Aspects of Radiative Symmetry Breaking in the Standard Model and Beyond

A Thesis Submitted to the

College of Graduate Studies and Research

in Partial Fulfillment of the Requirements

for the degree of Doctor of Philosophy

in the Department of Physics and Engineering Physics

University of Saskatchewan

Saskatoon

By

Wang, Zhi Wei

Permission to Use

In presenting this thesis in partial fulfilment of the requirements for a Postgraduate degree from the University of Saskatchewan, I agree that the Libraries of this University may make it freely available for inspection. I further agree that permission for copying of this thesis in any manner, in whole or in part, for scholarly purposes may be granted by the professor or professors who supervised my thesis work or, in their absence, by the Head of the Department or the Dean of the College in which my thesis work was done. It is understood that any copying or publication or use of this thesis or parts thereof for financial gain shall not be allowed without my written permission. It is also understood that due recognition shall be given to me and to the University of Saskatchewan in any scholarly use which may be made of any material in my thesis.

Requests for permission to copy or to make other use of material in this thesis in whole or part should be addressed to:

Head of the Department of Physics and Engineering Physics
Physics Building
116 Science Place
University of Saskatchewan
Saskatoon, Saskatchewan
Canada
S7N 5E2

Abstract

In this thesis, I discuss the conformally symmetric (CS) Standard Model (SM) and the hidden sector extensions to address the hierarchy/ naturalness problem, the origin of electroweak (EW) symmetry breaking (SB), dark matter (DM) candidates and the recent LHC (Large Hadron Collider) diphoton/ diboson anomalies where all the notions are discussed in the introduction. The main body of the thesis (chapter 2-6) where my original works are embedded studies different aspects of the CS hidden sector. The CS SM is the starting point, and further complexity is gradually introduced into the models. In chapter 2, I will show a 125 GeV Higgs mass with a large perturbative Higgs quartic coupling can be naturally realized in the conformal SM. In chapter 3, the minimal extension of the SM: the CS real singlet extension is studied, where the DM decay is protected by the Z_2 symmetry and two SB scenarios (the sequential scenario and dynamical scenario) are developed. In both scenarios, viable DM candidates are obtained. In chapter 4, I discuss the CS complex singlet extension of the SM with a global $U(1)$ symmetry which can be either broken or unbroken and both scenarios are studied to address DM, a second Higgs and the LHC diphoton excess. In the unbroken case, a viable cold DM candidate at ~ 100 GeV is obtained. In the broken case, a renormalization-scale optimization technique is developed to significantly narrow the parameter space and find a 550 GeV second Higgs boson. Upon including the interactions of the complex scalar with an additional vector-like fermion, a 720 GeV mass singlet is found to address the 750 GeV LHC diphoton excess. In chapter 5, the conformal scenario is combined with the asymptotic safety (AS) theory to study an asymptotically safe CS hidden sector. The AS is encoded in UV boundary conditions and renormalization group (RG) equations are used as a bridge to connect UV boundary conditions and EW/ TeV scale physics and furnish a detailed example in the context of a CS leptophobic $U(1)'$ model. In chapter 6, the multi-scale RG method is developed to address the two approximations within the implementation of Gildener Weinberg method: the weak coupling approximation and the simplification of the form of the logarithm. The introduction of an extra renormalization scale allows the mapping of the effective potential onto an RG-equivalent form with a certain symmetric structure, leading to a simplified form of the effective potential.

Acknowledgements

I would like to thank my mentor Dr. Tom Steele who has greatly shaped the way I think about this subject. I will tell two stories to show Tom is a great mentor and it has been a great experience to work with Tom. The first one I will call it as Magic Chicken Power. It was during the time when I almost finished the key calculations of my second PRL paper and we were attending CAP in Montreal. However, through the discussion, Tom and I found the result is completely chaos and almost no physical meaning. Instead of pushing me harder, Tom took me to a restaurant to have a big meal to make me calm down. I remembered I had half a chicken that night. During the night, when I was calmly rethinking about the calculations again, I found a simple rearrangement of the codes made everything in order again. After that night, I found a meaningful result and this work was published in PRL finally. The second story I will call Starting with the Simplest Case. It was during the time when I first got into the project of my first PRL paper. At that time, I don't understand why I need to start with such a simple $O(4)$ model rather than the one with more complication. Tom told me when you start to study one subject, you should always start with the simplest one which often captures the essential feature of the more complicated case. Finally, I find when I fully understand $O(4)$ model case, it's much easier for me to study my later on projects including further complexity.

I would like to thank Dr. Robert Mann whose deep insights into physics has greatly influenced the way I select research topics and formulate a physics problem with both global picture and local details. Also, he is one of the key persons leading me to the fantastic area of dark matter. I also thank Francesco Sannino whose works have indirectly influenced my PhD study.

I would also like to thank Dr. Rainer Dick, Dr. Gerry McKeon, Dr. F. A. Chishtie, Dr. Masoud Ghezelbash, Dr. Kaori Tanaka, Dr. Chris Soteros, Dr. Chijin Xiao, Dr. Doug Degenstein, Dr. Gap Soo Chang, Dr. Yansun Yao, Dr. Robin Kleiv, Dr. Wei Chen, Jason Ho and Fred Sage who have provided me lots of help during my PhD study.

Finally, I would like to thank my wife Lu Jiang, who always forgives me to be slow in daily life and has been accompanying me during the darkness time of my postdoctoral positions hunting. Also, I thank my parents and my grandparents who are always behind me.

To my wife, for not regretting the choice to marry a theoretical physicist. This thesis is also dedicated to my parents, my grandparents who are always behind me.

Contents

List of Tables

List of Figures

List of Abbreviations

AS	Asymptotic Safety
CW	Coleman Weinberg
CS	conformally symmetric
DM	dark matter
EW	electroweak
GW	Gildener Weinberg
ILC	International Linear Collider
LHC	Large Hadron Collider
LEP	Large ElectronPositron Collider
QCD	quantum chromodynamics
RG	renormalization group
SB	symmetry breaking
SM	Standard Model
VEV	vacuum expectation value
WIMP	weakly interacting massive particles

Chapter 1

Introduction

1.1 Motivation and Roadmap

The Standard Model (SM) [1, 2, 3, 4] which describes strong and electroweak interactions between quarks and leptons is the most successful particle physics theory human beings have achieved so far. However, it is almost universally believed that the SM is incomplete. The most severe problem is the hierarchy/ naturalness problem [5, 6] which has been the deep motivation for beyond the SM new physics in the last thirty years. Three main directions have been developed to address the hierarchy/ naturalness problem: supersymmetry, technicolor, global symmetry (little Higgs, twin Higgs) and the well-known strategy of extra dimension is considered as a dual of technicolor model (see e.g., [7, 8] for more detail). All the three main directions are deeply connected to the idea of custodial symmetries where the Higgs mass is protected by the symmetry against very large radiative corrections and the UV sensitivity of the Higgs mass is under control [6]. Recently, "conformal symmetry" as an alternative custodial symmetry to address hierarchy/naturalness problem has received much attention [9, 10, 11]. In this thesis, I will focus on the conformal symmetry and study its implication in the SM and beyond.

The SM also receives severe challenge from dark matter (DM) which provides another crucial motivation to go beyond the SM. Among the numerous ways to go beyond the SM, the hidden sector idea is particularly interesting. The hidden sector not only provides many exciting possibilities for DM but also produces interesting signatures at collider experiments and for cosmology. Moreover, it may address the origin of the electroweak symmetry breaking.

In this thesis, I will combine conformal symmetry with the notion of hidden sectors and study

conformally symmetric hidden sectors. The structure of the introduction will be composed of motivation, phenomenology and techniques. I will firstly provide a very brief introduction of the SM in section 1.2 and then introduce the hierarchy/ naturalness problem with a particular emphasis on conformal symmetry as a custodial symmetry in section 1.3. A follow up discussion about how conformal symmetry (scale invariance) is radiatively broken through the Coleman Weinberg mechanism [12] and a generalization to Gildener Weinberg method [13] will be in section 1.4. Connecting to the phenomenology and model building of dark matter, a brief discussion of the WIMP dark matter candidate and using hidden sector for model building will be in section 1.5. Also, connecting to the LHC (Large Hadron Collider) phenomenology, a mini review of the recent LHC diphoton excess will be in section 1.6. Finally, the two key techniques in this thesis: effective potential and renormalization group method will be discussed respectively in section 1.7 and section 1.8. The main body of the thesis will discuss different aspects of the conformally symmetric hidden sector and my original works [14, 15, 16, 17, 18] are embedded in chapter 2–6. In chapter 2, I will start with the conformally symmetric SM where we have shown that a 125 GeV Higgs mass can be naturally realized in this scenario associated with a large perturbative Higgs quartic coupling solution [14]. However, the SM is incomplete as we have discussed above and we study a conformal real singlet extension of the SM in chapter 3 [15]. In this scenario, the dark matter only couples to the SM through the Higgs portal interaction. In chapter 4, I will generalize the case discussed in chapter 3 and study the conformally symmetric complex singlet extension of the SM [16]. The complex singlet extension is particularly interesting since the hidden sector possesses a global $U(1)$ symmetry. The global $U(1)$ symmetry protects the dark matter from decaying and provides an ideal cold dark matter candidate. Moreover, gauging the global $U(1)$ symmetry, we can naturally construct the famous $U(1)'$ models. In chapter 5, I will combine the notion of asymptotic safety with conformal symmetry and apply this to a beyond the SM hidden sector in the context of $U(1)'$ leptophobic model [17]. This idea is broad and far-reaching, and we have provided a framework to show how UV boundary conditions can substantially affect electroweak/TeV scale physics, furnishing an explanation of the LHC diboson excesses. In chapter 6, I will develop a multi-scale renormalization group method to simplify the effective potential of the models with

multiple scalar fields while allowing an extension of the Gildener & Weinberg method beyond the weak coupling approximation [18]. Finally, a summary of the thesis will be in chapter 7.

1.2 Brief Introduction of the Standard Model

The Standard Model is based on the gauge group $SU(3)_C \otimes SU(2)_L \otimes U(1)_Y$ which provides fundamental interactions between the elementary particles where C, L, Y refer to color, left chiral nature, and weak hypercharge respectively [1, 2, 3, 4]. The Standard Model Lagrangian density is

$$L_{\rm SM} = L_{\rm gauge} + L_f + L_{\rm Higgs} + L_{\rm Yukawa} \tag{1.1}$$

where $L_{\rm gauge}$, L_f, $L_{\rm Higgs}$ and $L_{\rm Yukawa}$ correspond to gauge, fermion, Higgs and Yukawa sectors of the theory. The gauge sector is

$$L_{\rm gauge} = -\frac{1}{4}G^i_{\mu\nu}G^{\mu\nu i} - \frac{1}{4}W^i_{\mu\nu}W^{\mu\nu i} - \frac{1}{4}B_{\mu\nu}B^{\mu\nu} \tag{1.2}$$

where the field strength tensors $G^{\mu\nu}$, $W^{\mu\nu}$ and $B^{\mu\nu}$ correspond to $SU(3)_C$, $SU(2)_L$ and $U(1)_Y$ respectively. The fermion part of the SM involves 3 generations of quarks and leptons and each generation consists of

$$Q = \begin{pmatrix} u_L \\ d_L \end{pmatrix} \quad \ell = \begin{pmatrix} \nu_L \\ e_L \end{pmatrix}; \quad u_R,\ d_R,\ e_R,\ \nu_R \tag{1.3}$$

where Q, ℓ are quark and lepton $SU(2)$ doublets and R fields are $SU(2)$ singlets. The fermion sector can be written as

$$L_f = \sum_{m=1}^{3} \left(\bar{Q}_{mL} i \not{D} Q_{mL} + \bar{\ell}_{mL} i \not{D} \ell_{mL} + \bar{u}_{mR} i \not{D} u_{mR} + \bar{d}_{mR} i \not{D} d_{mR} + \bar{e}_{mR} i \not{D} e_{mR} + \bar{\nu}_{mR} i \not{D} \nu_{mR} \right) \tag{1.4}$$

where m is the family number and $\not{D} = D_\mu \gamma^\mu$ is the covariant derivative.

1.2.1 The Electroweak Symmetry Breaking and Higgs Mechanism

Electroweak symmetry breaking has been the crucial idea underneath the Higgs mechanism which provides masses for both the gauge bosons and the fermions in the SM. So far, the

origin of electroweak symmetry breaking is still an open question. In the SM, the electroweak symmetry is spontaneously broken by introducing a negative quadratic mass term in the Higgs effective potential which will be discussed in further detail later. However, there are still alternative ways to trigger the elctroweak symmetry breaking such as the well-known Coleman Weinberg Mechanism [12] which is a key focus of this thesis and the famous dynamical symmetry breaking [19].

The idea of spontaneous symmetry breaking was firstly introduced in [20, 21]. Here the symmetry breaking means the symmetry of the vacuum state is broken and the vacuum state does not possess the symmetry of the field system (the Lagrangian). In fact, there is no reason why an invariance of the Lagrangian of one quantum system should also be an invariance of the vacuum (ground) state of this system. Mathematically, after symmetry breaking the vacuum is non-invariant for certain generators of the symmetry group before symmetry breaking. In fact we can calculate how many generators are broken after the symmetry breaking and each broken generator corresponds to a massless particle called a Goldstone boson [22, 23]. However, the massless Goldstone bosons become a problem since massless particles can be easily produced, while there was no experimental evidence for them [22, 23]. Moreover, for the same reason, the massless gauge bosons in the theory are not observed and they require longitudinal degrees of freedom to become massive. If we can transfer all the degrees freedom of the Goldstone bosons to be the longitudinal degrees of freedom of the massive gauge bosons, then both the problems are solved. All the original massless gauge bosons will obtain mass and all the Goldstone bosons disappear since their physical degrees of freedom are "eaten" or absorbed to be the longitudinal degrees of freedom of the massive gauge bosons. The above points summarize the Higgs mechanism as rearrangement of degrees of freedom.

To connect the idea of spontaneous symmetry breaking to the Higgs mechanism, we need to introduce the a complex Higgs doublet:

$$\Phi \equiv \begin{pmatrix} G^+ \\ \frac{h+iG^0}{\sqrt{2}} \end{pmatrix},$$

where $G^{\pm}, G^0$ are the Nambu-Goldstone modes while h represents the physical Higgs field. The

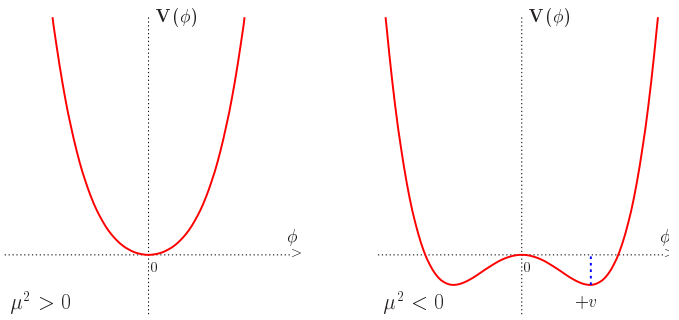

Figure 1.1: The potential V of the scalar field ϕ in the case $\mu^2 > 0$ (left) and $\mu^2 < 0$ (right).

Higgs potential can be written as

$$V(\Phi) = \mu^2 |\Phi|^2 + \lambda |\Phi|^4 \ . \tag{1.5}$$

It is useful to discuss a even simpler case of the Higss effective potential. We replace the complex Higgs doublet to a simple real scalar field ϕ and the Higgs potential Eq. (1.5) becomes:

$$V(\phi) = \frac{1}{2}\mu^2\phi^2 + \frac{1}{4}\lambda\phi^4, \tag{1.6}$$

which is shown in Fig. 1.1 (see e.g., [24]). The potential possesses a Z_2 symmetry $\phi \to -\phi$. If the mass term μ^2 is positive, the above Z_2 symmetry is not broken, the minimum of the potential is at the origin with vacuum expectation value (VEV) $\langle 0|\phi|0\rangle \equiv \phi_0 = 0$ shown in the left hand side of Fig. 1.1. If the mass term μ^2 is negative, the above Z_2 symmetry is broken, the minimum of the potential is not at the origin with non-zero VEV $\langle 0|\phi|0\rangle \equiv \phi_0 = -\frac{\mu^2}{\lambda} \equiv v^2$ shown in the right hand side of Fig. 1.1.

In the broken case, to determine particle masses and interactions, we must expand around one of the minima v by defining $\phi = v + \sigma$ where σ becomes the physical field degree of freedom. In terms of the new field degree of freedom σ, the Lagrangian becomes

$$L = \frac{1}{2}\partial_\mu\sigma\,\partial^\mu\sigma - (-\mu^2)\,\sigma^2 - \sqrt{-\mu^2\lambda}\,\sigma^3 - \frac{\lambda}{4}\,\sigma^4 + \text{const.}\,. \tag{1.7}$$

The occurrence of the cubic term σ^3 implies the Z_2 symmetry is broken. However, in fact, the underlying symmetry of the Higgs sector still exists. The symmetry breaking in the scalar sector is due to that some part of the symmetry is hidden through rearrangement of the degrees of freedom. In the real Higgs sector, the vacuum is degenerate (with the same ground state energy) and possesses a certain rotation symmetry $SO(4)$. Similar to the above simplified case where we select one of the two minima, in the real Higgs sector, however, we need to choose a specific direction in the vacuum and do the perturbation around the chosen vacuum direction. Moreover, the abnormal negative mass term is crucial to trigger the symmetry breaking. One of the reason Coleman and Weinberg proposed the radiative symmetry breaking is to get rid of the unnatural mass term [12].

Masses of Gauge Bosons

In this section, we will show how the gauge bosons obtain their masses through the Higgs mechanism [3, 4, 19, 25]. We will focus on the kinetic part of the Higgs sector since the masses of the gauge bosons come from the coupling of the Higgs field with the gauge field through the form of covariant derivative, i.e.,

$$\left| \left[i\partial_\mu + g\hat{\boldsymbol{T}} \cdot \boldsymbol{W_\mu} + \frac{1}{2} g' Y B_\mu \right] \Phi \right|^2 , \tag{1.8}$$

where W_μ and B_μ are respectively the gauge eigenstates of $SU(2)_L$ and $U(1)_Y$ and Y is the hypercharge of the Higgs field. $\hat{\boldsymbol{T}} = \left(\hat{T}_1, \hat{T}_2, \hat{T}_3\right)$ denotes the three generators of the $SU(2)$ group with $\hat{\boldsymbol{T}} \cdot \boldsymbol{W_\mu} = \hat{T}_1 W_\mu^1 + \hat{T}_2 W_\mu^2 + \hat{T}_3 W_\mu^3$ representing the dot product in gauge space. We choose a specific direction in the vacuum and do the perturbation on the chosen vacuum direction. To obtain the dynamics, we need to introduce a physical field η and change the variable from Φ to $\Phi = v + \eta$, where v is the vacuum expectation value of Φ. However, we don't need to consider η at this moment since the mass terms of the gauge bosons are independent of η. In this way, we can simply replace Φ with one constant matrix which contains the VEV of Φ and Eq. (1.8) becomes:

$$\begin{aligned} &\Phi^\dagger \left| g\hat{\boldsymbol{T}} \cdot \boldsymbol{W_\mu} + \frac{1}{2} g' Y B_\mu \right|^2 \Phi \\ =&W_\mu^i W_k^\mu g^2 \left(\Phi^\dagger \hat{T}_i \hat{T}_k \Phi \right) + g g' W_\mu^i B^\mu Y \left(\Phi^\dagger \hat{T}_i \Phi \right) + \frac{1}{4} g'^2 Y^2 B_\mu B^\mu \left| \Phi \right|^2 . \end{aligned} \tag{1.9}$$

By using the $SU(2)$ relation:

$$\hat{T}_i\hat{T}_k = \frac{1}{4}\delta_{ik} + \frac{i}{2}\varepsilon_{ikl}\left(\hat{T}_l\right) , \tag{1.10}$$

the term $\Phi^\dagger\hat{T}_i\hat{T}_k\Phi$ in Eq. (1.9) can be written as:

$$\Phi^\dagger\hat{T}_i\hat{T}_k\Phi = \frac{1}{4}\delta_{ik}\left|\Phi\right|^2 + \frac{i}{2}\varepsilon_{ikl}\left(\Phi^\dagger\hat{T}_l\Phi\right) . \tag{1.11}$$

Substituting the Eq. (1.11) into Eq. (1.9) and by noticing that $W^i_\mu W^\mu_k$ is symmetric with respect to the index i,k and the term $\frac{i}{2}\varepsilon_{ikl}\left(\Phi^\dagger\hat{T}_l\Phi\right)$ vanishes, we obtain:

$$\left(\frac{1}{4}g^2\boldsymbol{W_\mu}\cdot\boldsymbol{W^\mu} + \frac{1}{4}g'^2Y^2B_\mu B^\mu\right)\left|\Phi\right|^2 + gg'YB^\mu\boldsymbol{W_\mu}\cdot\left(\Phi^\dagger\hat{\boldsymbol{T}}\Phi\right) . \tag{1.12}$$

As mentioned above, Φ is just a constant matrix and $|\Phi|^2$ is just the square of the VEV, ie. $|\Phi|^2 = \frac{1}{2}v^2$. We now put vacuum states on both sides of the equation (1.12), and focus on the term: $\left(\Phi^\dagger\hat{\boldsymbol{T}}\Phi\right)$, since other terms will not change. The VEV of this term is given by:

$$\left\langle 0\left|\Phi^\dagger\hat{\boldsymbol{T}}\Phi\right|0\right\rangle = \frac{1}{2}v^2\boldsymbol{T_{vac}} , \tag{1.13}$$

where we have defined an isospin vector of the Higgs vacuum by $\boldsymbol{T_{vac}} = \frac{\langle 0|\Phi^\dagger\hat{\boldsymbol{T}}\Phi|0\rangle}{|\langle 0|\Phi|0\rangle|^2}$, $\left|\boldsymbol{T_{vac}}\right|^2 = \frac{1}{4}$. We decompose the isovector field $\boldsymbol{W_\mu}$ into an isospin component $W^\parallel_\mu$ parallel to $\boldsymbol{T_{vac}}$ and a component $W^\perp_\mu$ perpendicular to $\boldsymbol{T_{vac}}$,

$$\boldsymbol{W_\mu} = 2W^\parallel_\mu\boldsymbol{T_{vac}} + \boldsymbol{W^\perp_\mu} \tag{1.14}$$

with the relations

$$W^\parallel_\mu = 2\boldsymbol{W_\mu}\cdot\boldsymbol{T_{vac}} \qquad , \qquad \boldsymbol{W^\perp_\mu}\cdot\boldsymbol{T_{vac}} = 0 , \tag{1.15}$$

where $2\boldsymbol{T_{vac}}$ is a unit vector in isospin space. By using (1.14), we obtain:

$$\boldsymbol{W_\mu}\cdot\boldsymbol{W^\mu} = W^\parallel_\mu W^\mu_\parallel + \boldsymbol{W^\perp_\mu}\cdot\boldsymbol{W^\mu_\perp} . \tag{1.16}$$

We now put vacuum states on both sides of Eq. (1.12) and substitute for (1.13)–(1.16) to find:

$$\begin{aligned}&\frac{1}{8}v^2\left[g^2\boldsymbol{W^\perp_\mu}\cdot\boldsymbol{W^\mu_\perp} + g^2A^\parallel_\mu A^\mu_\parallel + 2gg'YA^\parallel_\mu B^\mu + g'^2B_\mu B^\mu Y^2\right] + \cdots \\ &\quad = \frac{1}{8}v^2g^2\left[\boldsymbol{W^\perp_\mu}\cdot\boldsymbol{W^\mu_\perp} + \left(A^\parallel_\mu + \frac{g'}{g}YB_\mu\right)^2\right] + \cdots \qquad .\end{aligned} \tag{1.17}$$

Let

$$Z_\mu = \frac{gW_\mu^{\parallel} + g'YB_\mu}{\sqrt{g^2 + g'^2}} \tag{1.18}$$

and after input (1.18) into (1.17) we get:

$$\frac{1}{8}v^2g^2\left[\boldsymbol{W}_{\boldsymbol{\mu}}^{\perp}\cdot\boldsymbol{W}_{\perp}^{\boldsymbol{\mu}} + Z_\mu Z^\mu\left(1+\frac{g'^2}{g^2}\right)\right]. \tag{1.19}$$

Let

$$\boldsymbol{W}_{\boldsymbol{\mu}}^{\perp} = \{W_\mu^1, W_\mu^2\}, \tag{1.20}$$

and the mass eigenstates $W_\mu^{\pm}$ can be written as the combination of W_μ^1 and W_μ^2 i.e.

$$W_\mu^{\pm} = \frac{W_\mu^1 \mp iW_\mu^2}{\sqrt{2}}, \tag{1.21}$$

It follows that:

$$\boldsymbol{W}_{\boldsymbol{\mu}}^{\perp}\cdot\boldsymbol{W}_{\perp}^{\boldsymbol{\mu}} = W_\mu^1W^{1\mu} + W_\mu^2W^{2\mu} = 2W_\mu^{(+)}W^{(-)\mu}, \tag{1.22}$$

and input (1.22) into (1.19) to get:

$$L \supset \frac{1}{8}v^2g^2\left[2W_\mu^{(+)}W^{(-)\mu} + Z_\mu Z^\mu\left(1+\frac{g'^2}{g^2}\right)\right]. \tag{1.23}$$

The above equation exactly represents the mass terms for both W bosons and Z boson and their masses given by $M_W = \frac{1}{2}vg$, $M_Z = \frac{1}{2}vg\sqrt{1+\frac{g'^2}{g^2}}$ where $v = 246$ GeV attaches to the electroweak scale. To sum up, by introducing the Higgs mechanism, the gauge bosons obtain their mass and at the same time gauge symmetry is maintained.

Masses of Fermions

In this section, I will show how fermions obtain their masses through the Higgs mechanism. Note that without Higgs mechanism, any explict mass term of the fermions will break the $SU(2)$ chiral symmetry. In the framework of Higgs mechanism, the fermions obtain their mass when coupled to the Higgs field through the Yuakwa couplings. Without losing generality, we take leptons as an example and the Yukawa coupling terms are written as follows:

$$h_l\left(\overline{R_l}\Phi^\dagger L_l + \overline{L_l}\Phi R_l\right), \tag{1.24}$$

where h_l is the Yukawa coupling constant, L, R are left-handed iso-doublets and right-handed iso-singlet respectively, and label l represents leptons (e, μ, τ). Note that the case for quarks is slightly more complicated where we employ the charge conjugate of Higgs doublet $\Phi_c \equiv \frac{i}{2}\hat{T}_2\Phi^*$ and Higgs field Φ to produce masses for the up- and down-type quarks respectively.

In the following, we first show that Eq. (1.24) does generate masses for the fermions. Writing L and R explicitly as

$$L = \begin{pmatrix} \psi_{\nu l} \\ \psi_l \end{pmatrix} \qquad R = \psi_{lR} \qquad \Rightarrow \qquad L = \begin{pmatrix} \nu \\ e \end{pmatrix} \qquad R = e_R \quad (for\ l = e) \tag{1.25}$$

the expression (1.24) becomes

$$\begin{aligned} \overline{R_l}\Phi^\dagger L_l + \overline{L_l}\Phi R_l &= \overline{\psi_R}\begin{pmatrix} 0, \frac{v}{\sqrt{2}} \end{pmatrix}\begin{pmatrix} \psi_\nu \\ \psi \end{pmatrix}_L + \begin{pmatrix} \overline{\psi_\nu}, \psi \end{pmatrix}_L \begin{pmatrix} 0 \\ \frac{v}{\sqrt{2}} \end{pmatrix}\psi_R \\ &= \frac{v}{\sqrt{2}}\left(\overline{\psi_R}\psi_L + \overline{\psi_L}\psi_R\right) . \end{aligned} \tag{1.26}$$

It should be noted that here I've chosen the direction of the vacuum which leaves the neutrino ν massless. Using

$$\psi_L = \frac{1-\gamma_5}{2}\psi \qquad , \qquad \overline{\psi_L} = \overline{\psi}\frac{1+\gamma_5}{2} \tag{1.27}$$

$$\psi_R = \frac{1+\gamma_5}{2}\psi \qquad , \qquad \overline{\psi_R} = \overline{\psi}\frac{1-\gamma_5}{2} \tag{1.28}$$

as well as

$$\left(\frac{1-\gamma_5}{2}\right)^2 = \frac{1-\gamma_5}{2} \qquad , \qquad \left(\frac{1+\gamma_5}{2}\right)^2 = \frac{1+\gamma_5}{2} \tag{1.29}$$

the expression (1.26) becomes

$$\overline{R_l}\Phi^\dagger L_l + \overline{L_l}\Phi R_l = \frac{v}{\sqrt{2}}\left(\overline{\psi}\frac{1-\gamma_5}{2}\psi + \overline{\psi}\frac{1+\gamma_5}{2}\psi\right) = \frac{v}{\sqrt{2}}\overline{\psi}\psi\,. \tag{1.30}$$

This above expression clearly shows that the Yukawa terms correspond to the (Dirac) mass terms of the fermions, with the fermion's mass proportional to the vacuum expectation value and Yukawa coupling.

Next, I want to show that the new Yukawa terms are actually gauge invariant. Since I have already shown these terms correspond to mass terms of the fermions, if these terms are also

gauge invariant it solves our original problem. We use the notation of gauge transformations $\hat{U} = \hat{U_1}\hat{U_2} = \hat{U_2}\hat{U_1}$, where $\hat{U_1}$ corresponds to a $U(1)$ gauge transformation and $\hat{U_2}$ corresponds to $SU(2)_L$ transformation. Note that, $\hat{U_2}$ operates only on the left-handed fermions not on the right-handed one. We can have:

$$\begin{aligned} \overline{R_L}\Phi^\dagger L_l &= \overline{R_l}\hat{U}^{-1}\hat{U}\Phi^\dagger\hat{U}^{-1}\hat{U}L_l \\ &= \overline{R_l}\hat{U_1}^{-1}\hat{U_1}\Phi^\dagger\hat{U_1}^{-1}\hat{U_2}^{-1}\hat{U_1}\hat{U_2}L_l \end{aligned} \tag{1.31}$$

with definition:

$$R_l' = \hat{U_1}R_l \quad , \quad L_l' = \hat{U_1}\hat{U_2}L_l \quad , \quad \Phi' = \hat{U_1}\hat{U_2}\Phi\hat{U_1}^{-1} = \hat{U_2}\Phi \tag{1.32}$$

we finally get:

$$\overline{R_L}\Phi^\dagger L_l = \overline{R_l}'\Phi'^\dagger L_l' \tag{1.33}$$

which is gauge invariant.

The above analysis show how the Higgs mechanism can give mass to the gauge bosons and to the fermions while maintaining gauge invariance.

1.3 Hierarchy/ Naturalness Problem and Custodial Symmetry

Hierarchy/ naturalness problem [5, 6] has been the main motivation for beyond the Standard Model (SM) new physics in the last 30 years and becomes even more important in the LHC era. The hierarchy problem/naturalness can be understood in the following way. Any physical states will give a threshold correction to the Higgs mass proportional to their own mass scale i.e. $\delta m_H^2 \propto M^2$, which is independent of any regularization and renormalization scheme. This is because m_H is renormalized additively (as opposed to multiplicatively), so that quantum corrections are parametricaly uncorrelated with the classical value of m_H and can be numerically much larger. Since most physicists believe from electroweak scale to Planck scale there must be new physics scale, it is unnatural for the Higgs mass to be at the electroweak scale (naturalness problem). The naturalness problem is the effect of the hierarchy problem where there is a big

hierarchy between the electroweak scale and the Planck scale and it requires lots of fine tuning to absorb the significant threshold corrections to the bare mass term of the Higgs (fine tuning problem) [5, 6, 8].

To address the hierarchy problem, we need to introduce the principle of naturalness by 't Hooft [6] which has been the guiding principle for beyond the Standard Model (SM) new physics. The principle of naturalness is that a quantity in nature should be small only if the underlying theory becomes more symmetric as that quantity tends to zero [6]. For example (see e.g., [7, 8] for more detail), consider a Dirac fermion Ψ. In the limit $m_\Psi \to 0$, there occurs an extra symmetry (chiral symmetry), and m_Ψ is the parameter measuring how much the chiral symmetry is broken. Since quantum corrections respect the symmetries of the action, quantum corrections will not generate a mass term if $m_\Psi = 0$ initially. Thus, the form of the quantum corrections of the Dirac fermion must be proportional to the parameter m_Ψ and a Dirac fermion mass is protected by the chiral symmetry. We call chiral symmetry the "custodial symmetry" of the Dirac fermions. Similarly, for spin-1 particles, the radiative corrections to the gauge boson masses are proportional to the mass itself and the gauge boson masses are protected from the gauge symmetry. Thus, we call gauge symmetry the "custodial symmetry" of the spin-1 particles (see e.g., [7, 8] for more detail).

For spin-0 particles, we also need a custodial symmetry to protect the Higgs mass from large radiative corrections. However, within the SM, no symmetry is enhanced when the Higgs mass is set to zero (there's a non-trivial symmetry the "conformal symmetry" which will be discussed in detail later on). So, our task is to search for the custodial symmetry for the spin-0 particles. The Coleman-Mandula theorem [26] tells us that the only possible options are: supersymmetry, global or gauge symmetry and conformal symmetry.

We start with **supersymmetry** and follow closely the nice reivew in [8]. In supersymmetry theory, the scalars and fermions are connected by supersymmetry. Since the fermions are protected by the chiral symmetry, through supersymmetry the scalars are now also protected by the chiral symmetry. Consider the radiative corrections to the Higgs mass. Since in the SM, the top quark Yukawa coupling y_t is the largest coupling and we can only focus on the top quark contribution to the Higgs mass. The result is well-known and propotional to $y_t^2\Lambda^2$

which is UV sensitive! With supersymmetry, there is an extra contribution to the Higgs mass from the top partner the stop $\widetilde{t}$. Amazingly, the contributions between top quark and the stop cancel each other and the UV sensitivity vanishes. We obtain (for up type Higgs H_u):

$$\delta m_{H_u}^2 = -\frac{6y_t^2}{16\pi^2}\Lambda^2 + \frac{6y_t^2}{16\pi^2}\Lambda^2 - \frac{3y_t^2}{4\pi^2}m_{\widetilde{t}}^2 \ln\left(\frac{\Lambda}{m_{\widetilde{t}}}\right) + \dots , \tag{1.34}$$

here the quadratic pieces Λ^2 explicitly cancel and no UV sensitivity remains. The only contributions left are the physical threshold contributions from new heavy states, which are at most logarithmically sensitive to Λ.

The second custodial symmetry we will discuss is a **global symmetry**. The idea is that the Higgs is considered as a pseudo-Nambu-Goldstone-boson (PNGB) of a spontaneously broken global symmetry. In this way, the Higgs mass is protected by the shift symmetry of PNGB (a very nice reivew of NGB/ PNGB can be found in [27]). This idea has been implemented to a few explicit model buildings such as the famous little Higgs model [28, 29] and the twin Higgs model [201]. In this scenario, the loop contribution to the Higgs mass by the top quark will also be cancelled by the fermionic top partner contribution, which is very similar to the supersymmetry case. The top partner is introduced to enlarge the quark content of the SM to make the Yukawa coupling satisfy a larger symmetry before it spontaneously breaks to a smaller symmetry which contains $SU(2) \times U(1)$. The radiative contribution to the Higgs mass is written as (see e.g., [8] for further detail):

$$\delta m_H^2 = -\frac{6y_t^2}{16\pi^2}\Lambda^2 + \frac{6y_t^2}{16\pi^2}\Lambda^2 - \frac{3y_t^2}{4\pi^2}m_T^2 \ln\left(\frac{\Lambda}{m_T}\right) + \dots \tag{1.35}$$

where m_T is the energy scale of the top partner T. It is evident that the quadratic pieces explicitly cancel and no UV sensitivity is left. The only contributions left are the physical threshold contributions from new heavy states, which are logarithmically sensitive to Λ.

The last custodial symmetry I will discuss here is the **conformal symmetry** which is the central idea of this thesis. It was pointed out firstly by Bardeen that if the Higgs scalar field were part of a conformal field theory, then the Higgs mass would be protected by the conformal symmetry (scale invariance) [9] (see also the nice explanations in [11, 10]). However, it is well known that the conformal symmetry is broken in the SM by the particle masses and running couplings. Thus, to make the scenario work, the conformal symmetry can only be broken softly

(i.e. no new divergences are introduced by the couplings which break conformal symmetry) and needs to be restored sufficiently quickly (non-Gaussian fixed point) [31]. Quantum mechanically, it requires the RG (renormalization group) flows of the SM to approach UV interacting fixed point. For a non-interacting (Gaussian) UV fixed point, the conformal symmetry is not restored sufficiently rapidly in the UV and new UV divergences which depend on conformal symmetry breaking arises. For example, in QCD (quantum chromodynamics) which is asymptotically free, the coupling logarithmically approaches to the free fixed point, and the contributions to the Higgs mass due to the scale invariance violation from the running QCD coupling persist to arbitrarily high energy scale [31].

Moreover, we know that if there exists new physics between the electroweak scale and the Planck scale, there will be threshold contributions to the Higgs mass. In supersymmetry theory, it is believed that the supersymmetry is softly broken at the Electroweak/TeV scale and is restored quickly. Thus, any threshold contributions will be exactly cancelled when supersymmetry is restored (particles at high energy scale should satisfy exact supersymmetry). In supersymmetry theory, we only need to worry about the threshold contributions below the scale where supersymmetry is broken. However, in conformal symmetry case, any new heavy particles will spoil the conformal symmetry. If we assume the conformal symmetry is restored quickly (the field system run into an interacting fixed point after the threshold), the system will be protected by the conformal symmetry from the UV sensitivity. However, the threshold contribution to the Higgs mass which is proportional to the threshold scale still exists [31]. Thus, to use conformal symmetry as a custodial symmetry, if there are new heavy particles between the Electroweak scale and Planck scale, the new heavy particles' masses should be fairly close to the Electroweak/ TeV scale or they must be sufficiently decoupled from the Higgs field (see e.g., the comment in [8]).

In addition, in the pioneering work by Schmaltz [31], they show that the Higgs mass will also be sensitive to the transition scale of two different scaling behaviours. They have considered the system which is IR free and flows to an interacting UV fixed point. The scaling behaviours (anomalous dimension) at two fixed points are different and Schmaltz assumed the physics involved in the transition to an interacting fixed point is nonperturbative [31]. It was shown that

the smoother the transition between two scaling behaviours the larger width of the transition region will be and the more contributions from higher energy scale can contribute to the Higgs mass. In the limit case, where the transition between the UV and IR fixed points is abrupt at scale M (least UV contribution), the transition itself (without involving any new heavy particle) will contribute to the Higgs mass and the contribution will be proportional to the scale M.

In conclusion, for the conformal symmetry as a custodial symmetry, we need to be careful about three points: the interacting (non-Gaussian) UV fixed point, the threshold contributions of the new heavy particles, and the transition scale (if the physics involved is nonperturbative). It is well-known that there is no non-trivial interacting fixed point at UV scale within the SM. Thus, for the conformal symmetry as a custodial symmetry, beyond the SM new physics has to be introduced in at fairly close to the Electroweak/ TeV scale without spoiling the naturalness. Also, if the transition to the interacting UV fixed point is nonperturbative, the naturalness of Higgs mass requires the transition scale to be sufficiently low at Electroweak/TeV scale no matter there existing new heavy particles at the transition scale or not. Either way, new physics near Electroweak/ TeV scale is inevitable in the conformal scenario. Since LHC has not found evidence of supersymmetry, the conformal symmetry as an alternative strategy could be very important at LHC era (TeV era).

1.4 Coleman Weinberg Mechanism and the Origin of Electroweak Symmetry Breaking

The importance of Coleman Weinberg (CW) Mechanism is in three aspects. Firstly, we have discussed the possibility to use Conformal symmetry as a custodial symmetry in the previous section and CW Mechanism provides a framework to study how the conformal symmetry (scale invariance) can be broken through the trace anomaly (shown in detail at the end of this section) dependent on the perturbative quantum loops [11, 10]. Secondly, the electroweak (EW) scale (the scale hierarchies between EW and Planck scale) can be dynamically generated through dimensional transmutation in CW framework, which addresses the origin of electroweak symmetry breaking and the hierarchy problem [12, 11, 10]. Thirdly, CW mechanism provides nice framework to give Higgs mass prediction in the SM (e.g., see chapter 2) and beyond (e.g., see chapter 3, 4) [12].

In the following, we give a brief introduction of the CW mechanism following the nice discussion in [32]. In the pioneering work of [12], Coleman and Weinberg first investigated the radiative symmetry breaking in a massless QED model. If we denote the two components of the complex singlet ϕ_1 and ϕ_2, we obtain the Lagrangian density of the model:

$$L = -\frac{1}{4}F_{\mu\nu}F^{\mu\nu} + \frac{1}{2}\left(\partial_\mu\phi_1 - eA_\mu\phi_2\right)^2 + \frac{1}{2}\left(\partial_\mu\phi_1 + eA_\mu\phi_2\right)^2 - \frac{\lambda}{4!}\left(\phi_1^2+\phi_2^2\right)^2 , \tag{1.36}$$

where we have set the tree level mass term for the scalar field to zero to satisfy the scale invariance. The one loop effective potential will be (calculation method is discussed in the following section of the computation of the effective potential):

$$V\left(\phi_c\right) = \frac{\lambda}{4!}\phi_c^4 + \frac{5\lambda^2}{1152\pi^2}\phi_c^4\ln\phi_c^2 + 3\frac{3e^4}{64\pi^2}\phi_c^4\ln\phi_c^2 + \frac{1}{2}B\phi_c^2 + \frac{1}{4!}D\phi_c^4 + C\,, \tag{1.37}$$

where $\phi_c \equiv \langle 0|\phi|0\rangle$, $\phi_c^2 \equiv \phi_{c1}^2 + \phi_{c2}^2$ and B, D, C are counterterms which can be determined from the renormalization conditions given by [12]:

$$\frac{d^4V}{d\phi_c^4} = \frac{d^4V_{tree}}{d\phi_c^4}\,. \tag{1.38}$$

As the result, we obtain:

$$V\left(\phi_c\right) = \frac{\lambda}{4!}\phi_c^4 + \left(\frac{5\lambda^2}{1152\pi^2} + \frac{3e^4}{64\pi^2}\right)\phi_c^4\left(\ln\frac{\phi_c^2}{\mu^2} - \frac{25}{6}\right)\,. \tag{1.39}$$

In [12], Coleman and Weinberg assumed $\lambda^2 \ll e^4$ and showed that under this condition, there is a nontrivial minimum with $\phi_c = v \neq 0$ indicating that the symmetry is radiatively broken. Although this condition may not be necessary (see e.g., [33]), we will stick to Coleman and Weinberg's assumption $\lambda^2 \ll e^4$ in the following. With this assumption, the effective potential is simplified to

$$V(\phi) \simeq \frac{\lambda}{4!}\phi_c^4 + \frac{3e^4}{64\pi^2}\phi_c^4\left(\ln\frac{\phi_c^2}{\mu^2} - \frac{25}{6}\right). \tag{1.40}$$

The nontrivial minimum is determined by using the VEV condition:

$$\left.\frac{dV(\phi_c)}{d\phi_c}\right|_{\phi_c=v} = 0\,. \tag{1.41}$$

Attaching the scale $\mu = v$, we obtain

$$\left(\frac{\lambda}{6} - \frac{11e^4}{16\pi^2}\right)v = 0\,, \tag{1.42}$$

leading to

$$\lambda = \frac{33}{8\pi^2}e^4\,, \tag{1.43}$$

which justifies the initial assumption $\lambda^2 \ll e^4$. Here, Coleman and Weinberg introduced a very profound concept called dimensional transmutation [12] which is based on the following insight. Initially, the Lagrangian contains two parameters λ and e. The renormalization generates one additional scale parameter μ in the theory. We are able to set a particular value for the scale $\mu = v$, leading to the constraint for the coupling i.e. Eq. (1.43). Thus, by using Eq. (1.43), we are able to transfer the two parameters in the theory from (λ, e) to (e, v). Since e, λ are dimensionless and v is dimensionful, the above transition obtains the name dimensional transmutation.

The scalar mass prediction is given by the second order terms:

$$M^2 = \left.\frac{dV^2(\phi_c)}{d\phi_c^2}\right|_{\phi_c=v} = \frac{3e^4}{8\pi^2}v^2\,. \tag{1.44}$$

By noticing the vector boson mass is given by $M_v^2 = e^2v^2$, we can obtain the mass ratio:

$$\frac{M^2}{M_v^2} = \frac{3e^2}{8\pi^2}\,. \tag{1.45}$$

The possibility of calculating the ratio $\frac{M^2}{M_v^2}$ may appear to be miracle. However, it is the consequence of the dimensional transmutation where all the dimensionless quantities in the model should be functions of e alone.

The Coleman-Weinberg mechanism can be summarized by using the trace anomaly (see e.g., [11, 10] for more detail). The trace of improved stress tensor can be written as:

$$\hat{T}_{\mu}^{\mu} = \phi \frac{\delta}{\delta \phi} V(\phi) - 4V(\phi) = -\beta(\lambda)\phi^4 \tag{1.46}$$

where we have used the simplest model $V(\phi_c) = \frac{\lambda}{4!}\phi_c^4$ and $\beta(\lambda) \equiv \frac{d\lambda(\mu)}{d\ln\mu}$. $\hat{T}_{\mu}^{\mu} = 0$ corresponds to the scale invariance and since $\beta(\lambda)$ is non-zero generally, the scale invariance is broken by the running coupling $\lambda(\mu)$. From high energy scale to low energy scale, the running coupling λ transfers from positive to negative ($\beta_\lambda > 0$ see next subsection [34]) triggering the EW symmetry breaking and the zero-crossing point approximately defines the EW symmetry breaking scale. Thus, the trace anomaly, RG functions, and radiative symmetry breaking are deeply connected to each other, which summarizes the Coleman-Weinberg mechanism.

1.4.1 Scale Hierarchies through Dimensional Transmutation

In this section, I want to show how scale hierarchies of electroweak scale and Planck scale can be dynamically generated through the dimensional transmutation in CW mechanism (see e.g., a nice discussion in [34]). We consider the simplest model to realize this idea where $V(\phi) = \frac{1}{4}\lambda\phi^4$. The radiative symmetry breaking occurs near the scale where the running coupling constant crosses zero. Note that in this simplest model, the RG function of λ (i.e. β_λ) satisfies the condition $\beta_\lambda > 0$ to make a physical scalar mass prediction (positive definite) [34]. Thus, the running coupling λ is negative at the low energy scale while positive at the high energy scale. From high energy scale to low energy scale, the running coupling λ transfers from positive to negative and the zero-crossing point approximately defines the symmetry breaking scale. For simplicity, we make an approximation $\beta_\lambda = b > 0$. In addition, the running coupling λ near the zero-crossing scale can be approximately treated as linear dependent on the scale:

$$\lambda(t) = b(t - t_0) = b(t - t_{UV}) + \lambda_{UV}, \tag{1.47}$$

where $t \equiv \log[\phi/\mu]$ and we have already implemented the boundary condition $\lambda(t_{UV}) = \lambda_{UV}$ resulting the zero-crossing scale $t_0 = t_{UV} - \lambda_{UV}/b$. By using Eq. (1.47), the RG-improved effective potential can be written as

$$V(\phi) = \frac{1}{4}\lambda(t)\,\phi^4 = \frac{b\mu^4}{4}(t - t_0)\,e^{4t} \tag{1.48}$$

where we have used $t \equiv \log[\phi/\mu] \to \phi = \mu e^t$. Minimizing the effective potential (1.48) by using (1.41), we obtain:

$$t_{min} = t_0 - \frac{1}{4} = t_{UV} - \frac{\lambda_{UV}}{b} - \frac{1}{4}\,. \tag{1.49}$$

If we attach t_{min} to the electroweak scale i.e. $t_{min} = \log\left[\frac{M_{EW}}{\mu}\right]$, we have

$$t_{min} - t_{UV} = \log\left[\frac{M_{EW}}{\mu}\right] - \log\left[\frac{M_{UV}}{\mu}\right] = \log\left[\frac{M_{EW}}{M_{UV}}\right] = -\frac{\lambda_{UV}}{b} - \frac{1}{4}\,, \tag{1.50}$$

leading to

$$M_{EW} = M_{UV}\exp\left(-\frac{\lambda_{UV}}{b} - \frac{1}{4}\right). \tag{1.51}$$

The above expression (1.51) shows that with a small value of b, a small electroweak scale M_{EW} can be dynamically generated from a much larger UV scale M_{UV}, addressing the large scale hierarchies. In this sense, the CW mechanism is similar to the dimensional transmutation in QCD [11, 10, 34]:

$$\Lambda_{QCD} = M_{UV}\exp\left(-\frac{2\pi}{b_0\alpha_s(M_{UV})}\right) \tag{1.52}$$

to make Λ_{QCD} stable against M_{UV}, where b_0 is defined by the RG functions of the strong coupling (α_s): $\beta_{\alpha_s} = -(b_0/2\pi)\,\alpha_s^2$. Note that the occurrence of the large scale hierarchies Eq. (1.51) is due to the slow logarithmic RG evolution of the coupling λ.

1.4.2 Gildener-Weinberg Method

Coleman Weinberg mechanism is applied to the case where there is only one single scalar field. In the case with multiple scalar fields, we need to employ the Gildener Weinberg method [13]. We will provide a brief discussion of Gildener Weinberg method following the nice review in [35, 36].

We consider a renormalizable gauge field theory with a set of n real scalar fields ϕ_i and $(i = 1, 2, \cdots, n)$. We also denote Φ as an n dimensional field with ϕ_i as its n components. The scale invariant tree level potential is generally given by

$$V^{\text{tree}}(\Phi) = \frac{1}{4!} f_{ijkl} \phi_i \phi_j \phi_k \phi_l \,, \tag{1.53}$$

where f_{ijkl} represents the quartic coupling of the potential. Different from the single scalar field case, with multiple scalar fields, we need to find a direction n along which there is the local minimum of the effective potential in the multi-dimensional field space and we will do perturbative analysis around this direction. There are three conditions along the direction n: **flat**, **stationary** and **non-negative definite**. For flat condition, it means one has $V^{\text{tree}}(\Phi) = 0$ everywhere along the ray $\Phi^{\text{flat}} = \varphi n$ where φ is the radial distance from the origin of the field space. This condition can also be written as

$$V^{\text{tree}}(N) = \frac{1}{4!} f_{ijkl}(\mu) N_i N_j N_k N_l = 0 \,. \tag{1.54}$$

We suppose this constraint (1.54) is satisified for a particular unit vector $N = n$ with $\phi_i = \varphi N_i$ and for a particular RG scale $\mu = \Lambda$. Note that Eq. (1.54) imposes only a single constraint on the coupling f_{ijkl} and we are not able to choose a renormalization scale to make all the couplings f_{ijkl} vanish. For the stationary condition (under which the ray $\Phi^{\text{flat}} = \varphi n$ is a stationary line), we have

$$\left.\frac{\partial V^{\text{tree}}(N)}{\partial N_i}\right|_{N=n} = 0 \qquad , \qquad \left(\text{equivalent to } \left.\nabla \mathrm{V}^{\text{tree}}(\Phi)\right|_{\Phi=\varphi \mathrm{n}} = 0\right) \tag{1.55}$$

which can be written explicitly as:

$$f_{ijkl}(\Lambda) n_j n_k n_l = 0 \,, \tag{1.56}$$

where we have used the assumption that this condition is satisified for a particular unit vector $N = n$ and a particular RG scale $\mu = \Lambda$. The non-negative definite condition is to make sure there is the local minimum in the ray rather than the local maximum. We thus have the condition:

$$(P)_{ij} \equiv \left.\frac{\partial V^{tree}(N)}{\partial N_i \partial N_j}\right|_{N=n} = \frac{1}{2} f_{ijkl} n_k n_l \tag{1.57}$$

to be none-negative definte (P matrix has either positive or zero value eigenvalues). We now have a well defined ray $\Phi^{\text{flat}} = \varphi n$ with local minimum, we are able to study the one loop perturbative analysis along this ray. Since $V^{\text{tree}}(N)$ vanishes along the flat direction $\Phi^{\text{flat}} = \varphi n$, the full effective potential (tree level contribution and loop level contribtuion) will be dominated by higher-loop order contributions. Adding higher loop order contributions will lead to two consequences. First, higher order contributions will generate a small curvature in the radial direction $\Phi^{\text{flat}} = \varphi n$, leading to a minimum along the ray where $\varphi = v_\varphi$. This is similar to the case in Coleman Weinberg mechanism where radiative symmetry breaking generates a non-trivial minimum. Second, higher order contributions will also shift the flat direction leading to a small shift $\delta\Phi = v_\varphi \delta n$ perpendicular to the flat direction n with $n \cdot \delta n = 0$. We can extend the stationary condition Eq. (1.55) to the full effective potential with one loop order contribution included:

$$\nabla \left(V^{\text{tree}}(\Phi) + V_{eff}^{1-loop}(\Phi) \right) \Big|_{\Phi = v_\varphi (n + \delta n)} = 0 \,. \tag{1.58}$$

We can expand the expression with $\delta\Phi$ as one loop order parameter and we obtain:

$$v_\varphi^2 P \cdot \delta\Phi + \nabla V_{eff}^{1-loop}(\Phi) \Big|_{\Phi = v_\varphi n} = 0 \,. \tag{1.59}$$

We may eliminate the first term in the above expression by contracting the expression from the left with n since $n \cdot P = 0$ by using Eq. (1.55) and Eq. (1.56). Thus, we obtain the VEV condition along the radial direction:

$$n \cdot \nabla V_{eff}^{1-loop}(\Phi) \Big|_{\Phi = v_\varphi n} = \frac{dV_{eff}^{1-loop}(\varphi n)}{d\varphi} = 0 \,. \tag{1.60}$$

This condition plays the same role as the VEV condition Eq. (1.41) in Coleman Weinberg mechanism. Along the flat direcion $\Phi^{\text{flat}} = \varphi n$, the one loop effective potential can be conveniently written in a form similar to the one in Coleman Weinberg case

$$V_{eff}^{1-loop}(\varphi n) = A(n)\,\varphi^4 + B(n)\,\varphi^4 \ln \frac{\varphi^2}{\Lambda^2} \,. \tag{1.61}$$

where A, B are n dependent constants. A, B are written out explicitly in the $\bar{M}S$ scheme as:

$$\begin{aligned} A =& \frac{1}{64\pi^2 v_\varphi^4}\left\{ \mathrm{Tr}\left[m_S^4\left(-\frac{3}{2}+\ln\frac{m_S^2}{v_\varphi^2}\right)\right] + 3\,\mathrm{Tr}\left[m_V^4\left(-\frac{3}{2}+\ln\frac{m_V^2}{v_\varphi^2}\right)\right]\right. \\ & \left. -4\,\mathrm{Tr}\left[m_F^4\left(-\frac{3}{2}+\ln\frac{m_F^2}{v_\varphi^2}\right)\right]\right\}, \\ B =& \frac{1}{64\pi^2 v_\varphi^4}\left(\,\mathrm{Tr}m_S^4 + 3\,\mathrm{Tr}m_V^4 - 4\,\mathrm{Tr}m_F^4\right), \end{aligned} \tag{1.62}$$

where m_S, m_V and m_F correspond to tree level scalar, vector and fermion mass matrices respectively. Comparing with the one loop effective potential in Coleman Weinberg case (see Eq. (1.39)), it is apparent they have similar form. This point is crucial when we employ the leading logarithmic summation technique to obtain the renormalization group improved effective potential in Chapter 3 and Chapter 4. We can minimize Eq. (1.61) by using Eq. (1.60) and we obtain an expression for scale hierarchies (dimensional transmutation):

$$\Lambda = v_\varphi \exp\left(\frac{A}{2B}+\frac{1}{4}\right), \tag{1.63}$$

which is similar to Eq. (1.51) in Coleman Weinberg case.

Now, we will consider the scalar mass prediction with the one loop contributions included. The mass predictions will be given by:

$$\left(m_S^2+\delta m_S^2\right)_{ij} = \left.\frac{\partial^2\left(V^{\mathrm{tree}}(\Phi)+V_{eff}^{1-loop}(\Phi)\right)}{\partial\phi_i\partial\phi_j}\right|_{\Phi=v_\varphi(n+\delta n)}. \tag{1.64}$$

Expand the above expression to first order:

$$\left(\delta m_S^2\right)_{ij} = v_\varphi f_{ijkl} n_k \delta\phi_l + \left.\frac{\partial^2 V_{eff}^{1-loop}(\Phi)}{\partial\phi_i\partial\phi_j}\right|_{\Phi=v_\varphi n}. \tag{1.65}$$

We are able to obtain the scalon mass m_h^2 by contracting the above expression with n_i and n_j:

$$m_h^2 = n_i n_j\left(\delta m_S^2\right)_{ij} = n_i n_j \left.\frac{\partial^2 V_{eff}^{1-loop}(\Phi)}{\partial\phi_i\partial\phi_j}\right|_{\Phi=v_\varphi n} = \left.\frac{d^2 V_{eff}^{1-loop}(\varphi n)}{d\varphi^2}\right|_{\varphi=v_\varphi} = 8Bv_\varphi^2, \tag{1.66}$$

which is similar to the expression (Eq. (1.44)) in Coleman Weinberg mechanism. So, along the flat direction, the one loop effective potential calculation from VEV condition to scalon mass prediction will be similar to the case of Coleman Weinberg mechanism. This point provides the foundation when we employ the leading logarithm summation technique to the multiple scalar extensions of the SM (see Chapter 3 and Chapter 4).

1.5 Dark Matter and Hidden Sector

The particle dark matter provides a fantastic motivation to go beyond the SM. It should be noted that the idea of dark matter has been existing for a long time. In 1933, Zwicky observed the velocities of galaxies in the Coma Cluster and found the amount of mass required for the cluster to have sufficient gravitational pull was 400 times greater than the contributions of the measured luminous masses [37]. Zwicky proposed the existence of what he named Dunkle Materie (German for Dark Matter). In 1970s, Rubin and Kent Ford measured the rotation curves and found similar rotational velocities of stars at any distance from the galactic center [38]. Recently, dark matter is supported by the evidence of Bullet Cluster [39], Big Bang nucleosynthesis (BBN) [40], and the cosmic microwave background (CMB) [41].

1.5.1 WIMP Dark Matter Candidates

WIMP dark matter is normally produced as a thermal relic of the Big Bang. In the early universe, the dark matter and other standard model particles are in thermal equilibrium. In this stage, the number density of dark matter drops exponentially as $e^{-m_\chi/T}$ where m_χ is the dark matter mass. However, during the time when the universe cools down, the universe is also expanding. At a certain point, the dark matter particle number density has been exponentially damped and has become so dilute that it is hard to find another dark matter particle to annihilate with. At this point, dark matter "freezes out" and the comoving dark matter particle number density asymptotically approaches a constant.

We follow the very nice reviews of WIMP dark matter in [42, 43]. To make it simple enough, we consider there only exists one species of dark matter χ in the following. The evolving dark matter number density is described by the Boltzmann equation

$$\frac{dn}{dt} = -3Hn - \langle \sigma_A v \rangle \left(n^2 - n_{\rm eq} \right), \tag{1.67}$$

where $n, H, \langle \sigma_A v \rangle, n_{\rm eq}$ correspond respectively to dark matter number density, Hubble parameter, thermally averaged annihilation cross section and dark matter number density in thermal equilibrium. When χ is extremely relativistic i.e. $T \gg m_\chi$, the equilibrium density

$n_{\rm eq} = 3g_\chi\zeta(3)T^3/\left(4\pi^2\right)$ for fermions and $n_{\rm eq} = g_\chi\zeta(3)T^3/\left(\pi^2\right)$ for bosons, where g_χ is the effective number of relativistic species. In contrast, when χ is non-relativistic i.e. $T \ll m_\chi$, the equilibrium density $n_{\rm eq} = g_\chi \left(\frac{m_\chi T}{2\pi}\right)^{\frac{3}{2}} e^{-m_\chi/T}$.

A rough analysis by using the condition at freeze-out temperature is useful to provide important information of the thermal relic density even without solving the Boltzmann equation numerically. At the freeze-out temperature $T = T_{\rm fo}$, we have

$$\Gamma_A\left(T_{\rm fo}\right) = \langle\sigma_A v\rangle_{T=T_{\rm fo}} n_{\rm eq} \simeq H\left(T_{\rm fo}\right) , \tag{1.68}$$

where Γ_A is the annihilation rate. For particles with $M_\chi \gg T_{\rm fo}$, $n_{\rm eq} = g_\chi \left(\frac{m_\chi T}{2\pi}\right)^{\frac{3}{2}} e^{-m_\chi/T}$ and eq. (1.68) becomes

$$\Gamma_A\left(T_{\rm fo}\right) = \langle\sigma_A v\rangle_{T=T_{\rm fo}} n_{\rm eq}\left(T_{\rm fo}\right) \simeq \langle\sigma_A v\rangle_{T=T_{\rm fo}} \left(\frac{m_\chi T_{\rm fo}}{2\pi}\right)^{\frac{3}{2}} e^{-m_\chi/T_{\rm fo}} \simeq H\left(T_{\rm fo}\right) \simeq \frac{T_{\rm fo}^2}{M_{pl}} , \tag{1.69}$$

where M_{pl} is the planck mass. Eq. (1.69) leads to

$$n_{\rm eq}\left(T_{\rm fo}\right) \simeq \frac{T_{\rm fo}^2}{M_{pl}\langle\sigma_A v\rangle_{T=T_{\rm fo}}} . \tag{1.70}$$

The thermal relic density is

$$\Omega_\chi = \frac{m_\chi n_0}{\rho_c} = \frac{m_\chi T_0^3}{\rho_c}\frac{n_0}{T_0^3} \sim \frac{m_\chi T_0^3}{\rho_c}\frac{n_{\rm fo}}{T_{\rm fo}^3} \sim \frac{x_f T_0^3}{\rho_c M_{pl}}\langle\sigma_A v\rangle^{-1}_{T=T_{\rm fo}} \tag{1.71}$$

where ρ_c is the critical density and subscripts 0 denote present day and $x_f \equiv m_\chi/T_{\rm fo}$ where a typical value is $x_f \sim 20$. Eq. (1.71) shows the thermal relic density is inversely proportional to the annihilation cross section $\langle\sigma_A v\rangle_{T=T_{\rm fo}}$ and is insensitive to the dark matter mass m_χ. The Boltzman equation can be conveniently rewritten as

$$\frac{dY}{dx} = \frac{\langle\sigma_A v\rangle s}{Hx}\left(Y_{eq}^2 - Y^2\right) , \tag{1.72}$$

where $s = \frac{2\pi^2}{45}\frac{g_s m^3}{x^3}$ is the entropy density, $Y \equiv \frac{n}{s}$ and $H = \sqrt{\frac{4\pi^3}{45}}\frac{m^2}{M_{pl}x^2}g_\rho^{1/2}$. If we define $\lambda = \langle\sigma_A v\rangle m M_{pl}\sqrt{\frac{\pi}{45}}\frac{g_s}{\sqrt{g_\rho}}$, Eq. (1.72) can be further simplified to

$$\frac{dY}{dx} = \sqrt{\frac{\pi}{45}}\frac{g_s}{\sqrt{g_\rho}} m M_{pl}\frac{\langle\sigma_A v\rangle}{x^2}\left(Y_{eq}^2 - Y^2\right) = \frac{\lambda}{x^2}\left(Y_{eq}^2 - Y^2\right) . \tag{1.73}$$

After freeze out, Y_{eq} will continue to decrease according to the Boltzman suppression, so that $Y \gg Y_{eq}$ when $x \gg 1$, which further simplify the Boltzman equation (1.73) to

$$\frac{dY}{dx} \simeq -\frac{\lambda}{x^2} Y^2 \,. \tag{1.74}$$

Eq. (1.74) can be easily solved:

$$\frac{1}{Y_0} - \frac{1}{Y_f} = \lambda \left(\frac{1}{x_f} - \frac{1}{x_0} \right) \,, \tag{1.75}$$

where x_f and x_0 denote freeze out time and present time respectively. Noticing $x_0 \gg x_f$ and $Y_0 \ll Y_f$, we obtain

$$Y_0 \simeq \frac{x_f}{\lambda} \,. \tag{1.76}$$

The present relic abundance is defined as

$$\Omega_A \equiv \frac{\rho_A}{\rho_c^0} \,, \tag{1.77}$$

where $\rho_A = m_\chi Y_0 s_0$ and the critical density $\rho_c^0 = 3H_0^2/8\pi G$. By using (1.76), we obtain

$$\Omega_A = \frac{m_\chi Y_0 s_0}{\rho_c^0} = \frac{m_\chi x_f}{\lambda} \frac{2\pi^2 g_s^0 T_0^3}{45 \rho_c^0} \tag{1.78}$$

where we have used $s_0 = \frac{2\pi^2}{45} \frac{g_s^0 m_\chi^3}{x_0^3}$ and $g_s^0 = 3.91$ is the effective degrees of freedom of today. Setting $g_s = g_\rho$, we find

$$\Omega_A h^2 \simeq 0.1 \left(\frac{x_f}{20} \right) \left(\frac{60}{g_\rho} \right)^{1/2} \frac{3 \times 10^{-26} \mathrm{cm}^3/\mathrm{s}}{\langle \sigma_A v \rangle} \tag{1.79}$$

where $h^2 \sim 0.5$ and h is the hubble constant in units of $100\,\mathrm{km}/\,(\mathrm{s} \times \mathrm{Mpc})$. Eq. (1.79) is normally called "WIMP Miracle", which means that for typical electroweak cross sections, Eq. (1.79) provides the surprisingly accurate dark matter abundance we observed today. WIMP dark matter candidate becomes important since it connects to the physics at the scale (electroweak scale) which has been well studied.

1.5.2 Dark Matter Candidates in Hidden Sectors

The hidden sector idea has received lots of attention recently. The "hidden" is named as opposed to the visible sector the Standard Model. A hidden sector consists of fields that do not feel the

strong and electroweak forces that the SM do (singlet under the SM gauge group). The hidden sector is particularly useful in the study of dark matter. Firstly, the particle contents in the hidden sector can be made feebly interacting (through a certain portal) with the SM particles, providing ideal dark matter candidates. Secondly, the hidden sector framework permits study of dark matter with much richer internal structure (see e.g., [44, 45]) such as multi-component dark matter [46], non-abelian dark gauge group [47] or interesting symmetry breaking patterns [16]. People used to expect very simple dark matter and recently they believe dark matter with richer internal structures. It may not be just one more stable particle, it could be another hidden world which is probably as rich as our visible world.

The hidden sector and the visible sector (the SM) are connected through different portals such as scalar portal (e.g., Higgs portal), vector portal (e.g., Z' portal) and Neutrino Portal (see e.g., a nice review in [48]). We focus on the scalar portal and vector portal in the following.

Scalar Portal

The scalar portal is defined where there are new particles in the hidden sector which are neutral singlet scalars and couple to the square of the Higgs field $|H|^2$:

$$L_{\text{scalar portal}} = \left(\lambda_i S_i^2 + g_i S_i\right)\left(H^\dagger H\right) \tag{1.80}$$

where λ_i and g_i are dimensionless and dimensionful couplings respectively. The scalar portal is of particular importance for the following reasons [48]. Firstly, the discovery of Higgs boson provides strong evidence that fundamental scalars exist in nature as well as a profound motivation to study and search for alternative scalar particles. Secondly, since the particles in the hidden sector are neutral under the SM gauge group, it requires an operator which is also a singlet under the SM gauge group to transfer the interaction between the hidden sector and the SM sector. The operator $|H|^2$ is among the simplest operators which can be constructed from the SM and with the lowest dimension, which makes the (renormalizable) Higgs portal interaction unique. Thirdly, the scalar portal provides the simplest dark matter candidate while rich enough to possess the key characteristics such as dark matter stability. For the simplest case where the dark matter is constructed from a real singlet, the stability of the dark matter is protected by the discrete symmetry Z_2. For the next to simplest case where the dark matter

is constructed from a complex singlet, the stability of the dark matter is protected by a global $U(1)$ symmetry.

The Phenomenology of the Scalar Portal Model

In the following discussion, we focus on the simplest Higgs portal model: the real singlet extension of the SM (for more detail see Chapter 3). The phenomenology of the scalar portal model can be divided into the broken case ($\langle S \rangle \neq 0$) and the unbroken case ($\langle S \rangle = 0$). We firstly discuss the unbroken case where the singlet can be a dark matter candidate. For singlet mass less than half of the Higgs mass i.e. $M_S \leq \frac{1}{2} M_H = 62.5\,\text{GeV}$, the parameter space is very tightly constrained by the Higgs invisible decay width where Higgs portal coupling λ larger than $0.02 \sim 0.03$ is ruled out [49]. For singlet mass larger than half of the Higgs mass i.e. $M_S \geq \frac{1}{2} M_H = 62.5\,\text{GeV}$ and the Higgs portal coupling is not very large, the direct detection experiments provide the strongest bound [50, 51]. For singlet mass larger than the Higgs mass $M_S \geq M_H$ with large Higgs portal coupling, the channel that two singlet particles annihilate into two Higgs bosons $SS \to HH$ dominiates. We can show in this case, the direct detection rate which is defined as the product of direct detection cross section and relic density i.e. $\sigma \times \Omega h^2$ is suppressed [52]. For the process $SS \to HH$, the annihilation cross section is proportional to λ^4 in the limit of large λ and thus the thermal relic density $\Omega h^2 \propto \lambda^{-4}$. Since the direct detection cross section is still proportional to λ^2, the product of direct detection cross section and relic density $\sigma \times \Omega h^2 \propto \lambda^{-2}$, which is suppressed. In this case, the collider searching becomes more sensitive compared with the direct detection searching [52]. From the above discussion, it is very clear the direct detection and collider searching are complementary to each other.

Next, we consider the broken case ($\langle S \rangle \neq 0$). This case is particularly interesting because of the mixing between the singlet field and the Higgs field. The mixing angle is defined in the following:

$$\begin{pmatrix} \tilde{h} \\ \tilde{H} \end{pmatrix} = \begin{pmatrix} \cos\theta & -\sin\theta \\ \sin\theta & \cos\theta \end{pmatrix} \begin{pmatrix} h_1 \\ h_2 \end{pmatrix},$$

where $\tilde{h}, \tilde{H}$ are mass eigenstates while h_1 and h_2 are the gauge eigenstates defined by

$$H \equiv \begin{pmatrix} 0 \\ \frac{h_1+v_1}{\sqrt{2}} \end{pmatrix}, \qquad S \equiv \frac{h_2+v_2}{\sqrt{2}}\,.$$

For the singlet mass smaller than the Higgs mass i.e. $M_S \leq 125$GeV, the mixing angle is constrained most strongly by the LEP (Large ElectronPositron Collider) experiment, which constrained the mixing angle to be $\sin\theta \leq 0.02$ [53]. For singlet mass $125\,\mathrm{GeV} \leq \mathrm{M_S} \leq 500\,\mathrm{GeV}$, the mixing angle is constrained most strongly by the LHC Higgs searching, which constrained the mixing angle to be $\sin\theta \leq 0.3$ [53]. For singlet mass $M_S \geq 500\,\mathrm{GeV}$, the mixing angle is constrained most strongly by the Higgs signal rates, which constrained the mixing angle to be $\sin\theta \leq 0.5$ [53]. Note that, it has also been claimed in Ref. [54] that the mixing angle is constrained most strongly by the one loop correction to the W boson mass where for singlet mass $M_S \geq 500\,\mathrm{GeV}$, the bound of the mixing angle is $\sin\theta \leq 0.25$.

Vector Portal

In this case, the new Abelian field A'_μ with the field strength $F'_{\mu\nu}$ couples to the hypercharge fields $F_Y^{\mu\nu}$ through the (gauge invariant) kinetic mixing term [55] i.e.

$$L_{\text{vector portal}} = \epsilon F'_{\mu\nu} F_Y^{\mu\nu}\,, \tag{1.81}$$

where ϵ is a dimensionless coupling characterizing the mixing. Since the mixing problem is of particular importance in $U(1)'$ model, in the following, I will expand in much further detail following the discussion in [56].

Generally, there exists three kinds of field transformation and two kinds of mixing. Firstly, for an initial Lagrangian with tree level kinetic mixing (first kind of mixing) between two $U(1)$ gauge fields, we are able to select a special basis (first kind of field transformation) to get rid of the mixing. Secondly, we can do the field transformation again (second kind of field transformation) to make the gauge fields into gauge eigenstates. Thirdly, we can do another field transformation to make the gauge eigenstates into the mass eigenstates (mass mixing).

To show the above explicitly, we start from the most general Lagrangian for the kinetic

terms of $U(1)_1 \times U(1)_2$ gauge theory:

$$L_{\rm kin} = -\frac{1}{4}F^1_{\mu\nu}F^1_{\mu\nu} - \frac{1}{4}F^2_{\mu\nu}F^2_{\mu\nu} - \frac{1}{2}\epsilon F^1_{\mu\nu}F^2_{\mu\nu}\,. \tag{1.82}$$

The most general covariant derivative of a matter field ψ_k is

$$D_\mu = \partial_\mu + i\sum_{a=1}^{2}\sum_{b=1}^{2} Y_k^a g_{ab} A_\mu^b \tag{1.83}$$

and the corresponding gauge transformations are

$$A_\mu^a \to A_\mu^a + \partial_\mu \theta^a, \qquad \psi_k \to \exp\left(-i\sum_{a=1}^{2}\sum_{b=1}^{2} Y_k^a g_{ab}\theta^b\right)\psi_k\,, \tag{1.84}$$

where A_μ^b, Y_k^a and g_{ab} denote the gauge fields, hypercharges of $U(1)$ and coupling constants respectively. Note that instead of one gauge coupling for each $U(1)$ group, there exists a matrix g_{ab}, which is a unique characteristic of the theory with multiple $U(1)$ groups. We can choose a basis under which the tree level kinetic mixing term vanishes and the field transformations are

$$A_\mu^1 = \frac{1}{\sqrt{2\,(1+\epsilon)}}A_\mu^Y + \frac{1}{\sqrt{2\,(1-\epsilon)}}A_\mu^E, \quad A_\mu^2 = \frac{1}{\sqrt{2\,(1+\epsilon)}}A_\mu^Y - \frac{1}{\sqrt{2\,(1-\epsilon)}}A_\mu^E \tag{1.85}$$

where $A_\mu^Y,\ A_\mu^E$ are the new gauge fields. The corresponding couplings and charges for a certain matter field ψ_k are now respectively $g_{YY}, g_{YE}, g_{EY}, g_{EE}$ and Y_k^E, Y_k^Y It might be useful to write the above transformation in an alternative way. Define $\epsilon \equiv \sin\chi$, we can have the following simple transformation [57]

$$A_\mu^1 \to \tilde{A_\mu^1} - \tan\chi\tilde{A_\mu^2}, \quad A_\mu^2 \to \frac{\tilde{A_\mu^2}}{\cos\chi}\,, \tag{1.86}$$

where $\tilde{A_\mu^1},\ \tilde{A_\mu^2}$ denote the new gauge fields.

Our next step is to do the field transformation again to make the fields into gauge eigenstates. We denote the new gauge eigenstates as E_μ and B_μ where B_μ corresponds to the weak hypercharge gauge field. The interaction terms for a generic matter field ψ_k coupling to E_μ and B_μ are

$$g_y Y_k B_\mu + \left(g_E Y_k^E + g' Y_k^Y\right) E_\mu \tag{1.87}$$

where the fields transformations are [56]

$$E_\mu = \frac{g_{EE}A^E_\mu + g_{EY}A^Y_\mu}{\sqrt{g^2_{EE}+g^2_{EY}}}, \quad B_\mu = \frac{-g_{EY}A^E_\mu + g_{EE}A^Y_\mu}{\sqrt{g^2_{EE}+g^2_{EY}}} \tag{1.88}$$

and the corresponding couplings are denoted by

$$g_y = \frac{g_{EE}g_{YY} - g_{EY}g_{YE}}{\sqrt{g^2_{EE}+g^2_{EY}}}, \quad g_E = \sqrt{g^2_{EE}+g^2_{EY}}, \quad g' = \frac{g_{YE}g_{EE} + g_{EY}g_{YY}}{\sqrt{g^2_{EE}+g^2_{EY}}}\,. \tag{1.89}$$

Note that the couplings' rotations are corresponding to the fields rotations and thus the transformations (1.88) will not reintroduce the kinetic mixing term [56]. It is sometimes convenient to introduce the effective charge e_k to rewrite the term $g_E Y^E_k + g' Y^Y_k$ as

$$g_E e_k \equiv g_E Y^E_k + g' Y^Y_k\,. \tag{1.90}$$

The third transformation is to make the gauge eigenstates to mass eigenstates where similar to the SM case $B_\mu, W^3_\mu \to A_\mu, Z_\mu$, we now have three fields $B_\mu, W^3_\mu, E_\mu \to A_\mu, Z_\mu, Z'_\mu$. To show explicitly, the fields transformations are given by

$$\begin{pmatrix} B_\mu \\ W^3_\mu \\ E_\mu \end{pmatrix} = \begin{pmatrix} c & -sc' & ss' \\ s & cc' & -cs' \\ 0 & s' & c' \end{pmatrix} \begin{pmatrix} A_\mu \\ Z^0_\mu \\ Z'_\mu \end{pmatrix}$$

where $c \equiv \cos\theta_W, s \equiv \sin\theta_W$ are the weinberg angles defined by $\tan\theta_W \equiv g_y/g_2$ and $c' \equiv \cos\theta', s' \equiv \sin\theta'$ are the new rotations, where

$$\tan 2\theta' = \frac{2\left(-\frac{1}{2}\sqrt{g_y^2+g_2^2}\,g_E e_H v_H^2\right)}{\frac{1}{4}\left(g_y^2+g_2^2\right)v_H^2 - g_E^2\left(e_H^2 v_H^2 + e_S^2 v_S^2\right)}\,. \tag{1.91}$$

The interaction term of the fermion ψ_f with the gauge fields Z^0_μ and Z'_μ is

$$L_{\text{int}} = -J^\mu_{Z^0} Z^0_\mu - J'^\mu_Z Z'_\mu\,, \tag{1.92}$$

where the currents have the form

$$\begin{aligned} J^\mu_{Z^0} &= \sum_{\text{f}=\nu,\text{e,u,d}} \left[\frac{e}{sc}\left(T^3_f - s^2 Q_f\right)c' + e_f g_E s'\right]\bar\psi_f\gamma^\mu P_L\psi_f \\ &\quad + \sum_{\text{f}=\nu,\text{e,u,d}} \left[\frac{e}{sc}\left(-s^2 Q_f\right)c' - e_{f^c} g_E s'\right]\bar\psi_f\gamma^\mu P_R\psi_f \\ J^\mu_{Z'} &= \sum_{\text{f}=\nu,\text{e,u,d}} \left[-\frac{e}{sc}\left(T^3_f - s^2 Q_f\right)s' + e_f g_E c'\right]\bar\psi_f\gamma^\mu P_L\psi_f \\ &\quad + \sum_{\text{f}=\nu,\text{e,u,d}} \left[-\frac{e}{sc}\left(-s^2 Q_f\right)s' - e_{f^c} g_E c'\right]\bar\psi_f\gamma^\mu P_R\psi_f\,. \end{aligned} \tag{1.93}$$

It is interesting to note that in the limiting case where $M_{Z'} \gg M_{Z^0}$, we have $\sin\theta' \ll 1$ and $\cos\theta' \sim 1$. The above currents (1.93) can be then greatly simplified to

$$\begin{aligned} J^{\mu}_{Z^0} &= \sum_{\text{f=}\nu\text{,e,u,d}} \left[\frac{e}{sc}\left(T^3_f - s^2 Q_f\right)\right] \bar{\psi}_f \gamma^\mu P_L \psi_f + \sum_{\text{f=}\nu\text{,e,u,d}} \left[\frac{e}{sc}\left(-s^2 Q_f\right)\right] \bar{\psi}_f \gamma^\mu P_R \psi_f \\ J^{\mu}_{Z'} &= \sum_{\text{f=}\nu\text{,e,u,d}} \left(e_f g_E\right) \bar{\psi}_f \gamma^\mu P_L \psi_f + \sum_{\text{f=}\nu\text{,e,u,d}} \left(-e_{f^c} g_E\right) \bar{\psi}_f \gamma^\mu P_R \psi_f \,. \end{aligned} \tag{1.94}$$

For non-SM fermions, the charge assignments of T^3_f and Q_f depend on detailed model building $U(1)_{B-xL}$ where x is a parameter constrained by anomaly cancellation. It should be noted that conventional $U(1)'$ models are constrained very strongly by the collider dilepton decay searches. To avoid this collider constraint, versions of leptophobic models have been proposed [58].

1.6 LHC Anomaly and Diphoton Excess

The LHC anomaly provides another important motivation to the beyond SM hidden sector. In this section, I will focus on only one of the recent anomalies: the LHC diphoton excess and provide a brief summary of the existing models to address this anomaly.

The ATLAS and CMS collaborations have recently reported a possible diphoton excess at around 750 GeV at 3.9σ and 2.6σ respectively [59, 60]. The ATLAS collaboration provides a best fit total decay width at around 45 GeV (large decay width) while the CMS collaboration prefers a narrow width. The cross section for the production rate times the branching ratio is roughly around $5 - 10$ fb for both collaborations.

It is important to note that there has to be new physics to address the diphoton excess. Since there is no clear hints of excesses in other SM channels, LHC run 1 (with pp collisions at energy $\sqrt{s} = 8$ TeV) provides strong upper bound of $\Gamma\left(S \to f\right)/\Gamma\left(S \to \gamma\gamma\right)$ (see table 1.1) where S represents the resonance and f represents the final states ($\gamma\gamma, ZZ, Z\gamma, W^+W^-, hh$, etc.). Thus, the resonance can't be just another heavy Higgs since it will directly couple to the SM particles, which provides a way too large branching ratio to the SM particles. We may be able to categorize the candidates of the resonance according to the total decay width. For large deacy width (45 GeV), the strongly coupled models will be the ideal candidates such as dilaton

[61], techni-pions [62], techni-eta [63]. For narrow decay width as CMS collaboration suggested, we could have various hidden sector models such as the famous universal model [61, 64].

1.6.1 Universal Model

In this model, we add one more scalar singlet S (real or complex) to the SM as the resonance. Following the above discussion we understand the singlet cannot directly couple to the SM (do not have SM charges) since it will provide large branching ratio to the SM particles and violate the experimental bounds. Thus, we need extra particles to mediate the processes $\Gamma(gg \to S)$ (the gluon gluon fusion) and $\Gamma(S \to \gamma\gamma)$ (the diphoton decay process) through the triangle loop diagram (see Fig. 1.2). It can be either vector like fermions or complex scalars [64] and the detailed charge assignments will be dependent on the representations which can be determined by the ratio of the branching ratios of the SM particle final states for the resonance S such as $\mathrm{Br}(\mathrm{S} \to \mathrm{Z}\gamma)/\mathrm{Br}(\mathrm{S} \to \gamma\gamma)$, $\mathrm{Br}(\mathrm{S} \to \mathrm{W}^+\mathrm{W}^-)/\mathrm{Br}(\mathrm{S} \to \gamma\gamma)$, etc [64, 66]. Thus, if the accurate branching ratios are provided by the LHC run 2 (with pp collisions at energy $\sqrt{s} = 13\,\mathrm{TeV}$), the representations will be known for the universal model. The Lagrangian for the complex scalar resonance with vector-like fermion F has the form [65]:

$$L = \frac{1}{2}\partial_\mu H^\dagger \partial^\mu H + \frac{1}{2}\partial_\mu S^\dagger \partial^\mu S - \lambda_2 |S|^2 H^\dagger H - \lambda_3 |S|^4 - \lambda_1 \left(H^\dagger H\right)^2 + i\bar{F}\gamma^\mu D_\mu F - \left(y_S \bar{F}_L F_R S + \mathrm{h.c.}\right) \tag{1.95}$$

where F transforms as $(R_C, R_W)_{Y_F}$, H is the (complex doublet) Higgs field and S is the complex singlet field. Note that the symmetry breaking pattern of the system will directly influence the diphoton excess. If there is symmetry breaking in both the Higgs sector and singlet sector, the branching ratios to the SM particles could be greatly increased in two ways. Firstly, the Higgs particle will mix with the singlet particle and if the mixing angle is not small enough, the branching ratios to the SM particles will be greatly increased through the Higgs decays. Secondly, when singlet field obtains a vacuum expectation value, the decay channel $S \to HH$ is open, which will also increase the branching ratios to the SM. Using the branching ratio bounds of Ref. [61] (given in Table 1.1), we find corresponding bounds on the Higgs portal interaction and the mixing angle ($\sin\theta \leq 0.16$ for W^+W^- channel using the model shown by eq. (1.95)

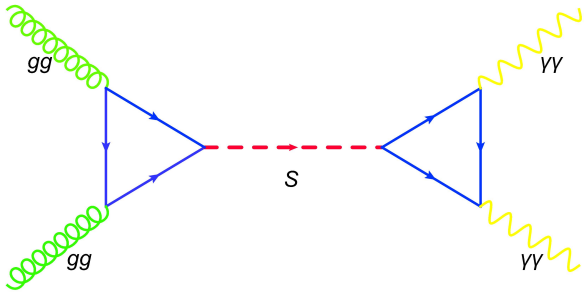

Figure 1.2: This figure shows the weakly coupled model for LHC diphoton excess. Here we have assumed the diphoton excess is realized through the process $gg \to S \to \gamma\gamma$ where g represents the gluon and two vector-like fermion F loops are required at both the production and decay process.

and please see Chapter 4 for more detail).

If the symmetry breaking only occurs in the Higgs sector, there is no mixing between the singlet field and Higgs field. In this case, the above two ways to increase the branching ratios to the SM particles will be prevented. When this case is considered in the conformal scenario, it becomes more interesting. If the field system possesses exact conformal symmetry in both the Higgs sector and hidden sector, there exist two upper bounds for the singlet mass which is much smaller than 750 GeV (see Chapter 4 for more detail). Thus, to address the diphoton excess, we have to introduce a bare mass term for the singlet to increase its mass and the conformal symmetry will be softly broken in the hidden sector. In addition, if the bare mass term is small, it may require a very large Higgs portal interaction in the conformal scenario to provide such a large singlet mass. A very large Higgs portal coupling will lead to a very large singlet annihilation cross section and results in very tiny dark matter abundance. In such case, we can only associate singlet with either dark matter candidate or 750 GeV diphoton resonance in conformal scenario but not both. In a non-conformal scenario, the case is very different since we can just input by hand a larger bare mass term and no large Higgs portal coupling is needed. For more detail, see Chapter 4.

In the following, I will show this universal model can easily provide the diphoton rate at the order of fb. For two body initial state, to leading order, the rate of the resonance S production

and decay to diphoton can be written as [64]

$$R_{\gamma\gamma} \sim \frac{\Gamma_{\rm in}}{m_S}\frac{\Gamma_{\gamma\gamma}}{\Gamma_{\gamma\gamma}+\Gamma_{\rm other}}\frac{dL}{dm_S^2} \tag{1.96}$$

where $\Gamma_{\rm in}$, $\Gamma_{\gamma\gamma}$, $\Gamma_{\rm other}$ and $\frac{dL}{dm_S^2}$ correspond to the partial width of resonance S to initial states, partial width to diphotons, total width from any other decay and parton luminosity function respectively. If we assume the resonance is produced through the gluon gluon fusion ($gg \to S$), and we obtain $\Gamma_{\rm in} = \Gamma_{gg}$. By assuming that there are no other modes for resonance S to decay to except for $\gamma\gamma$ and gg, we obtain

$$R_{\gamma\gamma} \sim \frac{\Gamma_{\rm gg}}{m_S}\frac{\Gamma_{\gamma\gamma}}{\Gamma_{\gamma\gamma}+\Gamma_{\rm gg}}\frac{dL}{dm_S^2} \sim \frac{\Gamma_{\gamma\gamma}}{m_S}\frac{dL}{dm_S^2} \sim \frac{10^{-3}{\rm GeV}}{750{\rm GeV}} \times 10^6{\rm fb} \sim 1{\rm fb}\,, \tag{1.97}$$

where in the second steps we have used $\Gamma_{\rm gg} \gg \Gamma_{\gamma\gamma}$. We find in this narrow width (universal model) case, the typical decay width to diphoton $\Gamma_{\gamma\gamma}$ is at the order of MeV scale and the diphoton excesses can be easily realized at the order of fb. We can go one step further to show the implications of $\Gamma_{\gamma\gamma} \sim$ MeV. The expression for the diphoton decay width is [64, 67]

$$\Gamma_{\gamma\gamma} = \frac{\alpha^2 N_c^2 N_F^2}{1024\pi^3}\frac{m_S^3}{m_F^2}\left|2y_S\left(\sum_i Q_i^2\right)A_{1/2}\left(\frac{m_S^2}{4m_f^2}\right)\right|^2\,, \tag{1.98}$$

where $A_{1/2} \simeq 4/3$ for $m_F \geq m_S/2$. If we choose F to be $(R_C, R_W)_{Y_F} = (3,2)_{7/6}$ as one of the charge assignments of the vector fermion where the electric charge $Q_1 = 1/2 + 7/6, Q_2 = -1/2 + 7/6$, $N_f = 1$, $\alpha \sim 1/128$, $y_S \sim 1$ and $m_F \sim 1$TeV, we obtain $\Gamma_{\gamma\gamma} \sim 0.58\,{\rm MeV}$. Thus, we have shown that in order to address the diphoton excess in this universal model, the scalar-vector fermion coupling y_S is at the order of $O(1)$.

To study the ratios of the branching ratios, it requires expressions for the decay widths of other channels. In the following, I will list two most important expressions. The expression for the decay widths to di-gluons and γZ are given by [64, 68]

$$\begin{aligned}
\Gamma_{gg} &= \frac{\alpha_s^2 N_F^2}{512\pi^3}\frac{m_S^3}{m_F^2}\left|2y_S A_{1/2}\left(\frac{m_S^2}{4m_f^2}\right)\right|^2 \\
\Gamma_{\gamma Z} &= \frac{\alpha^2 N_c^2 N_F^2}{256\pi^3}\frac{m_S^3}{m_F^2}\left|2y_S\left(\sum_i Q_i\frac{T_i^3 - Q_i\sin^2\theta_W}{\cos\theta_W\sin\theta_W}\right)A_{1/2}\left(\frac{m_S^2}{4m_f^2}\right)\right|^2\,.
\end{aligned} \tag{1.99}$$

It is useful to use the effective field theory notations. If we only consider the loop-induced decays, the effective lagrangian which describes the decay channels of S to the SM gauge bosons

is written (in terms of gauge eigenstates) as [68]:

$$L \supset c_G \frac{\alpha_s}{12\pi m_S} S\, G^a_{\mu\nu} G^{a,\mu\nu} + \frac{\alpha}{4\pi m_S} S\, \left(c_W W^i_{\mu\nu} W^{i,\mu\nu} + c_B B_{\mu\nu} B^{\mu\nu}\right) . \tag{1.100}$$

We can also rewrite the above expression in terms of the mass eigenstates as [68]

$$L \supset \frac{\alpha}{2\pi m_S} S\, \left(\frac{c_{\gamma\gamma}}{2} F_{\mu\nu} F^{\mu\nu} + c_{z\gamma} Z_{\mu\nu} F^{\mu\nu} + \frac{c_{zz}}{2} Z_{\mu\nu} Z^{\mu\nu} + c_{ww} W^+_{\mu\nu} W^{-\mu\nu}\right) , \tag{1.101}$$

where

$$\begin{aligned} c_{ww} &= c_W \ , & c_{\gamma\gamma} &= c_B \cos^2\theta_W + c_W \sin^2\theta_W \ , \\ c_{zz} &= c_B \sin^2\theta_W + c_W \cos^2\theta_W \ , & c_{z\gamma} &= (c_W - c_B) \sin\theta_W \cos\theta_W \ . \end{aligned} \tag{1.102}$$

In this universal model with vector like fermion, the above effective coupling $c_G, c_{\gamma\gamma}, c_{Z\gamma}$ can be written explicitly as [68]

$$\begin{aligned} c_G &= \sum_i y_S \frac{m_S}{M_F} \ , \\ c_{\gamma\gamma} &= \frac{2}{3} \sum_i y_S \frac{m_S}{M_F}\ N_c Q_i^2 \ , \\ c_{Z\gamma} &= \frac{2}{3} \sum_i y_S \frac{m_S}{M_F}\ N_c Q_i \frac{T_i^3 - Q_i \sin^2\theta_W}{\cos\theta_W \sin\theta_W} \ , \end{aligned} \tag{1.103}$$

where combining Eq. (1.102), we can obtain the expressions for c_W and c_B. By using Eq. (1.103), the above expressions for the decay widths to di-gluons and γZ can be written as

$$\Gamma(S \to \gamma\gamma) = \frac{m_S}{4\pi} \left(\frac{\alpha\, c_{\gamma\gamma}}{4\pi}\right)^2 \quad , \quad \Gamma(S \to gg) = \frac{2 m_S}{\pi} \left(\frac{\alpha_s c_G}{12\pi}\right)^2 , \tag{1.104}$$

where replacing $c_{\gamma\gamma}$ to $c_{Z\gamma}$ or c_{WW}, we obtain $\Gamma(S \to Z\gamma)$ and $\Gamma(S \to WW)$.

final	σ at $\sqrt{s} = 8\,\text{TeV}$			implied bound on
state f	observed	expected	ref.	$\Gamma(S \to f)/\Gamma(S \to \gamma\gamma)_{\text{obs}}$
$\gamma\gamma$	< 1.5 fb	< 1.1 fb	[69, 70]	$< 0.8\ (r/5)$
$e^+e^-, \mu^+\mu^-$	< 1.2 fb	< 1.2 fb	[71]	$< 0.6\ (r/5)$
$\tau^+\tau^-$	< 12 fb	< 15 fb	[72]	$< 6\ (r/5)$
$Z\gamma$	< 11 fb	< 11 fb	[73]	$< 6\ (r/5)$
ZZ	< 12 fb	< 20 fb	[74]	$< 6\ (r/5)$
Zh	< 19 fb	< 28 fb	[75]	$< 10\ (r/5)$
hh	< 39 fb	< 42 fb	[76]	$< 20\ (r/5)$
W^+W^-	< 40 fb	< 70 fb	[77, 78]	$< 20\ (r/5)$
$t\bar{t}$	< 450 fb	< 600 fb	[79]	$< 300\ (r/5)$
invisible	< 0.8 pb	-	[80]	$< 400\ (r/5)$
$b\bar{b}$	$\lesssim 1\,\text{pb}$	$\lesssim 1\,\text{pb}$	[81]	$< 500\ (r/5)$
jj	$\lesssim 2.5$ pb	-	[83]	$< 1300\ (r/5)$

Table 1.1: This table is adapted from [61]. Upper bounds of $\Gamma(S \to f)/\Gamma(S \to \gamma\gamma)$ at 95% confidence level at LHC 8 are provided, where the final states f are produced through a resonance S with mass $M_S = 750\,\text{GeV}$ and width $\Gamma/M_S \sim 0.06$. r is defined as $r = \sigma_{13\,\text{TeV}}/\sigma_{8\,\text{TeV}}$ and for gluon-gluon fusion, we have $r = \sigma_{13\,\text{TeV}}/\sigma_{8\,\text{TeV}} \sim 5$.

1.7 Effective Potential

1.7.1 From Effective Action to Effective Potential

In order to develop the mathematical structure of the effective potential [84], we first introduce the effective action in this section. In the next section, I will describe the physical meaning of the effective potential as the energy density of the ground state. Since the ground state of the field system is the vacuum, in this way, we can use effective potential to determine the vacuum structure of the quantum field system. The following is developed according to [84].

The connected generating functional, $W(J)$, is defined in terms of the transition amplitude from the vacuum state in the far past to the vacuum state in the far future, in the presence of

the source $J(x)$,

$$e^{iW(J)} = \left\langle 0^+ | 0^- \right\rangle_J \ . \tag{1.105}$$

We can expand W in a functional Taylor series

$$W = \sum_n \frac{1}{n!} \int d^4x_1 \cdots d^4x_n G^{(n)}\left(x_1 \cdots x_n\right) J\left(x_1\right) \cdots J\left(x_n\right) \ . \tag{1.106}$$

The successive coefficients $G^{(n)}\left(x_1 \cdots x_n\right)$ in the series are the connected Green's functions which represent the sum of all connected Feynman diagrams with n external lines. The effective action $\Gamma\left(\phi_c\right)$, is defined by a functional Legendre transformation:

$$\Gamma\left(\phi_c\right) = W\left(J\right) - \int d^4x J\left(x\right) \phi_c\left(x\right) \ , \tag{1.107}$$

where ϕ_c represents the classical field defined by

$$\phi_c\left(x\right) = \frac{\delta W}{\delta J\left(x\right)} = \left[\frac{\left\langle 0^+ \left| \phi\left(x\right) \right| 0^- \right\rangle}{\left\langle 0^+ | 0^- \right\rangle}\right]_J \ . \tag{1.108}$$

The effective action $\Gamma\left(\phi_c\right)$ in fact is the generating functional of the one-particle irreducible (1PI) Green functions. From the definition of $\Gamma\left(\phi_c\right)$ in Eq. (1.107), it follows directly that

$$\begin{aligned} \frac{\delta\Gamma}{\delta\phi_c\left(x\right)} &= \frac{\delta W\left[J\right]}{\delta\phi_c\left(x\right)} - \int d^4y \frac{\delta J\left(y\right)}{\delta\phi_c\left(x\right)} \phi_c\left(y\right) - J\left(x\right) \\ &= \int d^4y \frac{\delta W\left[J\right]}{\delta J\left(y\right)} \frac{\delta J\left(y\right)}{\delta\phi_c\left(x\right)} - \int d^4y \frac{\delta J\left(y\right)}{\delta\phi_c\left(x\right)} \phi_c\left(y\right) - J\left(x\right) \\ &= -J\left(x\right) \ . \end{aligned} \tag{1.109}$$

Comparing Eq. (1.108) with Eq. (1.109), we find ϕ_c plays the same role in the generating functional $\Gamma\left(\phi_c\right)$ as the source J in the generating functional $W(J)$. The effective action can also be expanded in a manner similar to that of (1.106), but with ϕ_c rather than the source J.

$$\Gamma\left(\phi_c\right) = \sum_n \frac{1}{n!} \int d^4x_1 \cdots d^4x_n \Gamma^{(n)}\left(x_1 \cdots x_n\right) \phi_c\left(x_1\right) \cdots \phi_c\left(x_n\right) \ . \tag{1.110}$$

Here the $\Gamma^{(n)}$ is the sum of all 1PI Feynman diagrams with n external lines and is defined as

$$\Gamma^{(n)}\left(x_1 \cdots x_n\right) = \left.\frac{\delta^n\Gamma}{\delta\phi_c\left(x_1\right) \cdots \delta\phi_c\left(x_n\right)}\right|_{\phi_c=0} \ . \tag{1.111}$$

However, the above expressions (1.110), (1.111) are only valid when the symmetry of the system is unbroken [32]. In the system with spontaneous symmetry breaking where $\phi_c(x,0) \equiv v \neq 0$, instead of expression (1.110), we have the following one:

$$\Gamma(\phi_c) = \sum_n \frac{1}{n!} \int d^4x_1 \cdots d^4x_n \Gamma_v^{(n)}(x_1 \cdots x_n) \tilde{\phi}_c(x_1) \cdots \tilde{\phi}_c(x_n) \ , \tag{1.112}$$

where $\tilde{\phi}_c(x) = \phi_c(x) - v$ and v is the vacuum expectation value (VEV). We can expand $\Gamma(\phi_c)$ in terms of the field $\phi_c(x)$ about a space-independent constant ϕ_0 which is in fact the VEV. Using

$$\phi_c(x) = \phi_0 + \tilde{\phi}_c(x) \ , \tag{1.113}$$

we obtain

$$\Gamma(\phi_c) = \Gamma(\phi_0) + \int d^4x \frac{\delta\Gamma}{\delta\phi_c(x)}\bigg|_{\phi_c=\phi_0} \tilde{\phi}_c(x) + \frac{1}{2}\int d^4x d^4y \frac{\delta^2\Gamma}{\delta\phi_c(x)\,\delta\phi_c(y)}\bigg|_{\phi_c=\phi_0} \tilde{\phi}_c(x)\,\tilde{\phi}_c(y) + \cdots \tag{1.114}$$

Instead of expanding in powers of $\tilde{\phi}_c$, we can also expand Γ in the following way (the derivative expansion):

$$\Gamma(\phi_c) = \int d^4x \left[-V(\phi_c) + \frac{1}{2}(\partial_\mu \phi_c)^2 Z(\phi_c) + \cdots \right] . \tag{1.115}$$

In fact, this equation gives the definition of the effective potential $V(\phi_c)$ as the sum of all the 1PI Green functions with the external lines carrying zero momentum. Now I want to show explicitly the relationship between the effective potential and the n point 1PI Green function. We first write $\Gamma^{(n)}$ in momentum space

$$\Gamma^{(n)}(x_1 \cdots \ x_n) = \int \frac{d^4k_1}{(2\pi)^4} \cdots \frac{d^4k_n}{(2\pi)^4} (2\pi)^4 \delta(k_1 + \cdots k_n) \times e^{i(k_1 \cdot x_1 + \cdots k_n \cdot x_n)} \Gamma^{(n)}(k_1 \cdots k_n) \ . \tag{1.116}$$

Input the above equation into (1.110) and expand in powers of k_i, we get:

$$\begin{aligned} \Gamma(\phi_c) &= \sum_n \frac{1}{n!} \int d^4x_1 \cdots d^4x_n \int \frac{d^4k_1}{(2\pi)^4} \cdots \frac{d^4k_n}{(2\pi)^4} \times \int d^4x e^{i(k_1 + \cdots k_n)\cdot x} e^{i(k_1 \cdot x_1 + \cdots k_n \cdot x_n)} \\ &\quad \times \left[\Gamma^{(n)}(0, \cdots 0)\, \phi_c(x_1) \cdots \phi_c(x_n) + \cdots \right] \\ &= \int d^4x \sum_n \frac{1}{n!} \left\{ \Gamma^{(n)}(0, \cdots 0) \left[\phi_c(x)\right]^n + \cdots \right\} . \end{aligned} \tag{1.117}$$

Comparing (1.115) with (1.117) we see that the nth derivative of $V(\phi_c)$ is just the sum of all IPI diagrams with n external lines carrying zero momenta

$$V(\phi_c) = -\sum_n \frac{1}{n!}\Gamma^{(n)}(0,\cdots 0)\left[\phi_c(x)\right]^n . \tag{1.118}$$

1.7.2 Physics Interpretation of the Effective Potential

In the previous section, we have shown the mathematical structure of the effective potential. In this section, I will explain its physical meaning following [32]. Let us consider a source J independent of t. The transition amplitude is defined as:

$$Z(J) = N\left\langle \phi_f(\mathbf{x}) \left| e^{-iH(J)\left(t_f - t_i\right)} \right| \phi_i(\mathbf{x}) \right\rangle , \tag{1.119}$$

where $H(J)$ is the Hamiltonian corresponding to the Lagrangian density:

$$\mathcal{L}(J) = \mathcal{L} + J(x)\phi(x) . \tag{1.120}$$

The normalization factor N is chosen in such a way that makes $Z(0) = 1$. We can write out N explicitly and input (1.119) to obtain:

$$Z(J) = \frac{\left\langle \phi_f(\mathbf{x}) \left| e^{-iH(J)\left(t_f - t_i\right)} \right| \phi_i(\mathbf{x}) \right\rangle}{\left\langle \phi_f(\mathbf{x}) \left| e^{-iH\left(t_f - t_i\right)} \right| \phi_i(\mathbf{x}) \right\rangle} . \tag{1.121}$$

Here the H is the Hamiltonian without source term. The relationship between H and $H(J)$ is given as follows:

$$H(J) = H - \int d^3x J(\mathbf{x})\phi(x) , \tag{1.122}$$

If we expand the transition amplitude in a complete set of energy eigenstates,

$$H(J)\left|n;J\right\rangle = E_n(J)\left|n;J\right\rangle , \tag{1.123}$$

then

$$Z(J) = \frac{\sum_n exp\left(-iE_n(J)T\right)\left\langle \phi_f(\mathbf{x})\left|n;J\right\rangle\left\langle n;J\right|\phi_i(\mathbf{x})\right\rangle}{\sum_n exp\left(-iE_nT\right)\left\langle \phi_f(\mathbf{x})\left|n\right\rangle\left\langle n\right|\phi_i(\mathbf{x})\right\rangle} \qquad , \qquad T = t_f - t_i \tag{1.124}$$

where

$$|n\rangle \equiv |n, J\rangle|_{J=0} \qquad , \qquad E_n \equiv E_n(J)|_{J=0} . \tag{1.125}$$

With $T \to \infty$, the strong oscillations damp the amplitude, and therefore only the leading term in this expression which corresponds to the lowest energy state is dominant:

$$Z(J) \simeq \exp\left(-i\left(E_0(J) - E_0\right)T\right) \frac{\langle \phi_f(\mathbf{x}) |0; J\rangle \langle 0; J|\phi_i(\mathbf{x})\rangle}{\langle \phi_f(\mathbf{x}) |0\rangle \langle 0|\phi_i(\mathbf{x})\rangle} . \tag{1.126}$$

Since $Z(J) = \exp(iW(J))$, then the above equation implies that, as $T \to \infty$,

$$W(J) = \left(E_0 - E_0(J)\right)T . \tag{1.127}$$

If we choose $E_0 = 0$ as a reference point, we get

$$W(J) = -E_0(J)\,T , \tag{1.128}$$

where $-W(J)/T$ is the energy of the ground state of the Hamiltonian with a source term. By using Eq. (1.122) we get:

$$-W(J) = \langle 0; J|H|0; J\rangle T - \int d^4x J(\mathbf{x}) \langle 0; J|\phi(x)|0; J\rangle . \tag{1.129}$$

Comparing with the definition of the effective action

$$\Gamma(\phi_c) = W(J) - \int d^4x J(x)\,\phi_c(x) , \tag{1.130}$$

we can find that:

$$\Gamma(\phi_c) = -\langle 0; J|H|0; J\rangle T . \tag{1.131}$$

In fact, here we should change a little bit the notation since after Legendre transformation in the definition of $\Gamma(\phi_c)$ the position of $J(\mathbf{x})$ is replaced by $\phi_c(\mathbf{x})$. So we should change the notation of the ground state:

$$|0; J\rangle \to |0; \phi_c\rangle , \tag{1.132}$$

where $\phi_c(\mathbf{x})$ is defined as:

$$\phi_c(\mathbf{x}) = \langle 0; J|\phi(x)|0; J\rangle . \tag{1.133}$$

After the replacement we get:

$$\Gamma(\phi_c) = -\langle 0; \phi_c | H | 0; \varphi_c \rangle T . \tag{1.134}$$

Here, it is easy to see the meaning of $-\frac{\Gamma(\phi_c)}{T}$ is the average energy of the ground state $|0; \phi_c\rangle$ which satisfies the constraint:

$$\phi_c(\mathbf{x}) = \langle 0; \phi_c | \phi(x) | 0; \phi_c \rangle . \tag{1.135}$$

With one more step, we can get the physical meaning of the effective potential. By using the equation (1.107), we find that for sources independent of x, i.e. when $\phi_c = \text{const.}$, the effective potential $V(\phi_c)$ is

$$V(\phi_c) = \langle 0; \phi_c | \mathcal{H} | 0; \phi_c \rangle . \tag{1.136}$$

Thus the effective potential is physically interpreted as the energy density of the ground state $|0; \phi_c\rangle$ with $\langle 0; \phi_c | \phi | 0; \phi_c \rangle = \phi_c$. Since the ground state in quantum field system is the vacuum, we can use effective potential as a tool to determine the vacuum structure.

Here, I want to make three comments. First, the value of ϕ_c which minimizes the effective potential yields information about spontaneous symmetry breaking. If the minimum occurs at $\phi_c \neq 0$, then all symmetries of $\mathcal{L}$ which do not leave ϕ_c invariant are broken [85]. From this view-point we can say that the structure of effective potential, i.e. where the minimum occurs, is the signal of spontaneous symmetry breaking. We can pick out one direction of the vacuum and then the symmetry breaks. Normally, in conventional EW symmetry breaking, it requires a mass term with minus sign in the effective potential to generate the "mexican hat shape" vacuum structure (see Fig. 1.1). However, this mass term seems artificial and provides one of the important motivations to develop the idea of radiative symmetry breaking to dynamically generate the mass term from radiative (quantum) corrections. Secondly, in the expansion of effective action (1.115), we assumed that the ϕ_c which the effective potential depends on is translationally invariant. This assumption is in fact the reason that the effective potential can be related to the energy of the ground state since the Hamiltonian will become a minimum when the field is constant (i.e. no kinetic energy). Another point we should mention is that the above proof is not the only way to show the physical idea of the effective potential. In fact, we can use variational methods to show the same result [85].

1.7.3 Computation of the Effective Potential

Since the effective potential is a quantum quantity rather than classical, we should see different orders of quantum corrections to it. Here, the different orders of quantum corrections in fact correspond to different number of loops. We normally call the perturbative calculation of effective potential the loop expansion. In the following, I will show the basic formulation of the loop expansion of the effective potential following the pioneering work [87]. We will first find a perturbative expansion for the generating functional Z and then take the logarithm to obtain the generating functional W. Finally, we take the Legendre transformation to obtain Γ. Since we will use renormalized perturbation theory, it is convenient to split the Lagrangian into a piece depending on renormalized parameters and one containing the counterterms $\delta\mathcal{L}$:

$$\mathcal{L} = \mathcal{L}_1 + \delta\mathcal{L}\,. \tag{1.137}$$

Since the generating functional Z is dependent on the source J while Γ is dependent on ϕ_c, we need to find one relation between J and ϕ_c in order to transfer J into ϕ_c. In fact, this equation is easy to find at lowest order and it is just the classical field equation

$$\left.\frac{\delta\mathcal{L}}{\delta\phi}\right|_{\phi=\phi_c} + J\left(x\right) = 0\,. \tag{1.138}$$

Let us define $J_1\left(x\right)$ to be whatever function satisfies the above equation exactly; when $\mathcal{L} = \mathcal{L}_1$:

$$\left.\frac{\delta\mathcal{L}_1}{\delta\phi}\right|_{\phi=\phi_c} + J_1\left(x\right) = 0\,. \tag{1.139}$$

We will use this classical field equation to eliminate the first order term in the expansion of Z and then the lowest order quantum correction is always second order (or quadratic). We will think of the difference between J and J_1 as a counterterm, analogous to $\delta\mathcal{L}$, and thus we write

$$J\left(x\right) = J_1\left(x\right) + \delta J\left(x\right)\,, \tag{1.140}$$

where δJ is determined order by order in perturbation theory. By using the above notations, we can write:

$$\begin{aligned} Z\left[J\right] = e^{-iW[J]} &= \int \mathcal{D}\phi \exp\left[i\int d^4x\left(\mathcal{L}\left[\phi\right] + J\phi\right)\right] \\ &= \int \mathcal{D}\phi\, e^{i\int d^4x(\mathcal{L}_1[\phi]+J_1\phi)} e^{i\int d^4x(\delta\mathcal{L}[\phi]+\delta J\phi)}\,. \end{aligned} \tag{1.141}$$

We focus on the first exponential and come back to the counterterm part later. We do the Taylor expansion of the first exponential at the point ϕ_c by replacing $\phi(x) = \phi_c + \eta(x)$. The exponent takes the form

$$\begin{aligned}\int d^4x \left(\mathcal{L}_1 + J_1\phi\right) = \int d^4x \left(\mathcal{L}_1\left[\phi_c\right] + J_1\phi_c\right) + \int d^4x\eta(x)\left(\frac{\delta\mathcal{L}}{\delta\phi} + J_1\right) \\ + \frac{1}{2}\int d^4xd^4y\eta(x)\eta(y)\frac{\delta^2\mathcal{L}_1}{\delta\phi(x)\delta\phi(x)} + \cdots \quad .\end{aligned} \tag{1.142}$$

Here, we only keep up to the second order in η. By using the equation (1.139), we can make the first order term vanish and then we obtain:

$$\int \mathcal{D}\eta \exp\left[i\left(\int\left(\mathcal{L}_1\left[\phi_c\right] + J_1\phi_c\right) + \frac{1}{2}\int \eta\frac{\delta^2\mathcal{L}_1}{\delta\phi\delta\phi}\eta\right)\right], \tag{1.143}$$

where we have changed the integral variable from $\phi(x)$ to $\eta(x)$. In Eq. (1.143), we find a pure Gaussian integral, which can be evaluated in terms of the functional determinant:

$$\begin{aligned}&\int \mathcal{D}\eta \exp\left[i\left(\int\left(\mathcal{L}_1\left[\phi_c\right] + J_1\phi_c\right) + \frac{1}{2}\int \eta\frac{\delta^2\mathcal{L}_1}{\delta\phi\delta\phi}\eta\right)\right] \\ &\quad = \exp\left[i\int\left(\mathcal{L}_1\left[\phi_c\right] + J_1\phi_c\right)\right] \times \left(\det\left[-\frac{\delta^2\mathcal{L}_1}{\delta\phi\delta\phi}\right]\right)^{-\frac{1}{2}} \quad .\end{aligned} \tag{1.144}$$

Now, we come back to the counterterm part which can be rewritten in the following way:

$$\delta\mathcal{L}\left[\phi\right] + \delta J\phi = \left(\delta\mathcal{L}\left[\phi_c\right] + \delta J\phi_c\right) + \left(\delta\mathcal{L}\left[\phi_c + \eta\right] - \delta\mathcal{L}\left[\phi_c\right] + \delta J\eta\right) . \tag{1.145}$$

It is convenient to do the above separation because the second part in fact corresponds to the counterterms higher than second order and can be neglected in our one-loop calculation. Thus, we only keep the first part of the counterterms. Combining Eq. (1.144) and Eq. (1.145), we obtain:

$$\begin{aligned}-iW\left[J\right] = i\int d^4x\left(\mathcal{L}_1\left[\phi_c\right] + J_1\phi_c\right) - \frac{1}{2}\log\det\left[-\frac{\delta^2\mathcal{L}_1}{\delta\phi\delta\phi}\right] \\ + i\int d^4x\left(\delta\mathcal{L}\left[\phi_c\right] + \delta J\phi_c\right) + \left(\text{connected diagrams}\right) ,\end{aligned} \tag{1.146}$$

where the connected diagrams represent the Feynman diagrams higher than one loop order including the higher order counterterms. Now, we take the Legendre transformation of $W\left[J\right]$ to find:

$$\Gamma\left[\phi_c\right] = \int d^4x\mathcal{L}_1\left[\phi_c\right] + \frac{i}{2}\log\det\left[-\frac{\delta^2\mathcal{L}_1}{\delta\phi\delta\phi}\right] + \int d^4x\delta\mathcal{L}\left[\phi_c\right] - i\cdot\left(\text{connected diagrams}\right) . \tag{1.147}$$

It is easy to find that the above equation has no explicit source dependence. Now, I want to show more detail in the diagrammatic correspondence with the calculation method we have developed above. To do so, we need to write out the Lagrangian a little bit more explicitly. We consider the Lagrangian of the following form:

$$\mathcal{L} = \frac{1}{2}\partial^{\mu}\varphi\partial_{\mu}\varphi - \left(\frac{1}{2}\mu^{2}\varphi^{2} + U_{0}\left(\varphi\right)\right) . \tag{1.148}$$

Then the second derivative of the Lagrangian is:

$$\frac{\delta^{2}\mathcal{L}_{1}}{\delta\varphi\delta\varphi} = -\partial^{\mu}\partial_{\mu} - \mu^{2} - U_{0}^{''}\left(\varphi_{c}\right) . \tag{1.149}$$

Thus, the one loop correction in the effective action is:

$$\begin{aligned}
\frac{i}{2}\log\det\left[-\frac{\delta^{2}\mathcal{L}_{1}}{\delta\varphi\delta\varphi}\right] &= \frac{i}{2}\log\det\left(\partial^{\mu}\partial_{\mu} + \mu^{2} + U_{0}^{''}\left(\varphi_{c}\right)\right) \\
&= \frac{i}{2}Tr\log\left(\partial^{\mu}\partial_{\mu} + \mu^{2} + U_{0}^{''}\left(\varphi_{c}\right)\right) \\
&= \frac{i}{2}\left(VT\right)\int\frac{d^{4}p}{\left(2\pi\right)^{4}}\log\left(-p^{2} + \mu^{2} + U_{0}^{''}\left(\varphi_{c}\right)\right) \\
&= \frac{i}{2}\left(VT\right)\int\frac{d^{4}p}{\left(2\pi\right)^{4}}\log\left(-p^{2} + \mu^{2}\right) - \frac{i}{2}\left(VT\right)\int\frac{d^{4}p}{\left(2\pi\right)^{4}}\sum_{n=1}^{\infty}\frac{1}{n}\left[\frac{U_{0}^{''}\left(\varphi_{c}\right)}{p^{2}-\mu^{2}}\right]^{n} ,
\end{aligned} \tag{1.150}$$

where in the last step we separate the one loop contributions into two terms and the reason will be clear shortly after. It is apparent that the one loop effective potential is:

$$\frac{i}{2}\int\frac{d^{4}p}{\left(2\pi\right)^{4}}\log\left(-p^{2} + \mu^{2}\right) - \frac{i}{2}\int\frac{d^{4}p}{\left(2\pi\right)^{4}}\sum_{n=1}^{\infty}\frac{1}{n}\left[\frac{U_{0}^{''}\left(\varphi_{c}\right)}{p^{2}-\mu^{2}}\right]^{n} . \tag{1.151}$$

For the first term, we can first do one Wick rotation and then integrate out the p_0, i.e.

$$\begin{aligned}
&\frac{i}{2}\int\frac{d^{4}p}{\left(2\pi\right)^{4}}\log\left(-p^{2} + \mu^{2}\right) \\
&= -\frac{1}{2}\int\frac{d^{4}p}{\left(2\pi\right)^{4}}\log\left(p^{2} + \mu^{2}\right) \qquad \text{after the wick rotation } \ \mathrm{p}_0 \to \mathrm{ip}_4 \ \text{ into Euclidean space} \\
&= -\frac{1}{2}\int\frac{d^{3}p}{\left(2\pi\right)^{3}}\left(\mathbf{p}^{2} + \mu^{2}\right) ,
\end{aligned} \tag{1.152}$$

where in the last step we have integrated over p_0 and $\mathbf{p}$ represents the momentum in three-dimensional space.

The physical meaning of this term is apparent. It is the zero point energy density of a free scalar field with the mass μ which can be removed by an appropriate vacuum energy density normalization. For the second term of Eq. (1.151). It's physical meaning is the sum of all the one loop diagrams which include the n propagators $\frac{i}{p^2-\mu^2}$ and n vertices $-iU_0''(\varphi_c)$. We find it is quite interesting that there exists an analytic function to represent the sum of all the one loop diagrams with zero momentum external lines.

To sum up, in this section, we have developed a method to calculate the one loop quantum correction to the effective potential and their correspondence to the Feynman diagrams.

1.7.4 Problem with the Loop Expansion of the Effective Potential

In this section I want to discuss problems that occur in the loop expansion. I will show the solution to the problem leads us to the renormalization group technique to improve the calculation [12, 91]. The loop expansion is in fact a perturbative expansion in powers of λ and $\log\frac{M^2(\varphi_c)}{\mu^2}$ with $M^2 = \frac{d^2V^{(0)}}{d\varphi_c^2}$ where μ is the renormalization scale. In general, effective potential with n loops will be in the form of $\left[\log\frac{M^2(\varphi_c)}{\mu^2}\right]^n$ since each loop will generate one more logarithm. Also, according to Feynman rules, each vertex will correspond to one coupling constant. Since one diagram with n loops will have $n+1$ vertices, in total the form of the potential at n loops order can be written as $\lambda^{n+1}\left[\log\frac{M^2(\varphi_c)}{\mu^2}\right]^n$. In this way, it is easy to see that the expansion is reliable only when λ and $\lambda\left[\log\frac{M^2(\varphi_c)}{\mu^2}\right]$ are both small enough. So the problem is we should not only make the coupling constant small, but we should also make the product of the coupling constant and the logarithm small. Thus, there is only a very small range of the scales which we can choose to make the product small enough to be a valid expansion.

Is there any other possibility that we can extend our effective region of the scale to do the expansion? The answer is yes. But we should first introduce another tool called the renormalization group. The renormalization group technique helps to cleverly rearrange the coupling constant and the logarithms into the form of the running coupling. Finally, only the running coupling will occur in the equation of the effective potential rather than the bare

coupling constant and the products with logarithms. Then, the condition under which it is reliable to do the expansion only depends on the size of the running coupling. In section 1.8.3 we will show that by introducing the running coupling, we can greatly extend our effective region of the expansion. But the whole mystery comes from the renormalization group. In the next section the renormalization group will be described in more detail.

1.8 Renormalization Group

Physics at different scales will have different kinds of phenomena and especially, these kinds of phenomena are decoupled between different scales, which means we can understand a limited range of scales of physical phenomena without having to understand everything at once. The renormalization group describes the change of our description of physics as we change the scale at which we probe nature.

In the following, we provide a brief discussion of Wilson's effective field theory approach to the renormalization group [88] (see also very nice review in e.g., [86, 92]). The key idea of the effective field theory is that if we are only interested in the low energy modes of the theory we can integrate out the high frequency modes to get an effective field theory which describes the low energy physics [88]. After integrating out the high frequency modes in the theory, the information of these high frequency modes does not disappear and will be encoded in the forms of the corrections of the parameters in the Lagrangian. The form of the correction terms can be divided into three categorizations according to the dimension of the operators: the relevant terms, the irrelevant terms and the marginal terms. The relevant and marginal terms are in exactly the same form as the terms in the original Lagrangian and the coefficients of the relevant terms grow from UV to IR while the irrelevant terms are greatly suppressed when the energy scale studied is much lower than the cut off. However, the characteristics (grow or decay) of the marginal operators normally depend on the higher order corrections. Moreover, the corrections of the parameters in the theory will be dependent on the interval of the scale which we integrated out. If we take the interval of the scale to be infinitesimally small, we will obtain continuous transformations (one for each parameter) about how the parameters evolve with the scale. For historical reasons, these continuous transformations of the parameters in the

theory are called renormalization group. In fact, we can even study how fast these parameters change with the scale. We can view the evolution of the parameters with the scale in the parameter space known as renormalization group flow. The renormalization group flow as a diagrammatic method is useful in presenting how the physics changes with the scale intuitively.

Note that the idea of renormalization group is consistent with the idea of renormalization. In the renormalization theory, we use the counterterms possessing the same forms as the terms in the original Lagrangian to absorb the high energy behaviour of the loop corrections. For renormalization group theory, the information of the high energy modes is organized into the corrections of the parameters in the original Lagrangian, which is actually equivalent to the case that counterterms absorbs the high energy behaviour. However, there is one key difference between the renormalization group theory and the renormalization theory. In the renormalization theory, we set the cut off Λ and absorb it into the counterterms in just one step, while in renormalization group theory, we deal with the cut off through successive integrations.

The Wilson approach provides us a deep insight and intuitive picture of the renormalization group. However, in some practical calculations it is not quite useful, especially when we want to connect the idea of renormalization group to the correlation functions which are directly related to the microscopic processes. In this case, we introduce another approach to the renormalization group called Callan's approach [89]. Both approaches are equivalent to each other but are represented in different ways. Compared with the Wilson's approach, Callan's approach emphasizes how the correlation functions of the system associated with different energy scales are connected to each other. In the next section I will show how to obtain Callan's equation.

1.8.1 Callan-Symanzik Equation

In this section, I will discuss the Callan-Symanzik equation in $\lambda\Phi^4$ theory according to [89, 90]. First, we note that differentiation of the unrenormalized Green's function with respect to the bare mass μ_0^2 is equivalent to an insertion of the composite operator $\Omega = \frac{1}{2}\Phi_0^2$ carrying zero momentum

$$\frac{\partial\Gamma^{(n)}\left(p_i\right)}{\partial\mu_0^2} = -i\Gamma^{(n)}_{\Phi^2}\left(0;p_i\right) , \tag{1.153}$$

where $\Gamma^{(n)}$ is the n points 1PI Green's function. In fact, the above formula is easy to understand since the derivative of the action with respect to the bare mass will bring down the term $\Omega = \frac{1}{2}\Phi_0^2$ in the Green function. The relations between the bare and renormalized (1PI) Green's functions are given by:

$$\begin{aligned} \Gamma_R^{(n)}\left(p_i;\lambda,\mu\right) &= Z_\Phi^{\frac{n}{2}}\Gamma^{(n)}\left(p_i;\lambda_0,\mu_0\right) \\ \Gamma_{\Phi^2 R}^{(n)}\left(p,p_i;\lambda,\mu\right) &= Z_{\Phi^2}^{-1}Z_\Phi^{\frac{n}{2}}\Gamma_{\Phi^2}^{(n)}\left(p,p_i;\lambda_0,\mu_0\right)\,, \end{aligned} \tag{1.154}$$

where we have considered the renormalization of composite operators through the factor Z_{Φ^2}. After substituting (1.154) into (1.153) and using the following relation:

$$\frac{\partial}{\partial\mu_0^2}\Gamma_R^{(n)}\left(p_i;\lambda,\mu\right) = \left[\frac{\partial\mu^2}{\partial\mu_0^2}\frac{\partial}{\partial\mu^2} + \frac{\partial\lambda}{\partial\mu_0^2}\frac{\partial}{\partial\lambda}\right]\Gamma_R^{(n)}\left(p_i;\lambda,\mu\right)\,, \tag{1.155}$$

we obtain the Callan-Symanzik equation in $\lambda\Phi^4$ theory

$$\left[\mu\frac{\partial}{\partial\mu} + \beta\frac{\partial}{\partial\lambda} - n\gamma\right]\Gamma_R^{(n)}\left(p_i;\lambda,\mu\right) = -i\mu^2\alpha\Gamma_{\Phi^2 R}^{n}\left(0,p_i;\lambda,\mu\right) \tag{1.156}$$

where α, β, and γ are dimensionless functions

$$\begin{aligned} \beta &= 2\mu^2\frac{\partial\lambda/\partial\mu_0^2}{\partial\mu^2/\partial\mu_0^2} \\ \gamma &= \mu^2\frac{\partial\log Z_\Phi/\partial\mu_0^2}{\partial\mu^2/\partial\mu_0^2} \\ \alpha &= \frac{\partial Z_{\Phi^2}/\partial\mu_0^2}{\partial\mu^2/\partial\mu_0^2}\,. \end{aligned} \tag{1.157}$$

The function α and γ are not independent to each other. We can easily see this by using the renormalization conditions for the two point Green's function:

$$\Gamma_R^{(2)}\left(0;\lambda,\mu\right) = i\mu^2 \qquad ; \qquad \Gamma_{\Phi^2 R}^{(2)}\left(0,0;\lambda,\mu\right) = 1\,. \tag{1.158}$$

Input the above renormalization conditions into (1.156), we obtain:

$$\alpha = 2\left(\gamma - 1\right)\,. \tag{1.159}$$

Since the renormalized quantities $\Gamma_R^{(n)}$ and $\Gamma_{\Phi^2 R}^{(2)}$ are both cut-off independent to all orders in λ, we expect that the functions α, β, and γ are also cut-off independent.

The Callan-Symanzik equation (1.156) can be generalized to involve several composite operators. If we denote the composite operators as $A, B, C \cdots$, the generalized Callan-Symanzik equation is written as

$$\left[\mu\frac{\partial}{\partial\mu}+\beta\frac{\partial}{\partial\lambda}-n\gamma+\gamma_{AB\cdots}\right]\left\{\Gamma^{(n)}_{AB\cdots}\left(p_i;\lambda,\mu\right)\right\}_R=-i\mu^2\alpha\left\{\Gamma^{n}_{\Phi^2 AB\cdots}\left(0,p_i;\lambda,\mu\right)\right\}_R\,. \quad (1.160)$$

1.8.2 The Asymptotic Solution of the Renormalization Group Equation

In this section, we will discuss the large-momentum asymptotic behaviour of the Green's function using the Callan-Symanzik equation. We will follow the excellent descriptions of this topic in [95]. Since we are interested in the large-momentum asymptotic behaviour of the Green's function, the right hand side of the Callan-Symanzik equation (1.156) can be reasonably dropped [94] following Weinberg's theorem [93] that we have $\Gamma^{(n)}_R >> \Gamma^{(n)}_{\Phi^2 R}$ to any finite order (we assume to all order) of λ in the deep Euclidean region ($\sigma\to\infty$). The asymptotic form of Callan-Symanzik equation (1.156) can be written as:

$$\left[\mu\frac{\partial}{\partial\mu}+\beta\left(\lambda\right)\frac{\partial}{\partial\lambda}-n\gamma\left(\lambda\right)\right]\Gamma^{(n)}_{as}\left(p_i,\lambda,\mu\right)=0\,, \quad (1.161)$$

where $\Gamma^{(n)}_{as}$ is the asymptotic form of $\Gamma^{(n)}_R$. Thus in the deep Euclidean region, a small change in the mass parameter (the $\mu\left(\partial/\partial\mu\right)$ term) can always be compensated for by an appropriate small change in the coupling (the $\beta\left(\partial/\partial\lambda\right)$ term) and an appropriate small rescaling of the fields the ($-n\gamma$ term) [95].

First we replace the change in the scale μ by the corresponding change in the rescaling parameter σ. From dimensional analysis we can write

$$\Gamma^{(n)}_{as}\left(p_i,\lambda,\mu\right)=\mu^{4-n}\Gamma^{(n)}_R\left(\frac{p_i}{\mu},\lambda\right)\,, \quad (1.162)$$

where $\Gamma^{(n)}_R\left(\frac{p_i}{\mu},\lambda\right)$ is a dimensionless quantity. We have used the Weinberg's theorem [93] that the 1PI Green's function $\Gamma^{(n)}_R$ grows in the deep Euclidean region ($\sigma\to\infty$) as σ^{4-n} times polynomials in $\ln\sigma$ to any finite order in the coupling λ. If we re-parametrize the p_i we can get:

$$\Gamma^{(n)}_{as}\left(\sigma p_i,\lambda,\mu\right)=\mu^{4-n}\Gamma^{(n)}_R\left(\frac{\sigma p_i}{\mu},\lambda\right)\,, \quad (1.163)$$

where $\Gamma_R^{(n)}$ satisfies

$$\left(\mu\frac{\partial}{\partial\mu}+\sigma\frac{\partial}{\partial\sigma}\right)\Gamma_R^{(n)}\left(\frac{\sigma p_i}{\mu},\lambda\right)\,. \tag{1.164}$$

We combine (1.163) and (1.164) to find

$$\left[\mu\frac{\partial}{\partial\mu}+\sigma\frac{\partial}{\partial\sigma}+(n-4)\right]\Gamma_{as}^{(n)}\left(\sigma p_i,\lambda,\mu\right)=0\,. \tag{1.165}$$

Comparing (1.161) and (1.165), we get:

$$\left[\sigma\frac{\partial}{\partial\sigma}-\beta\left(\lambda\right)\frac{\partial}{\partial\lambda}+n\gamma\left(\lambda\right)+(n-4)\right]\Gamma_{as}^{(n)}\left(\sigma p_i,\lambda,\mu\right)\,. \tag{1.166}$$

where $\mu\frac{\partial}{\partial\mu}$ has been replaced by $\sigma\frac{\partial}{\partial\sigma}$. This is the asymptotic form of the Callan-Symanzik equation with p re-parametrized.

Next, I will discuss the solutions of Eq. (1.166). We may first remove the non-derivative terms with the transformation:

$$\Gamma_{as}^{(n)}\left(\sigma p_i,\lambda,\mu\right)=\sigma^{4-n}\exp\left[n\int_0^{\lambda}\frac{\gamma\left(x\right)}{\beta\left(x\right)}dx\right]F^{(n)}\left(\sigma p_i,\lambda,\mu\right)\,. \tag{1.167}$$

Then, we can have the differential equation only with respect to $F^{(n)}\left(\sigma p_i,\lambda,\mu\right)$ and without the nonderivative terms:

$$\left[\sigma\frac{\partial}{\partial\sigma}-\beta\left(\lambda\right)\frac{\partial}{\partial\lambda}\right]F^{(n)}\left(\sigma p_i,\lambda,\mu\right)=0\,. \tag{1.168}$$

For convenience, define $t=\ln\sigma$ and the above equation can be transformed into:

$$\left[\frac{\partial}{\partial t}-\beta\left(\lambda\right)\frac{\partial}{\partial\lambda}\right]F^{(n)}\left(e^t p_i,\lambda,\mu\right)=0\,. \tag{1.169}$$

Now, we introduce the running coupling $\overline{\lambda}$ which will be shown to be the solution of the above equation. The running coupling is defined as:

$$\frac{d\overline{\lambda}\left(t,\lambda\right)}{dt}=\beta\left(\overline{\lambda}\right) \tag{1.170}$$

with the boundary condition $\overline{\lambda}\left(t=0,\lambda\right)=\lambda$. We first integrate the above equation with respect to t:

$$t=\int_{\lambda}^{\lambda(t,\lambda)}\frac{dx}{\beta\left(x\right)}\,, \tag{1.171}$$

and then differentiate both sides with respect to λ and get

$$0 = \frac{1}{\beta(\lambda)} \frac{d\overline{\lambda}}{d\lambda} - \frac{1}{\beta(\lambda)} . \tag{1.172}$$

The above expression (1.172) can be rearranged into a more familar form:

$$\left[\frac{\partial}{\partial t} - \beta(\lambda) \frac{\partial}{\partial \lambda} \right] \overline{\lambda}(t, \lambda) = 0 , \tag{1.173}$$

which becomes apparent that the running coupling is the solution to (1.169). Thus, the function $F^{(n)}(e^t p_i, \lambda, \mu)$ which depends on t and λ can be constructed to be dependent on a new function $\overline{\lambda}(t, \lambda)$ and the function $F^{(n)}(e^t p_i, \lambda, \mu)$ can be rewritten as:

$$F^{(n)}\left(e^t p_i, \lambda, \mu\right) = F^{(n)}\left(p_i, \overline{\lambda}(t, \lambda), \mu\right) . \tag{1.174}$$

Substituting Eq. (1.174) into Eq. (1.167), we obtain:

$$\Gamma^{(n)}_{as}(\sigma p_i, \lambda, \mu) = \sigma^{4-n} \exp\left[n \int_0^{\lambda} \frac{\gamma(x)}{\beta(x)} dx \right] F^{(n)}\left(p_i, \overline{\lambda}(t, \lambda), \mu\right) . \tag{1.175}$$

If we define the function

$$H\left(\overline{\lambda}\right) = \exp\left[n \int_0^{\overline{\lambda}} \frac{\gamma(x)}{\beta(x)} dx \right] , \tag{1.176}$$

we can simplify the equation (1.175) further to

$$\Gamma^{(n)}_{as}(\sigma p_i, \lambda, \mu) = \sigma^{4-n} \exp\left[-n \int_0^{t} \gamma\left(\overline{\lambda}(x', \lambda)\right) dx' \right] H\left(\overline{\lambda}(t, \lambda)\right) F^{(n)}\left(p_i, \overline{\lambda}(t, \lambda), \mu\right) . \tag{1.177}$$

In fact, the multiplication $H\left(\overline{\lambda}(t, \lambda)\right) F^{(n)}\left(p_i, \overline{\lambda}(t, \lambda), \mu\right)$ is just $\Gamma^{(n)}_{as}\left(p_i, \overline{\lambda}(t, \lambda), \mu\right)$. So, finally we obtain:

$$\Gamma^{(n)}_{as}(\sigma p_i, \lambda, \mu) = \sigma^{4-n} \exp\left[-n \int_0^{t} \gamma\left(\overline{\lambda}(x', \lambda)\right) dx' \right] \Gamma^{(n)}_{as}\left(p_i, \overline{\lambda}(t, \lambda), \mu\right) . \tag{1.178}$$

The physical meaning of the above equation is quite clear. It says that rescaling the momentum p_i in the Green function $\Gamma^{(n)}_{as}$ is equivalent to replacing the coupling constant λ by the running coupling constant $\overline{\lambda}$ apart from some multiplicative factors. In fact, it is the same to the idea of Wilson's approach. In Wilson's approach, we rescale the cut-off and the information from each rescaling step can be absorbed into the corrections of the parameters in the Lagrangian

(e.g. the running coupling λ in our example). In this way, both approaches are equivalent and the rescaling is absorbed into the running coupling constant.

One thing I want to mention here is that the above approaches are all based on the Callan Symanzik renormalization scheme. In fact, we can also derive the equation in some other schemes such as the minimal subtraction scheme. In the minimal subtraction scheme, it is much easier to derive the renormalization group equation and we do not need to use the Weinberg's theorem to get rid of the inhomogeneous term on the right hand side of the equation. However, although the form of the renormalization group equation may be different in different schemes the final solution should be independent of the scheme. The scheme dependence will only occur when we truncate the perturbative calculation to a particular order and the scheme dependence will disappear if we could include the terms to all orders.

1.8.3 Renormalization Group Improvement

In this section, I want to address the problem mentioned at the end of the effective potential section that there is only a very small range of the scales which can be chosen to make the product $\lambda \left[\log \frac{M^2(\varphi_c)}{\mu^2}\right]$ small enough to be a valid expansion. We will show the product of the coupling constant and the logarithm can be cleverly rearranged into a new compact form (i.e. the running coupling) to greatly improve the effective region of our perturbative calculation [12, 91].

In fact, based on the above analysis of the solution of the renormalization group, we can easily see this is true. The solution of the renormalization group tells us that rescaling the momentum is equivalent to replacing the original coupling constant with the running coupling. Also rescaling the momentum is equivalent to rescaling the system (i.e. changing the scale of the system) and the scale of the system always occurs in logarithmic form in our perturbative calculation. So, intuitively, we can see that the running coupling is a kind of combination of the original coupling constant and the logarithm. When we introduce the running coupling, we only need to worry about one quantity (i.e. the running coupling) instead of two (i.e. the original coupling constant and the logarithm).

We take the $O(4)$ model as an example where the one loop beta function is given as [86]:

$$\beta\left(\overline{\lambda}\right) = \frac{3\overline{\lambda}^2}{16\pi^2}\,. \tag{1.179}$$

By using the definition of the running coupling:

$$\frac{d\overline{\lambda}\left(t,\lambda\right)}{dt} = \beta\left(\overline{\lambda}\right)\,, \tag{1.180}$$

we obtain

$$\overline{\lambda} = \frac{\lambda}{1-\frac{3\lambda}{16\pi^2}t} = \frac{\lambda}{1-\frac{3\lambda}{16\pi^2}\log\sigma}\,. \tag{1.181}$$

The above expression show explicitly that the running coupling contains the product of the coupling constant and the logarithm. In particular, the valid perturbative region is much larger because if λ is small it is not necessary that the logarithm should also be small. In fact, the logarithm can be very large if it is negative and can still make the total running coupling in the valid region of perturbative analysis. This results in an improvement through the renormalization group method.

In addition, we can do the perturbative expansion of the running coupling with a product of the coupling constant and the logarithm leading to a series of the terms:

$$\lambda^{n+1}\left(\log\sigma\right)^n\,. \tag{1.182}$$

We normally call this series as the summation of the leading logarithms. For higher loop calculations, we will have the summation of the next-to-leading logarithm, the next-to-next-to leading logarithm and so on. In fact, all the information of Green's function is encoded in these summation of the logarithms. However, usually we are not able to calculate the β function to infinitely high order, we have to truncate the summation to some order, (e.g., the leading logarithm or the next-to leading logarithm). This technique of summation of the logarithms has been widely used in my research to calculate effective potential and will be discussed in much detail in later chapters.

1.9 Summary

In this chapter, a brief introduction of the SM is firstly provided in section 1.2 with a particular emphasis on the Higgs sector and the conventional EW symmetry breaking. The notion of

conformal symmetry is then introduced as a custodial symmetry to address the hierarchy/ naturalness problem in section 1.3. I have discussed that the conformal scenario may imply new physics around EW/ TeV scale, making this scenario particularly interesting at LHC era. A follow up discussion about how conformal symmetry is radiatively broken through the Coleman-Weinberg mechanism and a generalization to Gildener Weinberg method is in section 1.4. In addition, I have shown the EW scale can be dynamically generated through dimensional transmutation in Coleman-Weinberg framework, which addresses the origin of the EW symmetry breaking and the hierarchy problem. Also, the SM itself cannot address the dark matter. In section 1.5, a brief discussion of the WIMP dark matter is provided as well as the notion of hidden sector which provides the framework for model building. Connecting to the LHC phenomenology, a mini review of the recent LHC diphoton excess is in section 1.6. The notion that conformal symmetry as a custodial symmetry, Coleman Weinberg mechanism and the hidden sector extensions of the SM lay the foundation of the thesis.

In this chapter, I have also introduced two key techniques in this thesis: the effective potential method in section 1.7 and the renormalization group technique in section 1.8. Combining these two techniques results in the leading logarithmic summation technique where the RG improvement of the effective potential is obtained. The effective potential and the renormalization group technique lay the technical foundation of this thesis.

The following chapters of the thesis will discuss different aspects of the conformally symmetric hidden sector and my original works [14, 15, 16, 17, 18] are embedded in chapter 2–6. It will start with the simplest case of conformally symmetric SM and gradually add further complexity to the models. In chapter 2, I will show a 125 GeV Higgs mass with a large perturbative Higgs quartic coupling can be naturally realized in the conformal SM. In chapter 3, the minimal extension of the SM: the CS real singlet extension is studied, where the DM decay is protected by the Z_2 symmetry and two SB scenarios (the sequential scenario and dynamical scenario) are developed. In both scenarios, viable DM candidates are obtained. In chapter 4, I discuss the CS complex singlet extension of the SM with a global $U(1)$ symmetry which can be either broken or unbroken and both scenarios are studied to address DM, a second Higgs and the LHC diphoton excess. In the unbroken case, a viable cold DM candidate at $\sim 100\,\text{GeV}$ is

obtained. In the broken case, a renormalization-scale optimization technique is developed to significantly narrow the parameter space and find a 550 GeV second Higgs boson. Upon including the interactions of the complex scalar with an additional vector-like fermion, a 720 GeV mass singlet is found to address the 750 GeV LHC diphoton excess. In chapter 5, the conformal scenario is combined with the asymptotic safety (AS) theory to study an asymptotically safe CS hidden sector. The AS is encoded in UV boundary conditions and renormalization group (RG) equations are used as a bridge to connect UV boundary conditions and EW/ TeV scale physics and furnish a detailed example in the context of a CS leptophobic $U(1)'$ model. In chapter 6, the multi-scale RG method is developed to address the two approximations within the implementation of Gildener Weinberg method: the weak coupling approximation and the simplification of the form of the logarithm. The introduction of an extra renormalization scale allows the mapping of the effective potential onto an RG-equivalent form with a certain symmetric structure, leading to a simplified form of the effective potential.

Chapter 2

Is Conformal Standard Model Consistent with a 125 GeV Higgs Mass?

The work presented in this chapter was done in collaboration with Tom Steele and has been published in Phys. Rev. Lett. [14].

In this chapter, we will study the conformally symmetric SM. We start with this simplest case (within the SM) in this chapter and in the next few chapters, we will gradually add complications and explore the case beyond the SM. The conformal SM captures some essential features of more complicated conformal models such as the well-known radiative symmetry breaking through the Coleman Weinberg mechanism. In addition, in this chapter, we will present the essential techniques without further complications. The technique of the leading logarithmic summation to obtain the renormalization group improvement of the effective potential will be crucial and throughout this thesis. Moreover, the reader may obtain a conceptual understanding of the coupling solutions and the mass prediction, which will be useful in helping understanding the parameter space in more complicated models such as the SM with hidden sector in later chapters.

The highlight of this article is we are able to show a 125 GeV Higgs mass can be naturally realized in the conformally symmetric SM with a large perturbative Higgs quartic coupling solution. This large coupling solution will lead to a significant enhancement of the process $HH \to HH$ and will be testable in the future ILC (International Linear Collider).

2.1 Introduction and Motivation

2.1.1 Abstract

The mechanism of radiative electroweak symmetry breaking occurs through loop corrections, and unlike conventional symmetry breaking where the Higgs mass is a parameter, the radiatively-generated Higgs mass is dynamically predicted. Padé approximations and an averaging method are developed to extend the Higgs mass predictions in radiative electroweak symmetry breaking from five- to nine-loop order in the scalar sector of the Standard Model, resulting in an upper bound on the Higgs mass of 141 GeV. The mass predictions are well-described by a geometric series behaviour, converging to an asymptotic Higgs mass of 124 GeV consistent with the recent ATLAS/CMS observations. Similarly, we find that the Higgs self-coupling converges to $\lambda = 0.23$, which is significantly larger than its conventional symmetry breaking counterpart for a 124 GeV Higgs mass. In addition to this significant enhancement of the Higgs self-coupling and $HH \to HH$ scattering, we find that Higgs decays to gauge bosons are unaltered and the scattering processes $W_L^+W_L^+ \to HH$, $Z_LZ_L \to HH$ are also enhanced, providing signals to distinguish conventional and radiative electroweak symmetry breaking mechanisms.

2.1.2 Introduction

The observation of a 125 GeV Higgs candidate by ATLAS and CMS [96, 97], along with supporting evidence from CDF and D0 [98], provides preliminary information for evaluating different mechanisms of electroweak (EW) symmetry breaking. Coleman & Weinberg originally demonstrated that spontaneous symmetry breaking can occur through loop (radiative) corrections to the effective potential in the absence of a tree-level Lagrangian quadratic scalar term [12]. This radiative EW symmetry-breaking mechanism is conceptually appealing because the Higgs mass is no longer a free-parameter as it is in conventional EW symmetry breaking, but is a dynamical quantity which can be self-consistently predicted by the theory. The absence of a conventional-symmetry-breaking quadratic scalar term also addresses aspects of the scale hierarchy problem [99] and the fine-tuning problem [5].

The small-Higgs-coupling radiative symmetry-breaking solution originally discovered by Coleman & Weinberg leads to an order 10 GeV Higgs mass which has been excluded by experiment. This result relies upon the dominance of gauge couplings over Yukawa couplings

in the effective potential; the large Yukawa coupling of the top quark (which was not known at the time of Coleman & Weinberg) destabilizes the small-Higgs-coupling solution. However, it has been demonstrated that a large-Higgs-coupling solution exists that results in a significantly larger Higgs mass prediction [33, 100]. Similar radiative-symmetry-breaking solutions have been found in extensions of the Standard Model [101].

The large-Higgs-coupling solutions for radiative symmetry breaking are intrinsically challenging because higher-loop corrections can become important. Fortunately, one can demonstrate that Yukawa and gauge couplings have minimal effect on the analysis, and hence the scalar field sector of the Standard Model (a globally-symmetric $O(4)$ scalar field theory) captures the essential features of the effective potential and radiative symmetry breaking in the full Standard Model [102], providing a simpler field theory for evaluating higher-loop corrections. In particular, at leading-order the largest secondary effect of the top-quark Yukawa coupling $x = x_t = 0.025$ only has a 2% effect on the Higgs mass [102, 103]. This arises as a combination of two main effects: x_t represents 15% of the one-loop β function for the Higgs self-coupling in the large-coupling solution, and the x-independent tree-level contribution suppresses the x dependence in the Higgs mass prediction.

Although such higher-loop calculations of the effective potential would initially seem daunting, in the Coleman-Weinberg (CW) renormalization scheme [12, 104], the effective potential for scalar field theories with global $O(N)$ symmetry can be uniquely determined from the renormalization-group functions [105]. Because the renormalization-group functions for $O(N)$-symmetric scalar ϕ^4 theories are known to five-loop order in the MS scheme [106], and methods are known for converting them to the CW scheme [107], calculation of the five-loop effective potential in $O(N)$ ϕ^4 theory has been achieved [105, 108]. The Higgs mass prediction resulting from these higher-loop corrections shows evidence of slow convergence as loop order is increased, resulting in a Higgs mass upper bound of 165 GeV from the five-loop effective potential [103].

The purpose of this paper is to assess whether radiative EW symmetry-breaking can accommodate a 125 GeV Higgs mass as observed by ATLAS and CMS [96, 97] by estimating higher-loop effects on the Higgs mass prediction. This is achieved by exploiting the success of Padé approximation methods for the renormalization-group functions of $O(N)$ ϕ^4 theory

[109, 110, 111] to estimate higher-loop contributions to the effective potential and Higgs mass. We also argue that averaging subsequent orders of the effective potential further extends the estimates to two loops higher accuracy. By combining these estimation methods, we obtain a nine-loop Higgs mass upper bound of 141 GeV and observe an empirical pattern of Higgs mass estimates that extrapolates the Higgs mass prediction to a value in close agreement with ATLAS and CMS [96, 97]. However, mass predictions alone are not sufficient to distinguish conventional and radiative EW symmetry breaking. Following Ref. [112] we identify possible phenomenological signatures, including the Higgs self-coupling, that would distinguish a 125 GeV Higgs in conventional and radiative EW symmetry breaking.

2.2 Theoretic Framework

In $O(N)$-symmetric massless $\lambda\phi^4$ theory (i.e. the Standard Model scalar sector corresponds to $N = 4$), the effective potential in the CW scheme takes the form [12]

$$V(\lambda, \phi, \mu) = \sum_{n=0}^{\infty} \sum_{m=0}^{n} \lambda^{n+1} T_{nm} L^m \phi^4 \tag{2.1}$$

where $L = \log(\phi^2/\mu^2)$, $\phi^2 = \sum_{i=1}^{N} \phi_i^2$, and μ is the renormalization scale. The summation includes leading logarithm (LL), next-to-leading logarithm (NLL), next-to-next-to-leading logarithm N^2LL, and in general N^nLL terms. The N^nLL term S_n can be isolated by rearranging the summation in the form

$$V(\lambda, \phi, \mu) = \sum_{n=0}^{\infty} \lambda^{n+1} S_n(\lambda L) \phi^4 \tag{2.2}$$

where $S_n(\lambda L) = \sum_{m=0}^{\infty} T_{n+m\,m} (\lambda L)^m$. The renormalization group (RG) equation

$$\left(\mu \frac{\partial}{\partial \mu} + \beta(\lambda) \frac{\partial}{\partial \lambda} + \gamma(\lambda) \phi \frac{\partial}{\partial \phi} \right) V(\lambda, \phi, \mu) = 0 \tag{2.3}$$

$$\beta(\lambda) = \mu \frac{d\lambda}{d\mu} = \sum_{k=2}^{\infty} b_k \lambda^k \,, \;\; \gamma(\lambda) = \frac{\mu}{\phi} \frac{d\phi}{d\mu} = \sum_{k=1}^{\infty} g_k \lambda^k \tag{2.4}$$

leads to the following coupled differential equations for the functions $S_n(\xi)$ [105]

$$\begin{aligned} 0 = & \left[(-2 + b_2 \xi) \frac{d}{d\xi} + (n+1) b_2 + 4 g_1 \right] S_n \\ & + \sum_{m=0}^{n-1} \left\{ \left(2 g_{n-m} + b_{n+2-m} \xi \frac{d}{d\xi} \right) \right. \\ & \left. + \left[(m+1) b_{n+2-m} + 4 g_{n+1-m} \right] \right\} S_m \,, \end{aligned} \tag{2.5}$$

where we show below that $g_1 = 0$. We thus see that the $n+1$-loop renormalization-group functions are needed to determine S_k for $k = 0, 1, 2, \ldots, n$. The boundary conditions $S_n(0) = T_{n0}$ needed to solve (2.5) emerge from the CW renormalization condition $\frac{d^4 V}{d\phi^4}|_{\phi=\mu} = 24\lambda$ [12, 104], resulting in the constraints [105]

$$\begin{aligned} 0 = & 16 \frac{d^4}{d\xi^4} S_k(0) + 80 \frac{d^3}{d\xi^3} S_{k+1}(0) + 140 \frac{d^2}{d\xi^2} S_{k+2}(0) \\ & + 100 \frac{d}{d\xi} S_{k+3}(0) + 24 S_{k+4}(0) \quad (k = 0, 1, 2 \cdots) \,. \end{aligned} \tag{2.6}$$

The boundary condition $S_n(0)$ for the differential equation (2.5) can then be obtained by iteratively solving for the lower-order S_k, where $k = \{n-1, n-2, n-3, n-4\}$. Thus in the CW scheme, the effective potential to $N^p LL$ order is uniquely determined by the $p+1$-loop RG functions. However, since we only have the limited information of the renormalization group functions, we need to truncate the process at a certain $N^p LL$ order

$$V_p = \sum_{n=0}^{p} \lambda^{n+1} S_n (\lambda L) \phi^4 + \sum_{i=p+1}^{p+4} T_{i\,0} \lambda^{i+1} \phi^4 \,, \tag{2.7}$$

where the last term represents a counter-term which is constrained by the CW renormalization condition. It should be noted that this procedure can reproduce the explicit two-loop calculation of the effective potential [104].

In general, the effective action also has divergences in the kinetic term which are addressed in the CW scheme via a condition which maintains the tree-level form. With this additional condition, the Higgs mass M_H is given by

$$M_H^2 = \frac{1}{Z} \frac{d^2 V}{d\phi^2} \bigg|_{\phi=\mu} = \frac{d^2 V}{d\phi^2} \bigg|_{\phi=\mu} . \tag{2.8}$$

where $Z(\phi) = 1$ in the CW scheme. Finally, the coupling λ is determined by the spontaneous-symmetry-breaking condition that the effective potential has a non-trivial minimum $\frac{dV}{d\phi}|_{\phi=\mu} =$

0 . Contact with the Standard Model is achieved by identifying the scale μ with the EW scale $\mu = v = 246.2\,\text{GeV}$. We note that although higher-loop calculations of the effective potential exist in other schemes, there are very few corresponding calculations of $Z(\phi)$, so for pragmatic purposes higher-loop calculations of the Higgs mass are currently limited to the CW scheme. By contrast, RG functions $\tilde{\beta}$ and $\tilde{\gamma}$ are generally calculated in MS-like schemes, and hence it is necessary to convert these RG functions to the CW scheme [107]. We can thus use the five-loop MS-scheme determinations of the $O(N)$-symmetric ϕ^4 RG functions [106] to determine their five-loop CW-scheme counterparts. Note that in the MS-scheme $\tilde{g}_1 = 0$, and hence we also have $g_1 = 0$ in the CW scheme.

In Ref. [103] it was demonstrated that for p even, V_p provides an upper bound on the Higgs mass M_H which slowly drops from 221 GeV at one-loop order (LL order) to 165 GeV at five-loop order (N^4LL). Thus we can exclude radiative symmetry breaking if the upper bound drops below the ATLAS/CMS value of 125 GeV. We thus focus on improving the upper bound by approximating higher-loop terms in the RG functions which enables higher-loop approximations to the effective potential.

2.3 Pade Approximation and Averaging Method

Padé approximation methods, particularly when improved with an asymptotic error correction [109, 113, 114], have been successfully applied to the MS-scheme RG functions of $O(N)$ massive scalar field theory [109, 110, 111]. For example, using four-loop results as input, the Padé-predicted and exact five loop term in the beta function agree to better than 5% for $N = 4$ [111].

For Padé approximations to the MS-scheme beta function $\tilde{\beta}$ we write

$$\tilde{\beta} = \tilde{b}_2\lambda^2\left(1 + \frac{\tilde{b}_3}{\tilde{b}_2}\lambda + \frac{\tilde{b}_4}{\tilde{b}_2}\lambda^2 + \frac{\tilde{b}_5}{\tilde{b}_2}\lambda^3 + \frac{\tilde{b}_6}{\tilde{b}_2}\lambda^4\right) \tag{2.9}$$

and apply Padé approximation methods to the bracketed quantity. Using the methods outlined in Refs. [109, 113, 114], the asymptotic-improved Padé prediction of the R_5x^5 term with known

coefficients $\{R_1, R_2, R_3, R_4\}$ in the series $P(x) = 1 + R_1 x + R_2 x^2 + R_3 x^3 + R_4 x^4$ is given by

$$R_5 = \frac{R_4^2 \left(R_1 R_3^3 - 2R_2^3 R_4 + R_1 R_2 R_3 R_4\right)}{R_3 \left(2R_1 R_3^3 - R_2^2 R_3^2 - R_4 R_2^3\right)} \ . \tag{2.10}$$

From this expression, the resulting asymptotic-improved Padé prediction of the $O(4)$ MS six-loop beta function is $\tilde{b}_7 = -1.07$. Because we also want the seven-loop beta function, a [2|2] Padé approximant to $P(x)$ is then used to predict its x^5 and x^6 terms. The resulting prediction of the six- and seven-loop MS-scheme $O(4)$ beta function coefficients are $\tilde{b}_7 = -0.992$ and $\tilde{b}_8 = 1.96$. The agreement of the [2|2] and asymptotic-improved predictions for $\tilde{b}_7$ to approximately 10% provides a validation of the [2|2] methodology and establishes a characteristic error for our analysis below. Converting these MS-scheme beta function coefficients to the CW scheme results in $b_7 = -0.695$ and $b_8 = 1.37$.

For Padé approximations to the MS-scheme anomalous dimension we follow the same procedure except there is less information than in the beta function because the leading-order $\tilde{g}_1$ term in the anomalous dimension is zero. Given knowledge of $\{R_1, R_2, R_3\}$ in the series $P(x)$, the asymptotic-improved Padé prediction of R_4 [110] results in the asymptotic-improved Padé prediction of the six-loop coefficient $\tilde{g}_6 = -0.692 \times 10^{-3}$ and $g_6 = -0.135 \times 10^{-3}$ after conversion to the CW scheme. As argued above, we can now use $\tilde{g}_6$ to form a [2|2] Padé approximant to predict the seven-loop MS coefficient $\tilde{g}_7 = 0.961 \times 10^{-3}$ which corresponds to CW-scheme value $g_7 = -0.225 \times 10^{-4}$.

Equipped with Padé estimates of the RG functions up to seven-loop order, we can solve (2.5) and (2.6) to obtain S_5 and S_6, which enables the construction of the N^6LL effective potential V_6. Analysis of the effective potential results in the Higgs mass $M_H = 150\,\text{GeV}$ and the CW-scheme weak-scale coupling $\lambda(v) = 0.308$. Including 10% uncertainties in the RG coefficients only gives a 0.1 GeV Higgs mass difference which shows the method is quite robust.

Now, we develop methods to extrapolate the Higgs mass estimates to higher-loop orders. We begin with the averaging method motivated by the field-theoretical contributions to the Higgs mass in the absence of a counter-term contribution

$$\tilde{M}_n = \frac{1}{v^2} \frac{d^2 \left(V_n - K_n \phi^4\right)}{d\phi^2}\bigg|_{\phi=\mu} , \tag{2.11}$$

where $K_n = \sum_{i=n+1}^{n+4} T_{i,0} \lambda^{i+1}$ is the corresponding counter-term at that order. The quantity

$\tilde{M}_n$ is shown in Fig. 2.1, and as argued in Ref. [103], demonstrates that the effective potential over-estimates the Higgs mass at even orders and under-estimates it at odd orders. Moreover, we can imagine that at higher orders, the field theoretical contributions to the Higgs mass will lie in the envelope between the even and odd orders. Indeed, for small λ Fig. 2.1 already shows close agreement between even and odd orders. It thus seems plausible that the average of an even- and odd-order effective potential will provide a better approximation to the full effective potential than a single-order result. This averaging method can be justified by identifying $\tilde{M}_n$ as the Eq. (2.7) partial sum of S_n contributions that alternate in sign as demonstrated by Fig. 2.1. In particular, moving from p-loop order to $p+1$-loop order involves the addition of S_p, and the sign of this contribution sequentially raises/lowers the curves in Fig. 2.1. Thus for any fixed value of λ, we can employ Euler's transformation for alternating series to accelerate its convergence [115]:

$$\sum_{n=0}^{\infty}(-1)^n u_n = u_0 - u_1 + \ldots - u_{N-1} + \sum_{s=0}^{\infty}\frac{(-1)^s}{2^{s+1}}\left[\Delta^s u_N\right] \tag{2.12}$$

and setting $s=0$ as the lowest order approximation, we obtain:

$$\sum_{n=0}^{\infty}(-1)^n u_n \approx u_0 - u_1 + \ldots - u_{N-1} + \frac{1}{2}u_N = \bar{P}_N\,, \tag{2.13}$$

where the partial sums $P_N = \sum_{n=0}^{N}(-1)^n u_n$ and $\bar{P}_N = \frac{1}{2}\left(P_N + P_{N-1}\right)$. In our case, the averaged effective potential $\bar{V}_n$ can be written as $\bar{V}_n = \frac{1}{2}\left(V_n + V_{n-1}\right)$.

For example, the average of four-loop (N^3LL) and five-loop (N^4LL) contributions to the effective potential $\bar{V}_4 = V_3/2 + V_4/2 = \left(\lambda S_0 + \ldots + \lambda^4 S_3 + \frac{1}{2}\lambda^5 S_4 + \bar{K}_4\right)\phi^4$ shown in Fig. 2.1 gives the Higgs mass prediction $M_H = 153\,\text{GeV}$ and the corresponding coupling $\lambda = 0.418$. Although the averaging results in a coupling close to the three-loop value, the mass is in close agreement with the seven-loop Padé result. Thus the average of the five-loop effective potential with its lower-loop four-loop counterpart, leads to a much better Higgs mass estimate than the five-loop contribution alone.

The same pattern holds at lower orders as well; the Higgs mass and coupling resulting from averaging the two- and three-loop effective potentials is in remarkably-close agreement with the five-loop Higgs mass and one-loop coupling (see Table 2.1). Based on this pattern that the

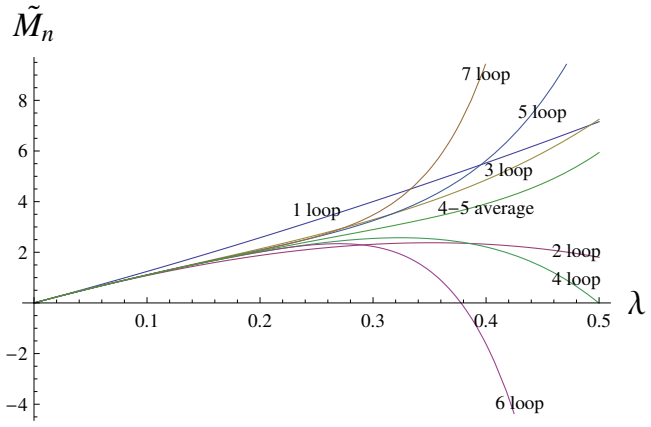

Figure 2.1: The dimensionless quantity $\tilde{M}_n$ (2.11) is plotted as a function of λ for the $O(4)$ scalar theory. Upper curves represent the even N^pLL ($p+1$-loop) orders ($p = 0, 2, 4, 6$) and the lower curves represent the odd orders ($p = 1, 3, 5$). The average of the four- and five-loop contributions is also shown.

average of the $n-1$ and n-loop effective potentials approximates the $n-2$ loop coupling and $n+2$ loop Higgs mass, we expect that the average of the six- and seven-loop Padé approximations to the effective potential will provide a good estimate of the nine-loop Higgs mass prediction and the five-loop coupling. Using this method, our nine-loop estimates are $M_H = 141\,\text{GeV}$ with the corresponding coupling $\lambda(v) = 0.352$. We note that the agreement between the five-loop coupling and the six- and seven-loop average (see Table 2.1) provides further confirmation of the pattern, and gives us confidence in the nine-loop Higgs mass estimate.

Loop	λ	M_H	λ_{CSB}	Average	λ	M_H	λ_{CSB}
1 loop	0.534	221	0.101				
3 loops	0.417	186	0.072	2,3 loop	0.514	167	0.230
5 loops	0.354	165	0.056	4,5 loop	0.418	153	0.194
7 loops	0.308	150	0.047	6,7 loop	0.352	141	0.041
Extrapolate	0.233	124	0.032				

Table 2.1: Higgs mass in GeV and self-coupling predictions at different loop orders in both the standard (left half) and averaging method (right half). The extrapolated values emerging from the geometric series behaviour are also shown. For comparison, the Higgs coupling λ_{CSB} in conventional symmetry breaking corresponding to the predicted Higgs mass is also provided.

Thus by combining Padé estimates and the averaging method, the seven- and nine-loop Higgs mass predictions have been estimated. These estimates demonstrate a continued slow convergence towards a Higgs mass bounded from above by 141 GeV. To determine whether the Higgs mass will eventually converge to a value consistent with the 125 GeV Higgs mass seen by ATLAS/CMS [96, 97], we first note that the differences between subsequent loop orders in Table 2.1 decrease in a fashion consistent with a geometric series

$$M_n - M_{Higgs} = \Lambda \sigma^n \ , \tag{2.14}$$

where M_n is the n-loop Higgs prediction, Λ has dimensions of mass, and $\sigma < 1$ is a dimensionless quantity which leads to $\lim_{n\to\infty} M_n = M_{Higgs}$. In Figure 2.2 the plot of $\log(M_n - M_{Higgs})$ shows clear linear behaviour with n consistent with the geometric series (2.14) when $M_{Higgs} = 125\,\text{GeV}$. The dependence of the χ^2 deviation from this linear fit is shown as a function of M_{Higgs} in Fig. 2.3, providing an optimized value $M_{Higgs} = 124\,\text{GeV}$. We thus speculate that the radiatively-generated Higgs mass ultimately converges to a value consistent with the 125 GeV ATLAS/CMS value [96, 97]. A similar geometric series pattern exists for the Higgs self-coupling; Figure 2.2 shows linear behaviour for $\log(\lambda_n - \lambda_{Higgs})$ for the least-squares optimized value $\lambda_{Higgs} = 0.23$. The similarity in slope between the mass and coupling plots in Fig. 2.2 is intriguing; we speculate that this is connected to the underlying rate of convergence of the effective potential.

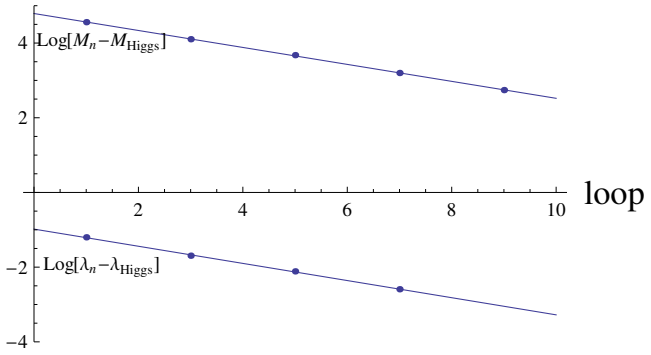

Figure 2.2: The quantities $\log(M_n - M_{Higgs})$ and $\log(\lambda_n - \lambda_{Higgs})$ are plotted versus loop order n for Table 2.1 values with $M_{Higgs} = 125\,\text{GeV}$ and $\lambda_{Higgs} = 0.23$. The lines are a linear fit to the data points based on the geometric series (2.14).

The extrapolated value λ_{Higgs} is a factor of 2 smaller than the leading logarithm result, so it

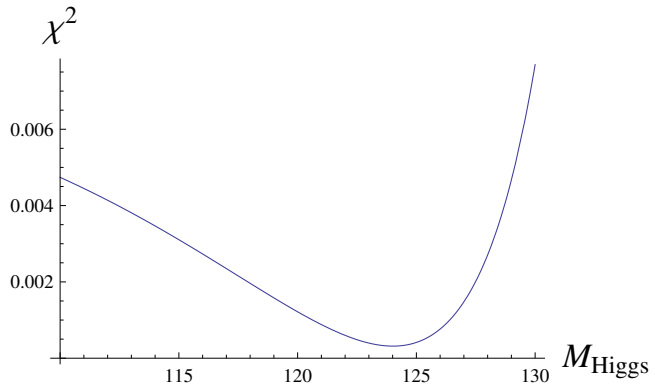

Figure 2.3: The χ^2 of the linear fit of Table 2.1 values to $\log(M_n - M_{Higgs})$ is plotted as a function of M_{Higgs} resulting in the least-squares prediction $M_{Higgs} = 124\,\text{GeV}$.

is necessary to re-examine whether the scalar field theory sector of the Standard Model is still a valid approximation. Because the top-quark Yukawa coupling is the dominant secondary effect on the Higgs mass [102], we have calculated the leading-logarithm (one-loop) ratio of the Higgs mass with top-quark effects included and omitted. For the extrapolated value $\lambda_{Higgs} = 0.23$, the top-quark effects are less than a 5% effect at leading-log order and hence the scalar field sector still captures the dominant features of the Standard Model.

Using Padé approximation methods and an averaging technique, we have extended the radiatively-generated Higgs mass prediction to nine-loop order. Two important trends emerge from this result: both the Higgs mass and CW-scheme coupling λ decrease with increasing loop order. Both the Higgs mass and self-coupling are well-described by a geometric series in the loop-order, converging to approximately $M_{Higgs} = 124\,\text{GeV}$ and $\lambda_{Higgs} = 0.23$.

The value of the coupling provides a phenomenological signal that distinguishes between radiative and conventional EW symmetry breaking. For example, in Table 2.1 the conventional symmetry-breaking λ value corresponding to the predicted Higgs mass is smaller than the radiatively-generated value at all orders, implying a significant enhancement of Higgs-Higgs scattering in radiative EW symmetry-breaking [33]. This trend is upheld in the extrapolation to $\lambda_{Higgs} = 0.23$ and a 125 GeV Higgs mass. It seems feasible for the Higgs self-coupling to be measured by the LHC [116, 117]; an enhancement of the coupling compared to conventional symmetry breaking could be evidence for the radiative scenario.

However, the Goldstone-boson replacement theorem [118] leads to identical results for the

Higgs decay processes $H \to W_L^+ W_L^-$, $H \to Z_L Z_L$ in conventional and radiative symmetry breaking independent of the extrapolated Higgs coupling, and similar equivalences are found for the scattering processes $W_L^+ W_L^- \to W_L^+ W_L^-$, $W_L^+ W_L^- \to Z_L Z_L$ [112]. This implies that these Higgs decays and gauge boson scattering processes are unable to distinguish between radiative and conventional EW symmetry breaking. By contrast, the processes $W_L^+ W_L^+ \to HH$, $Z_L Z_L \to HH$ are enhanced in radiative EW symmetry breaking independent of the extrapolated Higgs coupling. For example, the seven-loop Padé prediction leads to a three-fold enhancement comparable to the lower-loop analysis of Ref. [112].

2.4 Results and Conclusions

In summary, we have combined Padé approximation methods with averaging techniques to extend Higgs mass predictions in radiative EW symmetry breaking to the nine-loop estimate $M_H = 141\,\text{GeV}$ for the upper bound on the Higgs mass. Evidence of geometric-series convergence of the Higgs mass to 125 GeV suggests that radiative EW symmetry breaking is a viable mechanism for the ATLAS/CMS observation of a Higgs. Similar evidence of geometric series convergence for the Higgs self-coupling leads to the corresponding limiting value of the radiatively-generated Higgs coupling $\lambda_{Higgs} = 0.23$, a value significantly larger than its conventional symmetry-breaking counterpart. This implies that the processes $HH \to HH$, $W_L^+ W_L^+ \to HH$, $Z_L Z_L \to HH$ are enhanced, so discrepancies between experiment and conventional symmetry-breaking predictions may provide signals of radiative symmetry breaking.

Chapter 3

Viable Dark Matter in a Conformal Real Singlet Extension of the Standard Model

The work presented in this chapter was done in collaboration with Tom Steele, Robert Mann and Dago Contreras and has been published in Phys. Rev. Lett. [15].

In the previous chapter, we have studied the simplest case: the conformally symmetric SM. However, it is believed now that the SM itself is incomplete. There are many motivations for new physics beyond the SM such as dark matter, dark energy, the strong CP problem, baryogenesis, inflation and so on. In this chapter, we will study the minimum extension of the SM where only one extra real singlet is introduced. The real singlet only interacts with the SM through the Higgs portal interaction. Note that this model is also the simplest hidden sector model which complicated enough to capture the essential features of the conformal hidden sector such as the symmetry breaking pattern. However, in this work we only study the case where symmetry in the singlet is unbroken which provides an ideal cold dark matter. In the next chapter, we will provide a more thorough study of the symmetry breaking pattern where both the symmetry is either unbroken or broken in the hidden sector. In addition, the Coleman Weinberg mechanism employed in the previous chapter only applies to the case with single scalar field. With one extra real singlet included, we have to employ the well-known Gildener Weinberg method which is a generalization of Coleman Weinberg mechanism to multiple scalar fields.

The highlights of this chapter are in three points. First, we generalize the leading logarithmic summation technique (discussed in detail in the previous chapter) to the case with multiple scalar fields based on the Gildener Weinberg method and two symmetry breaking scenarios have

been proposed the dynamical scenario and the sequential scenario. Second, as far as I know, this is the first work in this area to propose the symmetry breaking pattern that radiative symmetry breaking first occurs in the Higgs sector and is then transmitted to the hidden sector through the Higgs portal interaction. Our symmetry breaking pattern is opposite to the conventional one widely discussed in other works. Thirdly, using the dynamical method we proposed, we are able to obtain an ideal cold dark matter candiate within the detection region of the next generation XENON experiment.

3.1 Introduction and Motivation

3.1.1 Abstract

We consider generation of dark matter mass via radiative electroweak symmetry breaking in an extension of the conformal Standard Model containing a singlet scalar field with a Higgs portal interaction. Generating the mass from a sequential process of radiative electroweak symmetry breaking followed by a conventional Higgs mechanism can account for less than 35% of the cosmological dark matter abundance for dark matter mass $M_s > 80\,\text{GeV}$. However in a dynamical approach where both Higgs and scalar singlet masses are generated via radiative electroweak symmetry breaking we obtain much higher levels of dark matter abundance. At one-loop level we find abundances of 10%–100% with $106\,\text{GeV} < M_s < 120\,\text{GeV}$. However, when the higher-order effects needed for consistency with a 125 GeV Higgs mass are estimated, the abundance becomes 10%–80% for $80\,\text{GeV} < M_s < 96\,\text{GeV}$, representing a significant decrease in the dark matter mass. The dynamical approach also predicts a small scalar-singlet self-coupling, providing a natural explanation for the astrophysical observations that place upper bounds on dark matter self-interaction. The predictions in all three approaches are within the $M_s > 80\,\text{GeV}$ detection region of the next generation XENON experiment.

3.1.2 Introduction

One of the most important outstanding challenges in physics is to reveal the underlying nature of dark matter. Amongst the numerous proposed dark matter candidates, the singlet scalar extension of the Standard Model is conceptually appealing and has been the subject of much investigation [119, 120, 121, 122, 123, 101, 124, 125] (see Ref. [121] for a clear and detailed discussion). This model was first introduced by Silverira and Zee [119] and then generalized

to a complex scalar by McDonald [120]. More detailed analyses that included nuclear recoil detection and implications for collider experiments were subsequently studied [121], along with the electroweak phase transition of this singlet extension of the Standard Model [101, 125]. Because it consists of one scalar singlet beyond the Standard Model, it is one of the simplest scenarios for nonbaryonic dark matter. However, it is complicated enough to offer rich properties, such as dark matter stability, because the Standard Model gauge singlet does not interact with ordinary matter except through the Higgs field (i.e., Higgs portal interactions [124]). In these models, the stability of dark matter is protected by a scalar singlet Z_2 symmetry that prohibits the dark-Higgs-Higgs decay process.

Versions of singlet scalar models with classical conformal symmetry are particularly interesting as a means for addressing the hierarchy and fine-tuning problems [5, 9] associated with the conventional Higgs mechanism. Classical scale invariance provides a custodial symmetry for Higgs loop corrections [9, 6], and similar to dimensional transmutation in QCD, leads to natural scale hierarchies in a unification context [99] (see also Ref. [11] for a recent discussion). In these scalar-singlet models, radiative symmetry breaking (i.e., the Coleman-Weinberg mechanism [12]) in the hidden (dark) sector gets communicated to the electroweak sector via the Higgs portal interaction [126, 127, 128, 129, 131, 130, 132, 133, 35]. Typically this requires a vacuum expectation value (VEV) for the scalar singlet field which breaks the Z_2 symmetry, and hence additional mechanisms are needed to incorporate dark matter (e.g., mirror dark matter [129], CP symmetry protected dark matter [134, 135], inert doublet dark matter [136] and Majorana Dark matter [137]).

In this article we take the approach of radiative electroweak symmetry breaking in the Standard Model sector, and explore its implications for the scalar singlet (dark matter) sector. Decays of the dark matter field are protected by Z_2 symmetry without introducing any extra mechanisms. In the Coleman-Weinberg mechanism [12], the VEV for the Higgs is radiatively generated directly in the Higgs sector. The small Higgs coupling Coleman-Weinberg solution [12] is destabilized by top-quark Yukawa contributions, but a large Higgs-self-coupling solution exists [33, 100]. Recently it has been shown that the 125 GeV Higgs mass observed by LHC [96, 97] can be described by radiative electroweak symmetry breaking in the large Higgs self coupling

regime [14]. The purpose of this article is to show that radiative symmetry breaking in the large Higgs self-coupling perturbative regime can dynamically generate a dark matter (scalar singlet) mass in a Higgs-portal extension of the Standard Model that provides a significant proportion of the dark matter abundance. The resulting dark matter mass and the corresponding dark-Higgs coupling are within the parameter space that will be probed by the next generation XENON experiment.

3.2 Theoretic Framework and Sequential Method

The dark matter scalar singlet extension of the conformal Standard Model has the following scalar sector [119, 120, 121, 122, 123, 101, 124, 125]:

$$L = \frac{1}{2}\partial_\mu H \partial^\mu H + \frac{1}{2}\partial_\mu S \partial^\mu S - \frac{k}{2} S^2 H^\dagger H - \frac{h}{4!} S^4 - \lambda (H^\dagger H)^2 \,, \tag{3.1}$$

where H is the Higgs field and S is the dark matter (real scalar) singlet field which has no interactions with other Standard Model fields except via the Higgs portal interaction. As discussed in Ref. [121], from an effective field theory perspective the absence of higher-dimensional non-renormalizable terms in Eq. (6.2) assumes other beyond-Standard-Model particles are much heavier than the electroweak scale. Because we are interested in Standard-Model extensions that are conformal at tree level, there are no quadratic terms for the Higgs and dark scalar and there are no S^3, $SH^\dagger H$, or similar terms that violate the Z_2 ($S \to -S$) symmetry. The stability of dark matter is protected by assuming the Z_2 symmetry is unbroken, precluding $SH^\dagger H$ terms in (6.2) induced by $\langle S \rangle \neq 0$, and thereby preventing dark matter from decaying through the Higgs portal. With zero VEV, the dark matter field can enter radiative symmetry breaking in two ways: either S is on an equal footing with all other Standard-Model non-Higgs fields, or else both Higgs and scalar singlet masses are radiatively generated.

In the first case, S influences the Higgs effective potential via the Higgs portal interaction. Radiative symmetry breaking first generates the Higgs VEV and then the dark matter gains its mass through the conventional Higgs mechanism via the the dark matter-Higgs coupling $\frac{k}{2} S^2 H^\dagger H|_{H \to v} = \frac{k}{2} v^2 S^2$. Thus in this scenario we consider the effective potential of the Higgs field, which can be rewritten as $O(4)$ symmetric massless $\lambda\phi^4$ theory because the gauge couplings

and top quark Yukawa coupling effects are numerically small in the large Higgs self-coupling regime of interest [100]. The effective potential in Coleman-Weinberg (CW) renormalization scheme then has the form [12, 104]:

$$V(\lambda, \Phi, \mu) \;=\; \sum_{n=0}^{\infty} \sum_{m=0}^{n} \lambda^{n+1} T_{nm} L^m \Phi^4 \tag{3.2}$$

where $L = \log\left(\Phi^2/\mu^2\right)$, $H^\dagger H = \Phi^2 = \sum_{i=1}^{4} \phi_i^2$, and μ is the renormalization scale which connects the $O(4)$ theory to the Standard Model when μ equals the electroweak scale $v = 246\,\mathrm{GeV}$. The summation includes leading logarithm (LL), next-to-leading logarithm (NLL), next-to-next-to-leading logarithm N^2LL, and in general N^nLL terms. For the leading logarithm summation we obtain

$$V_{LL} = \sum_{m=0}^{\infty} T_{m\,m} \lambda^{m+1} L^m \Phi^4 \,. \tag{3.3}$$

Generalizing to the multi-coupling case, assuming the two couplings are λ, k, the leading logarithm contribution to V can be written as

$$V_{LL} = \sum_{m=0}^{\infty} \sum_{r=0}^{m} T_{m-r+1,\,r} \lambda^{m-r+1} k^r L^m \Phi^4 \,. \tag{3.4}$$

The form of the multi-coupling case can be further extended to additional couplings for the dark singlet extension model. Because of the Coleman-Weinberg renormalization condition [12, 104]

$$\left.\frac{d^4 V}{d\Phi^4}\right|_{\Phi=\mu} = 24\pi^2 y \,,\; y = \lambda/\pi^2 \,, \tag{3.5}$$

it is only necessary to consider terms up to order L^4 in the effective potential to predict the scalar mass spectrum:

$$V_{LL} = \pi^2 y \Phi^4 + (BL + CL^2 + DL^3 + EL^4)\Phi^4 + \cdots \tag{3.6}$$

where B, C, D, E are (dimensionless) functions of (y, k, x, h), which respectively are the Higgs self-coupling $\lambda = \pi^2 y$, Higgs-dark matter coupling, top quark Yukawa coupling and dark matter self-coupling; these functions have the form $\left(y^\alpha k^\beta x^\gamma h^\delta\right) L^p$ where $p - (\alpha + \beta + \gamma + \delta) = 1$ in the leading logarithm approximation. All other Standard Model contributions such as $SU(2)$, $U(1)$ and $SU(3)$ gauge couplings are numerically sub-dominant [100, 103] and have therefore

been neglected. The effective potential V_{LL} can be determined from the renormalization group equation

$$\left(\mu\frac{\partial}{\partial\mu}+\beta^x\frac{\partial}{\partial x}+\beta^y\frac{\partial}{\partial y}+\beta^k\frac{\partial}{\partial k}+\beta^h\frac{\partial}{\partial h}\right.$$
$$\left.+\gamma_\Phi\Phi\frac{\partial}{\partial\Phi}+\gamma_s S\frac{\partial}{\partial S}\right)V_{LL}=0 \tag{3.7}$$

where the corresponding one loop renormalization group functions are [122]

$$\beta^y=6y^2+3xy-\frac{3}{2}x^2+\frac{k^2}{128\pi^4} \tag{3.8}$$

$$\beta^h=3\frac{h^2}{(4\pi)^2}+12\frac{k^2}{(4\pi)^2} \tag{3.9}$$

$$\beta^k=4\frac{k^2}{(4\pi)^2}+3ky+\frac{kh}{(4\pi)^2}+\frac{3}{2}xk \tag{3.10}$$

$$\beta^x=\frac{9x^2}{4}\,,\ \gamma_\Phi=\frac{3x}{4}\,,\ \gamma_s=0\,. \tag{3.11}$$

Note that $\gamma_s=0$ because the S field has no Yukawa coupling with Standard Model matter fields. Since we only have limited information on the renormalization group functions (to one loop order in the dark singlet model), we need to add counterterms to the effective potential to compensate for information lost due to truncation at LL order

$$V=V_{LL}+K\left(x,y,k,h\right)\Phi^4 \tag{3.12}$$

where $K\Phi^4$ is the counterterm and K is a function of the couplings. The counter terms in the full LL order effective potential can be determined by the Coleman Weinberg condition (3.5).

The coupling constants can be determined from the VEV conditions that spontaneous symmetry breaking will cause a nontrivial minimum in the vacuum structure: $\frac{dV}{d\Phi}|_{\Phi=\mu=v}=0$. Contact with the Standard Model is thus achieved by identifying the scale μ with the electroweak scale $\mu=v=246.2$ GeV. The mass generated for the Higgs doublet M_H and dark singlet M_S are only dependent on the quadratic terms in the effective potential and can be determined respectively from

$$M_H^2=\left.\frac{dV^2}{d\Phi^2}\right|_{\Phi=\mu=v}\quad,\quad M_S^2=\left.k\Phi^2\right|_{\Phi=\mu=v}\,, \tag{3.13}$$

where we have implicitly used the result that the effective potential kinetic term renormalization constant is unity in the Coleman-Weinberg renormalization scheme [12, 104].

To determine the dark matter mass, Higgs mass and the corresponding Higgs coupling y we need to input k and h. However, M_H shows almost no dependence on the values of these couplings in the range $0 < k < 1$ and $0 < h < 1$, with a large suppression of h contributions compared with k. At the one loop level, the predicted Higgs mass is around 216 GeV and Higgs self-coupling is $y = 0.054$ (which is 5 times larger than the Higgs self-coupling in conventional symmetry breaking mechanism indicating the large Higgs coupling regime [14]) for $0 < k < 1$, in close agreement with the one loop order result given in the simplified radiative $O(4)$ model [14, 103]. This implies that the singlet extension has very little effect on the Higgs mass in the considered range of k. This is understandable since the tree-level term $y\Phi^4$ in the Higgs mass contribution is only dependent on y which makes the k contribution to the Higgs mass a sub-leading loop contribution and also since $6y^2 >> \frac{k^2}{128\pi^4}$ in β^y the Higgs-dark coupling k contribution is much smaller compared with the Higgs self-coupling y. Similarly, the dark self-coupling h has an even smaller effect because it must first enter through the Higgs portal. Because of the small effect of the extended sector in the $O(4)$ model calculation, the radiatively-generated Higgs mass prediction can then converge to 125 GeV when the higher loop order contributions are included [14]. Although large values of k are ruled out as dark matter solutions because of extremely small abundances, at one loop level we reproduce the $k \approx 6$ Higgs mass result of Ref. [138].

Dark matter abundance provides a strong constraint on the dark matter mass and the corresponding dark-Higgs coupling. In Fig. 3.1, the curve of dark matter mass intersects the dark matter abundance curves corresponding to a solution for the coupling k and dark matter mass M_s at certain dark matter abundance. The dark matter abundance is calculated using the results of Refs. [139, 125, 140]. However, Refs. [125, 49] have performed a comprehensive analysis of the XENON results [50] in the context of the scalar singlet model (6.2), and apart from a small region of parameter space in the $M_S \approx M_H/2$ resonant region, dark matter masses below 80 GeV are excluded. The resonant fine tuning region near $M_H/2$ is generally considered unnatural, and $M_S < M_H/2$ is already strongly constrained by experimental bounds on the invisible width of the Higgs [141]. We thus focus on the region $M_S > 80\,\text{GeV}$ in Fig. 3.1 which intersects with abundance curves below 35%.

Thus, the sequential scenario of radiative electroweak symmetry-breaking followed by the conventional Higgs mechanism for the dark-singlet model explains less than 35% dark matter abundance with a lower bound of $M_s > 80\,\text{GeV}$ on the dark matter mass and $k > 0.11$ on Higgs-dark matter coupling .

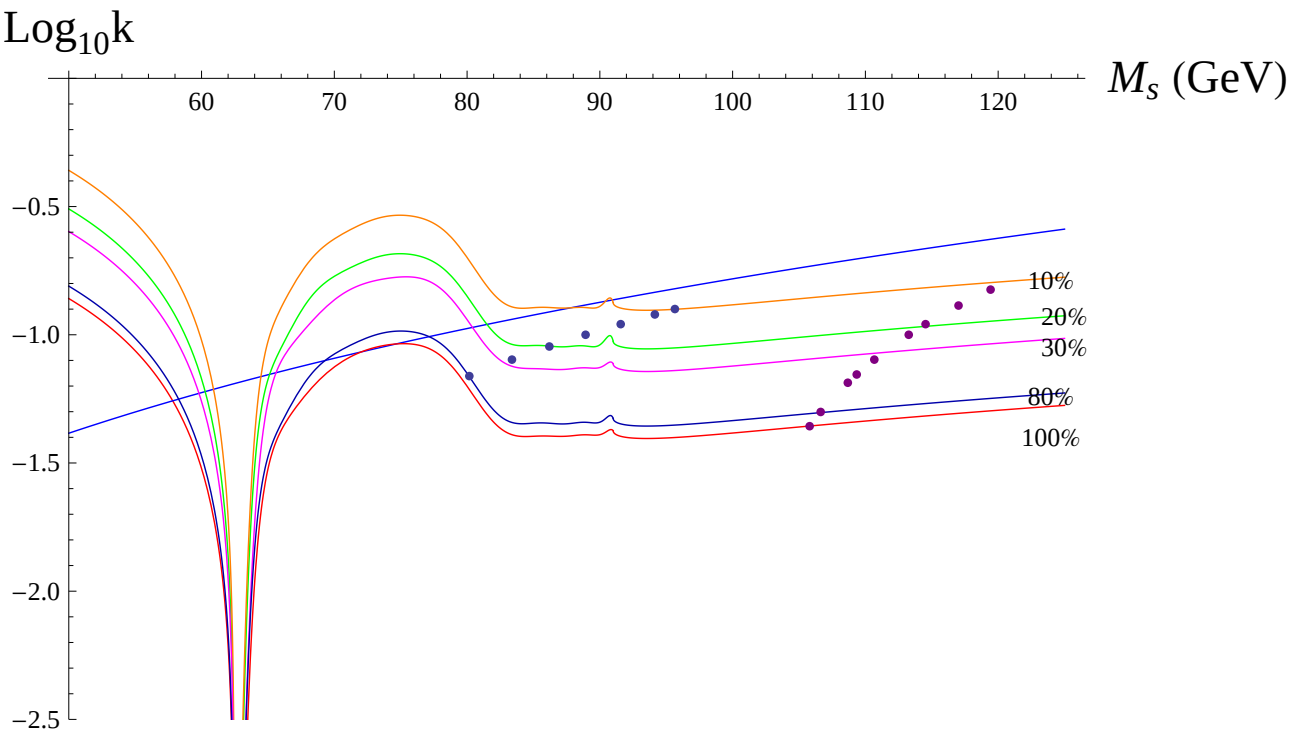

Figure 3.1: The conventional Higgs mechanism relationship between the dark matter mass and the dark-Higgs coupling (blue curve) is shown along with various dark matter abundance curves to constrain the dark singlet model. The points correspond to the dynamical symmetry-breaking approach for both the Higgs and dark fields at one-loop order (right set of points) and estimated higher-loop order (left set of points).

3.3 Dynamical Method

Consider next the alternate scenario where the Higgs and scalar singlet masses are generated simultaneously through radiative electroweak symmetry breaking. Inspired by the approach of Ref. [13], in this case the S field will enter the vacuum structure along with the Higgs doublet as the fifth (gauge neutral) degree of freedom of the scalar field space. However, it should be

noted that though this singlet can be viewed as an extension of the scalar sector, it is different from the Higgs because it is neutral under gauge interaction and does not couple to the quarks and leptons as the Higgs doublet does. In the dynamical case, both the Higgs doublet and dark singlet enter the tree level of the effective potential and the loop corrections are of the form $L = \log\left(\frac{\Phi^2+S^2}{\mu^2}\right)$ [13]. By contrast, in the non-dynamical case only the Higgs doublet enters the tree level effective potential, and loop corrections are of the form $L = \log\left(\frac{\Phi^2}{\mu^2}\right)$ i.e. the S field does not couple directly into the logarithm. The form of the effective potential to one loop order in the dynamical case can be written as [13]

$$\begin{aligned} V_{LL} =& \pi^2 y\Phi^4 + \frac{k}{2}\Phi^2 S^2 + \frac{h}{24}S^2 \\ &+ BL + CL^2 + DL^3 + EL^4 + \ldots \end{aligned} \tag{3.14}$$

where $L \equiv \log\left(\frac{\Phi^2+S^2}{\mu^2}\right)$. The quantities B, C, D, E are the functions of (y, k, x, h, ϕ_i, S) which are dimension-4 combinations of Φ^2 and S^2 as required by $O(4)$ and Z_2 symmetry and contain leading-logarithm combinations of couplings $\left(y^\alpha k^\beta x^\gamma h^\delta\right) L^p$ where $p - (\alpha + \beta + \gamma + \delta) = 1$. It should be noted that $L \equiv \log\left(\frac{\Phi^2+S^2}{\mu^2}\right)$ signals that dark field S affects the vacuum structure along with the Higgs field and works as a fifth scalar degree of freedom within the effective potential. The effective potential V_{LL} can be determined from the renormalization group equation which is given by Eq. (3.7) where the one loop renormalization group functions are the same as Eq. (3.8)–(3.11). It is useful to define $\rho^2 = \Phi^2 + S^2$ [13] and so truncation of the effective potential at LL order

$$V = V_{LL} + K\left(x, y, k, h\right)\rho^4 \tag{3.15}$$

requires the $K\rho^4$ counterterm which can be determined by the Coleman Weinberg condition [12, 104, 142]

$$\left.\frac{d^4V}{d\rho^4}\right|_{\rho=\mu} = \left.\frac{d^4V_{tree}}{d\rho^4}\right|_{\rho=\mu} \tag{3.16}$$

where V_{tree} is the tree level part of the effective potential. The vacuum structure is much more complicated in this case compared with the sequential symmetry-breaking scenario and we need two VEV conditions consisting of one scale constraint and one nontrivial directional constraint

for the minimum of the vacuum [13]

$$\left.\frac{dV}{d\rho}\right|_{\rho=\mu=v} = 0 \quad , \quad \left.\frac{dV}{d\phi_3}\right|_{\substack{\phi_3=\mu=v \\ s=0}} = 0 \tag{3.17}$$

where ϕ_3 is the component of the Higgs doublet that contains the VEV and $\mu = v = 246.2$ GeV to make contact with the Standard Model. The directional constraint $\frac{dV}{dS}|_{\phi_3=\mu,s=0} = 0$ is trivial since it identically vanishes. The dynamical mass generated for the Higgs doublet and dark singlet can be determined respectively from

$$M_H^2 = \left.\frac{dV^2}{d\phi_3^2}\right|_{\substack{\phi_3=\mu=v \\ s=0}} \quad , \quad M_S^2 = \left.\frac{dV^2}{dS^2}\right|_{\substack{\phi_3=\mu=v \\ s=0}} , \tag{3.18}$$

where we have again used the result that the the effective potential kinetic term renormalization constant is unity in the Coleman-Weinberg renormalization scheme [12, 104].

Now we have two VEV constraints, while we have three parameters y, k, h to be determined leaving one unconstrained coupling, which we choose to be k, to parameterize the solutions. As discussed below, we find solutions that are perturbatively-close to $h = 0$. We have chosen to parameterize our solutions through k because Fig. 3.1 shows that the dark matter abundance generally decreases with increasing k. The one-loop results are $0.044 < k < 0.15$ corresponding to scalar singlet mass predictions $106\,\mathrm{GeV} < M_s < 120\,\mathrm{GeV}$ and 10%–100% dark matter abundance (see right-hand set of dots in Fig. 3.1). We also note that there are no one-loop leading-log solutions for $k < 0.03$. The Higgs mass and Higgs self-coupling are remarkably close to the leading-log results of Ref. [14, 103]; hence the extended scalar sector does not destabilize radiative symmetry breaking in the Higgs sector. Comparing with the sequential symmetry-breaking scenario, the dynamical method can provide much higher levels of dark matter abundance at LL order. It is interesting that the solutions lead naturally to a small scalar-singlet self interaction $h = \epsilon_1 y + \epsilon_2 k$ ($\epsilon_i \ll 1$) consistent with astrophysical evidence for weakly self-interacting dark matter [39, 143]. The dark matter abundance condition is surprisingly effective in constraining k and the scalar singlet mass; as shown in Fig. 6 of Ref. [49] the one-loop predictions are in the sensitivity region of the next generation XENON experiment.

The large Higgs self-coupling that results from the dynamical scenario can clearly influence M_s through higher loop effects. Because the solution for M_H and y is very close to the radiatively-broken Standard Model result [33], higher-loop effects from the Higgs portal will

have a negligible effect on M_H and thus the higher-loop extrapolation to $M_H = 125\,\text{GeV}$ [14] will persist. However, these higher-loop corrections from the large Higgs self-coupling could have a similar effect of decreasing the scalar singlet mass. It is important to estimate these higher-loop effects to check if the dark matter mass either decreases far below the 80 GeV lower boundary extracted from the XENON results [125, 49, 50] or requires resonant fine-tuning of M_s and k for acceptable dark matter abundance.

The higher order estimation is based on detailed analysis of contributions to the dark matter mass from the different couplings. Because dark matter abundance constrains k to be small, we assume that corrections beyond leading order to the renormalization group functions are well approximated by the $O(4)$ model. Then using the five loop results for the $O(4)$ renormalization group functions [106] combined with the extrapolation methods of [14], we obtain the following result for the dark matter mass:

$$\begin{aligned} M_s^2 = &-1461.56\left(\frac{k}{0.05}\right)\left(\frac{y}{0.0534}\right) \\ &+ 3025.8\left(\frac{k}{0.05}\right) + 100^2\left(\frac{y}{0.0534}\right)^{1.4}, \end{aligned} \tag{3.19}$$

where we are working in GeV units and the top quark Yukawa coupling contributions are embedded in the numerical coefficients. Only the dominant leading order contributions in k have been retained in (3.19) (i.e. higher order terms in k are numerically suppressed because $k \sim 0.1$). By using this formula, we can estimate the dark matter mass at the convergence value $y = 0.0233, M_{Higgs} = 125$ GeV of Ref. [14]. As discussed earlier, we use the lower-bound $M_s > 80\,\text{GeV}$ which is the lowest mass consistent with analysis of the XENON results [125, 49, 50] without $M_S \approx M_H/2$ resonance fine-tuning. The higher order estimation gives the dark-Higgs coupling $0.07 < k < 0.13$ for dark matter mass $80\,\text{GeV} < M_s < 96\,\text{GeV}$, and dark matter abundance 10%–80% as shown by the left-hand set of dots in Fig. 3.1. In general, the estimated higher-loop effects result in a significant reduction of the dark matter mass compared to the one-loop predictions for comparable levels of abundance.

We have also studied the possibility of spontaneous breaking of the Z_2 symmetry by allowing a non-zero rotation angle in the VEV (i.e., $\langle S\rangle = v\sin\theta$, $\langle\Phi\rangle = v\cos\theta$) and self-consistently determining the couplings in each case using the procedure outlined above. For physical solutions of the couplings, the vacuum energy of the Z_2-symmetric case is always found to be

smaller, providing evidence that Z_2 symmetry remains unbroken.

3.4 Results and Conclusions

We have studied radiative symmetry breaking in an extension of the conformally invariant Standard Model containing a scalar singlet field with a Higgs portal interaction. The sequential symmetry-breaking scenario, where electroweak symmetry-breaking occurs via a large Higgs self coupling and the scalar singlet mass is then generated by the conventional Higgs mechanism, can explain at most 35% of the dark matter abundance without resonant fine-tuning. By contrast, the dynamical approach inspired by Ref. [13], where the electroweak and the Z_2-symmetric scalar-singlet vacuum simultaneously result from radiative symmetry-breaking in the large Higgs-coupling regime can accommodate larger dark matter abundances and results in a weakly self-interacting scalar singlet. Estimating the higher-loop effects needed to maintain consistency with a radiatively-generated 125 GeV Higgs mass dominated by the large Higgs self-coupling leads to the bounds $80\,\mathrm{GeV} < M_s < 96\,\mathrm{GeV}$ and a corresponding dark matter abundance in the range 10%–80%. The dark matter mass and Higgs-portal coupling predictions of the dynamical scenario, both at one-loop and estimated higher-loop levels, are within the range of sensitivity of the next generation of the XENON experiment [125, 49].

Chapter 4

Conformal Complex Singlet Extension of the Standard Model: Scenario for Dark Matter and a Second Higgs

The work presented in this chapter was done in collaboration with Tom Steele, Robert Mann and Tanvir Hanif and has been published in JHEP [16].

In the previous chapter, we have discussed the minimum extension of the SM. In this chapter, we will study the next to minimum extension: the complex singlet extension of the SM. The importance of this model is there exists a global $U(1)$ symmetry in the hidden sector. Compared with the discrete symmetry Z_2 in real singlet case, the continuous symmetry $U(1)$ can be gauged to construct more complicated models such as $U(1)'$ model (discussed in next chapter). In addition, in the previous chapter, we have only studied the case where the symmetry is not broken in the hidden sector while in this chapter, we will provide a more thorough study of the symmetry breaking patterns. We will consider the case where the symmetry in the hidden sector is either broken or unbroken.

The highlights of this chapter are in three points. First, the technique in the previous chapter is further developed. The generalized version of the leading logarithmic summation technique based on the Gildener Weinberg method can be directly employed to the model here, but in this chapter, we will push the technique even further. We have developed the so called generalized optimization method which provides extra constraints in the case where symmetry is broken in the hidden sector. By using the combination of generalized summation technique and the generalized optimization method, we are able to significantly narrow the parameter space and provide unique predictions. Seond, we employ this framework to study the recent

LHC diphoton excesses and found a set of solutions which is testable in the next run of LHC. Thirdly, we have provided a very detail study of the symmetry breaking pattern and some of the features are general and useful in further conformal model building.

4.1 Introduction and Motivation

4.1.1 Abstract

We consider a conformal complex singlet extension of the Standard Model with a Higgs portal interaction. The global $U(1)$ symmetry of the complex singlet can be either broken or unbroken and we study each scenario. In the unbroken case, the global $U(1)$ symmetry protects the complex singlet from decaying, leading to an ideal cold dark matter candidate with approximately 100 GeV mass along with a significant proportion of thermal relic dark matter abundance. In the broken case, we have developed a renormalization-scale optimization technique to significantly narrow the parameter space and in some situations, provide unique predictions for all the model's couplings and masses. We have found there exists a second Higgs boson with a mass of approximately 550 GeV that mixes with the known 125 GeV Higgs with a large mixing angle $\sin\theta \approx 0.47$ consistent with current experimental limits. The imaginary part of the complex singlet in the broken case could provide axion dark matter for a wide range of models. Upon including interactions of the complex scalar with an additional vector-like fermion, we explore the possibility of a diphoton excess in both the unbroken and the broken cases. In the unbroken case, the model can provide a natural explanation for diphoton excess if extra terms are introduced providing extra contributions to the singlet mass. In the broken case, we find a set of coupling solutions that yield a second Higgs boson of mass 720 GeV and an 830 GeV extra vector-like fermion F, which is able to address the 750 GeV LHC diphoton excess. We also provide criteria to determine the symmetry breaking pattern in both the Higgs and hidden sectors.

4.1.2 Introduction

The Standard Model (SM) of particle physics is incomplete since it does not provide an explanation for dark matter. Amongst the numerous ways to go beyond the SM, Higgs portal models [119, 120, 121, 122, 123, 101, 125] are conceptually appealing because they provide a link between Higgs hunting in collider experiments and dark matter direct detection experiments [144]. Complex singlet extensions with global $U(1)$ symmetry yield rich phenomenological properties,

such as a second Higgs particle mixed with the ordinary Higgs particle along with WIMP dark matter candidates [145, 146, 147]. The global $U(1)$ symmetry also provides a foundation for further model-building [148, 34, 149], in particular interactions with an extra vector-like fermion [64, 65] that may explain the LHC diphoton excesses [59, 60].

Versions of hidden sector extensions with classical conformal symmetry are particularly interesting since they can address the hierarchy and naturalness problems [5, 6, 9] associated with the conventional electroweak symmetry breaking mechanism. Conformal symmetry as a custodial symmetry protects the Higgs mass from large UV contributions, which addresses the naturalness problem [9, 6]. In this case, the conformal symmetry can only be softly broken and needs to be restored sufficiently quickly [31]. In addition, if the electroweak symmetry breaking is realized by Coleman-Weinberg (CW) mechanism within conformal models, a natural scale hierarchy is generated through the dimensional transmutation similar to the QCD case [99, 11]. In these models, there exists two main interpretations for the origin of electroweak (EW) symmetry breaking that are usually associated with different ranges of the couplings. In the first, radiative symmetry breaking (RSB, or the Coleman-Weinberg (CW) mechanism [12]) in the hidden (dark) sector gets communicated to the Higgs sector. This triggers EW symmetry breaking via the Higgs portal interaction [126, 127, 128, 129, 130, 131, 132, 133, 35] , which is normally negative (see e.g. Ref. [150]). Alternatively, RSB could occur in the SM Higgs sector first and then be communicated to the hidden sector. In this second interpretation, a reasonably large Higgs quartic coupling is usually required to balance the large top quark Yukawa coupling and a positive Higgs portal interaction is permitted [15, 33, 100, 14].

We consider here two main scenarios depending on whether or not the global $U(1)$ symmetry is spontaneously broken by a vacuum expectation value of the hidden-sector complex field. For the broken $U(1)$ case, we extend the optimization method proposed in [151] to multiple scalar fields to accommodate the addition of a complex-singlet vacuum expectation value. Generalizing this method to incorporate RSB, we find that in addition to the SM Higgs particle, there exists a second Higgs boson with a 554 GeV mass. We also explore including extra vector-like fermions and find a set of viable solutions where the mass of the second Higgs boson increases to around 720 GeV, which is able to address the 750 GeV diphoton anomaly observed at the LHC

[59][60]. This also leads to an axion dark matter candidate whose properties depend on detailed model building. This improved optimization method depends on local properties rather than global searchers, and therefore has very strong predictive power, affording dynamical generation of all the parameters in the model. In the unbroken case, we find a large Higgs self-coupling perturbative regime similar to Refs. [33, 100, 14], along with a scalar dark matter candidate that provides a significant proportion of dark matter abundance. We have also explored the possibility of diphoton excess in the unbroken case and find that a natural explanation of the diphoton excess can be provided only if extra terms are introduced in the singlet (hidden) sector to increase the singlet mass.

4.2 Model

The complex singlet extension of the SM with an extra vector-like fermion F has the Lagrangian [145, 64, 65]:

$$\begin{aligned} L = & \frac{1}{2}\partial_\mu H^\dagger \partial^\mu H + \frac{1}{2}\partial_\mu S^\dagger \partial^\mu S - \lambda_2 |S|^2 H^\dagger H - \lambda_3 |S|^4 \\ & - \lambda_1 \left(H^\dagger H\right)^2 + i\bar{F}\gamma^\mu D_\mu F - \left(y_S \bar{F}_L F_R S + \text{h.c.}\right) \end{aligned} \tag{4.1}$$

where F transforms as $(R_C, R_W)_{Y_F}$, H is the (complex doublet) Higgs field and S is the complex singlet field. Here we assume the diphoton excess is realized through the process $gg \to S \to \gamma\gamma$ where g represents the gluon and two vector-like fermion F loops are required at both the production and decay process. The LHC so far has not provided any hints in other channels, leading to strong upper bounds on other decay channels of the S-resonance [61]. It is therefore crucial that S has no direct interactions with SM fields except via the Higgs portal interaction proportional to λ_2, which prevents the large decay channels of the resonances to the SM particles as well as preventing large suppression of the diphoton excesses by the large decay width of S to top quark $\Gamma_{S\to tt}$ [64]. The above Lagrangian obeys a global $U(1)$ symmetry for S. This symmetry may either be unbroken ($\langle S\rangle = 0$) or broken ($\langle S\rangle \neq 0$), and we consider each case in turn. Note that the diphoton excess will also be dependent on the above symmetry breaking pattern. In the broken case, the singlet S will mix with the SM Higgs, which opens other decay channels of S through the mixing. If the mixing angle is not small enough, the upper bounds

of S decay to other SM particles [61] will be violated.

4.3 Unbroken Phase

For the unbroken case, S decay is protected by the $U(1)$ global symmetry, making it an ideal cold dark matter candidate when y_S is set to zero. In addition, this case may also provide a natural explanation for the diphoton excess when y_S is turned on since S will not mix with the Higgs and the decay channels of S to other SM particles are greatly suppressed. Our analysis builds upon the Gildener-Weinberg method [13] that generalizes the CW technique [12] to incorporate multiple scalar fields. Letting $H = \frac{1}{\sqrt{2}}(\phi_1 + i\phi_2, \phi_3 + i\phi_4)$, $S = \frac{1}{\sqrt{2}}(\varphi_1 + i\varphi_2)$ and defining $\phi^2 = \sum_i \phi_i^2$ and $\varphi^2 = \sum_i \varphi_i^2$, we obtain leading-logarithm expression for the effective potential [15]

$$\begin{aligned} V_{LL} &= \frac{1}{4}\lambda_1\phi^4 + \frac{1}{4}\lambda_2\phi^2\varphi^2 + \frac{1}{4}\lambda_3\varphi^4 \\ &\quad + BL + CL^2 + DL^3 + EL^4 + \dots \end{aligned} \tag{4.2}$$

where $L \equiv \log\left(\frac{\phi^2+\varphi^2}{\mu^2}\right)$. The quantities B, C, D, E are the functions of $(\lambda_1, \lambda_2, \lambda_3, g_t, \phi, \varphi)$ which are dimension-4 combinations of ϕ^2 and φ^2 as required by symmetry and contain leading-logarithm (LL) combinations of couplings $\left(\lambda_1^\alpha \lambda_2^\beta \lambda_3^\gamma g_t^{2\delta}\right) L^p$ where g_t is the top Yukawa coupling and $p - (\alpha + \beta + \gamma + \delta) = 1$. The coefficients B, C, D, E are determined by RG equation

$$\left(\mu\frac{\partial}{\partial\mu} + \beta_{g_t}\frac{\partial}{\partial g_t} + \sum_{i=1}^{3}\beta_i\frac{\partial}{\partial\lambda_i} + \gamma_\phi\phi\frac{\partial}{\partial\phi}\right) V_{LL} = 0 \tag{4.3}$$

where the RG functions β_i, β_{g_t} and anomalous dimensions γ_ϕ are given by [152][65]

$$\begin{aligned} \beta_1 &= \frac{1}{16\pi^2}\left(24\lambda_1^2 + \lambda_2^2 - 6g_t^4 + 12\lambda_1 g_t^2\right) \\ \beta_2 &= \frac{1}{16\pi^2}\lambda_2\left(8\lambda_3 + 12\lambda_1 + 4\lambda_2 + 6g_t^2 + 2R_C R_W y_S^2\right) \\ \beta_3 &= \frac{1}{16\pi^2}\left(2\lambda_2^2 + 20\lambda_3^2 + 2R_C R_W y_S^2\left(2\lambda_3 - y_S^2\right)\right) \\ \beta_{g_t} &= \frac{1}{16\pi^2}\left(\frac{9}{2}g_t^3\right) \quad , \quad \gamma_\phi = \frac{1}{64\pi^2}\left(12g_t^2\right) . \end{aligned} \tag{4.4}$$

and the anomalous dimension for the singlet field $\gamma_\varphi = 0$. Truncation of the effective potential at LL order requires counter terms corresponding to those in the Lagrangian

$$V_{eff} = V_{LL} + K_1\phi^4 + K_2\phi^2\varphi^2 + K_3\varphi^4 \tag{4.5}$$

where K_i are functions of the couplings. Defining $\rho^2 = \phi^2 + \varphi^2$ [13], the three renormalization conditions in CW (or Jackiw) scheme [12, 104] used to determine K_i are conveniently expressed as [142]

$$\left.\frac{d^4 V_{eff}}{d\rho^4}\right|_{\rho=\mu} = \left.\frac{d^4 V_{tree}}{d\rho^4}\right|_{\rho=\mu} \tag{4.6}$$

where V_{tree} is the tree level effective potential.

To determine the couplings, we need to employ the vacuum expectation value (VEV) conditions which provides constraint for the minimum of the vacuum

$$\left.\frac{dV_{eff}}{d\phi}\right|_{\substack{\phi=v\\ \varphi=v_1}} = 0 \quad , \quad \left.\frac{dV_{eff}}{d\varphi}\right|_{\substack{\phi=v\\ \varphi=v_1}} = 0\,. \tag{4.7}$$

where v is identified with the electroweak scale $v = 246.2\,\text{GeV}$. In the unbroken case ($v_1 = 0$), the above singlet VEV condition is trivial since it identically vanishes whereas this is not true in the broken case ($v_1 \neq 0$). In the unbroken case, we also identify μ with the electroweak scale $\mu = v = 246.2$ to eliminate the higher-logarithmic terms. The mass generated for the Higgs doublet M_H and singlet M_S are only dependent on the quadratic terms in the effective potential and can be determined from the eigenvalues of the mass matrix M

$$M = \left.\begin{pmatrix} \frac{dV_{eff}^2}{d\phi^2} & \frac{dV_{eff}^2}{d\phi d\varphi} \\ \frac{dV_{eff}^2}{d\varphi d\phi} & \frac{dV_{eff}^2}{d\varphi^2} \end{pmatrix}\right|_{\substack{\phi=v\\ \varphi=v_1}} \tag{4.8}$$

where in the unbroken case, the off-diagonal terms are zero and we obtain $M_H^2 = \left.\frac{dV_{eff}^2}{d\phi^2}\right|_{\substack{\phi=v\\ \varphi=v_1}}$, $M_S^2 = \left.\frac{dV_{eff}^2}{d\varphi^2}\right|_{\substack{\phi=v\\ \varphi=v_1}}$. Note that we have implicitly used the result that the effective potential kinetic term renormalization constant is unity in the CW scheme [12, 104].

Consider first the unbroken symmetry case with $y_S = 0$ (no contributions from F). Eq. (4.7) only contains one non-trivial constraint, and hence it is not possible to constrain all the couplings. We find that altering the singlet self-interaction coupling within the range $0 < \lambda_3 < 1$ affects the physical dark matter mass predictions by less than 2.4%. We therefore set $\lambda_3 = 0$, corresponding to the case of weakly self-interacting dark matter, commenting on $\lambda_3 \neq 0$ as appropriate. The Higgs portal interaction λ_2 is then the only input parameter; it will be strongly constrained by dark matter abundance and direct detection experiments XENON100 [50] and

LUX [51]. The Higgs mass prediction in this case is consistent with our previous findings and converges to approximately 125 GeV when higher loop contributions are included [15, 14].

We illustrate our predicted dark matter mass/coupling relation in the green curve in Fig. 4.1, which intersects the 10% (orange) and 100% (blue) dark matter abundance curves. These abundance curves are calculated using the results of Refs. [139, 125, 140]. Compared to the real scalar model [15], the complex singlet leads to a higher dark matter abundance because both components of the complex singlet contribute. Setting the dark matter self-interaction coupling to $\lambda_3 = 1$ shifts the results slightly from the green to the purple curve in the figure, retaining this qualitative feature. The shaded region in Fig. 4.1 represents the parameter space excluded by the LUX experiment at 95% CL [51], where we have followed the analysis of [49] and used the most conservative effective Higgs-nucleon coupling [153] in the dark matter nucleon recoil cross section. Most of the parameter space below 85 GeV is ruled out by the LUX experiment [51], apart from a small region of parameter space in the $M_S \approx M_H/2$ resonant region, which is strongly constrained by the Higgs decay width [144, 154] (see Refs. [125, 49] for a comprehensive analysis). Combining the LUX [51] and dark matter abundance constraints, the complex singlet model admits a viable dark matter candidate $100\text{GeV} \leq \text{M}_\text{s} \leq 110\text{GeV}$ with Higgs portal interaction $0.05 \leq \lambda_2 \leq 0.2$ corresponding to $10\% - 100\%$ dark matter abundance. The viable dark matter candidates resulting from our analysis are very close to the boundary of the current direct detection experiments and will be in the detection region of the coming experiments XENON1T [155] and LUX 300 day results [51].

We next consider the unbroken symmetry case with $y_S \neq 0$. The advantage of addressing diphoton excess in the unbroken case is twofold. First, in the unbroken case, there is no mixing between the singlet and the Higgs field, thereby greatly suppressing the decay processes of the S to SM particles, in turn ideally satisfying the bounds in ref.[61]. Second, the SHH term is forbidden by the global $U(1)$ symmetry; consequently the decay channels of the S to SM particles through SHH are prohibited, making this case an even better candidate for satisfying the bounds in [61].

We find when $\lambda_2 \geq 3$, there exist two sets of coupling solutions. More interestingly, there occur two upper bounds for the singlet mass M_S, one for each set of the coupling solutions.

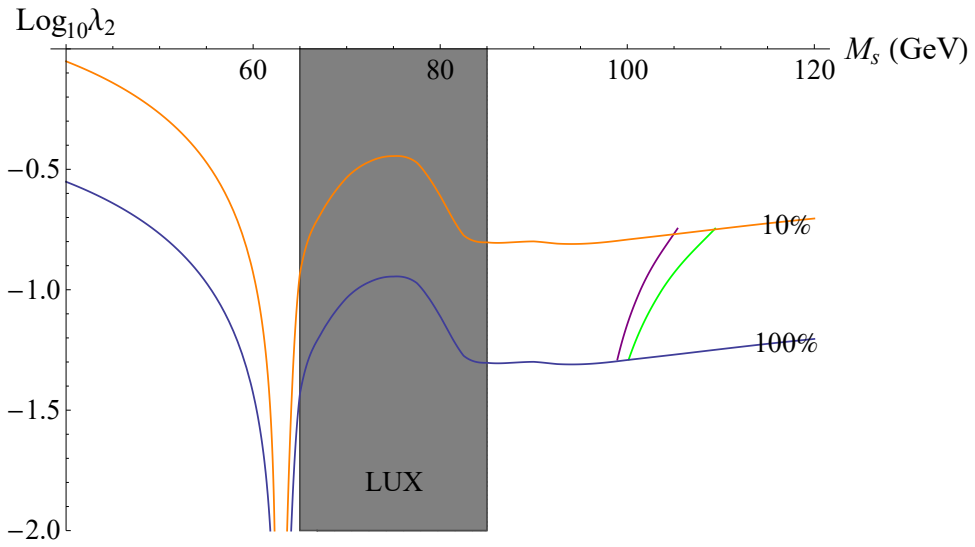

Figure 4.1: Relationship between predicted dark matter mass and Higgs portal coupling λ_2 with $\lambda_3 = 0$ is shown by the green curve and $\lambda_3 = 1$ shown by purple curve along with various dark matter abundance curves 10% in yellow and 100% in blue to constrain the complex singlet model. The shaded region represents the parameter space which is excluded by the LUX experiment at 95% CL.

For the first upper bound, we find $M_S \leq 217\,\text{GeV}$ corresponding to $y_S \sim 0$. The maximal value of the Higgs portal coupling is $\lambda_2 = 5.6$; a larger Higgs portal coupling ($\lambda_2 \geq 5.6$) will be non-perturbative and the above calculation method fails. Moreover, this upper bound will be sensitive to y_S, which decreases the bound. If we set $y_S \sim 1$ we find the upper bound decreases to $M_S \leq 133\,\text{GeV}$. For the second upper bound, we find $M_S \leq 290\,\text{GeV}$, corresponding to $y_S \sim 0$ and a Higgs portal coupling of $\lambda_2 = 4.5$. This upper bound is also be sensitive to y_S; at $y_S \sim 1$ it decreases to $M_S \leq 247\,\text{GeV}$.

It is therefore almost impossible to push the singlet mass to 750 GeV for which the system possesses exact conformal symmetry with the global $U(1)$ symmetry unbroken. To address the diphoton excess, we will have to extend our model and introduce extra terms that provide extra contributions to the singlet mass (e.g. another scalar portal couples to the singlet). A sample set of coupling solutions to address the 7 fb diphoton rate will be $y_S = 1.35,\ \lambda_1 = 2,\ \lambda_3 = 0,\ \lambda_2 = 2$ with the corresponding vector-like fermion mass at $M_F \sim 830\,\text{GeV}$ and the charge assignment $(R_C, R_W)_{Y_F} = (3,2)_{\frac{7}{6}}$. The predicted singlet mass is only around 90 GeV; an extra term is required to contribute the remaining 660 GeV in order to properly address the 750 GeV

diphoton excess.

4.4 Broken Phase

The broken-symmetry case $\langle S \rangle \neq 0$ is particularly interesting since the real component of the complex singlet will mix with the SM Higgs field, leading to one heavy and one light Higgs field. The light state corresponds to the 125 GeV observed Higgs boson [96, 97] and the heavy state can potentially explain the recently observed 750 GeV diphoton resonance [59, 60] following the argument in [64]. In this situation dark matter is associated with an axion decoupled from the effective potential, which in turn does not provide dark matter phenomenological constraints on the coupling present in the unbroken case. Consequently the guiding principles used to extract a meaningful range of the free parameter space of (λ_2, λ_3) that remains after imposing Eqs. (4.7) are lost. To address this difficulty, we generalize our unbroken-symmetry methodology to incorporate a renormalization-scale optimization technique [151]. This technique was used to obtain an optimized renormalization scale in the MSSM with conventional symmetry breaking (CSB) [151], and is based on the idea that the complete effective potential should be scale independent. Since we do not have full information about the effective potential, which must be truncated at a particular loop order, the best that can be achieved is to find an optimized scale at which the scale-dependent minimum of the truncated effective potential self-consistently satisfies its RG equation.

It is nontrivial to generalize this optimization method to incorporate RSB. In the CSB scenario of the SM, all the couplings are known , and we only need to implement these known couplings as initial values and use the renormalization-group to run the couplings with the scale. The optimized scale is then explicitly determined by the point where the minimum of the effective potential satisfies its RG equation [151]. However, in the case of RSB, all the couplings are unknown and should be determined dynamically from the theory itself [12]. Without boundary values for the running couplings an intractable non-linear numerical problem occurs in determining the optimized scale. To address this difficulty we modify the optimization method to only depend on local quantities near the optimized scale, and define the scale-

dependent minima $H_m(t)$ and $S_m(t)$ of the effective potential via

$$F\left(H_m(t), S_m(t), t, \lambda_i(t)\right) = \left.\frac{dV_{eff}}{dH}\right|_{\substack{H=H_m(t)\\S=S_m(t)}} = 0\,, \tag{4.9}$$

$$G\left(H_m(t), S_m(t), t, \lambda_i(t)\right) = \left.\frac{dV_{eff}}{dS}\right|_{\substack{H=H_m(t)\\S=S_m(t)}} = 0\,, \tag{4.10}$$

where $\mu = M_z \exp(t)$. We then differentiate these constraints with respect to t, and impose the condition [151]

$$\frac{dH_m(t*)}{dt} = -\gamma(t*)H_m(t*)\,,\ \frac{dS_m(t*)}{dt} = 0 \tag{4.11}$$

for the optimized scale $t*$, resulting in the two constraints

$$0 = \frac{\partial F}{\partial t^*} - \gamma(t*)H_m(t^*)\frac{\partial F}{\partial H_m} + \beta_i(t^*)\frac{\partial F}{\partial \lambda_i}\,, \tag{4.12}$$

$$0 = \frac{\partial G}{\partial t^*} - \gamma(t*)H_m(t^*)\frac{\partial G}{\partial H_m} + \beta_i(t^*)\frac{\partial G}{\partial \lambda_i}\ . \tag{4.13}$$

Finally we connect the optimized minimum field configurations with the physical VEVs

$$H_m(t^*) = \langle H\rangle = v\,,\ S_m(t^*) = v_1\,. \tag{4.14}$$

Thus rather than requiring a global solution for $H_m(t)$ and $S_m(t)$ that is then used to determine t^* via (4.11), we have encoded the same information into the local constraints (4.12),(4.13) and the RG functions of the theory [152]. Note that the CW renormalization condition (4.6) is unaffected except for the replacement $\mu = M_Z \exp(t^*)$. It should be noted that in the case discussed in [151], only one optimization condition for the Higgs field is needed since they assumed supersymmetry is at a much higher scale and decoupled from the SM. We have generalized this optimization condition for both the Higgs and singlet fields, since the vacuum expectation value predicted here for the singlet may be near the electroweak scale, which cannot be decoupled. The above optimization conditions can be generalized further for more complicated models with multiple scalar fields.

Setting $y_S = 0$, we have four constraints (4.7), (4.12), (4.13) for five parameters $\lambda_1(t^*), \lambda_2(t^*)$, $\lambda_3(t^*), v_1, t^*$ where $\langle S\rangle = v_1$ is the VEV of the singlet field. Using the 125 GeV Higgs mass as an extra constraint, we find $\lambda_1(t^*) = 0.53,\ \lambda_3(t^*) = 1.926,\ \lambda_2(t^*) = -2.95,\ \langle S\rangle = 156\,\text{GeV},\ \text{t}^* =$

-1.59 yielding an additional heavy Higgs at 554 GeV. The small scale $t^* = -1.59$ results from CW to MS scheme transformation $\mu_{CW} = \mu_{MS}/\lambda$ [18, 107], naturally leading to $\mu_{CW} \leq \mu_{MS}$. We have also studied these couplings to assess their perturbative convergence using two loop RG functions [156]. We found $\beta_1^{2loop}/\beta_1^{1loop} = 5 \times 10^{-5},\ \beta_2^{2loop}/\beta_2^{1loop} = 0.04,\ \beta_3^{2loop}/\beta_3^{1loop} = 0.13$, which implies that higher-loop contributions are under control. Numerically similar Higgs portal couplings in two doublet models were found in Ref. [11]. The mixing angle is strongly constrained by the LHC and electroweak precision measurements [53] where LHC Higgs signal rates provide the strongest constraint $\sin\theta \leq 0.5$ in the region around a 500 GeV Higgs mass. In our model, we find a mixing angle $\sin\theta = 0.467$, within the LHC run 2 detection region and not yet excluded. Note that higher loop effects might decrease the mixing angle further or alter the mass prediction of the heavier Higgs.

We now set $y_S \neq 0$ and impose the constraints (4.7), (4.12), (4.13), requiring a 125 GeV Higgs mass and a second Higgs in the 750 GeV range. With these six constraints we find $y_S(t^*) = 1.35,\ \lambda_1(t^*) = 1.73,\ \lambda_3(t^*) = 1.45,\ \lambda_2(t^*) = -3.2,\ \langle S\rangle = 270\,\text{GeV},\ \text{t}^* = -0.55$ and the second Higgs to have mass 720 GeV. Moreover, using the 7 fb fit value of the rate of the 750 GeV resonant production and decay to diphotons with the charge assignment $(R_C, R_W)_{Y_F} = (3,2)_{\frac{7}{6}}$ for the vector like fermion F [64], we obtain a value of 830 GeV for its mass M_F. The 830 GeV vector-like fermion mass satisfies the lower bounds 600 GeV–800 GeV provided in [157]. Note that this value cannot be purely generated by the singlet fermion Yukawa term, since the y_S Yukawa term only contributes 256 GeV to M_F and a bare mass term is required. Thus, all the parameters in the system are determined. The mixing angle predicted in this case is $\sin\theta = 0.67$, which satisfies the upper bounds ($\sin\theta \sim 0.7$) of LHC SM Higgs searches and EW observables (S, T, U) for a second Higgs at 750 GeV provided in [53]. Further experimental results for the diphoton excess especially the searching of S decay channels to other SM particles will soon tell whether this scenario is viable [61]. As a conclusion, our results of a 720 GeV second Higgs mass, 830 GeV vector-like fermion and a mixing angle of $\sin\theta = 0.67$ are compatible with the current experimental bounds to address the 7 fb LHC diphoton excess. Note also that we have used the strongest version of the optimization method with Eq. (4.7), (4.12), (4.13).

When the real component of the complex singlet obtains a VEV, the $U(1)$ global symmetry

is spontaneously broken and generates a massless Goldstone boson containing the imaginary degree of freedom of the complex singlet. The complex singlet is conventionally written as $S(x) = \phi(x) \exp\left(\frac{ia(x)}{\sqrt{2}f_a}\right)$ where $a(x)$ is the axion field and f_a is the axion decay constant. Associating the $U(1)$ global symmetry with the Peccei-Quinn PQ symmetry [158, 159], the above Goldstone boson can be explained as the axion [160, 161] which addresses the dark matter problem. Normally, a large intermediate scale is required to connect to the large PQ symmetry breaking scale to address the smallness of the axion coupling. However, any intermediate scale between the EW scale and UV scale is not allowed in the CW mechanism [9, 162]. In [160, 161], the authors cleverly connect the smallness of the axion coupling to the lightness of the neutrino mass and generate an effective large f_a without introducing any large intermediate scale. Moreover, the $U(1)$ global symmetry considered in this work could also be made into a local symmetry, providing a new gauge interaction boson Z′; symmetry breaking at the TeV scale in this model was studied in Ref. [34].

It is interesting to analyze the underlying symmetry breaking mechanism for the broken case. We use the ratio of the tree-level VEV conditions as a measure of whether CSB or RSB is dominant. The ratio r is defined by

$$r = \left.\frac{dV_{tree}/d\phi^2}{dV_{tree}/d\varphi^2}\right|_{\substack{\phi=v \\ \varphi=v_1}} = \frac{2\lambda_1\left(\frac{v^2}{v_1^2}\right) + \lambda_2}{2\lambda_3 + \lambda_2\left(\frac{v^2}{v_1^2}\right)} \tag{4.15}$$

where $r \ll 1, r \gg 1, r \simeq 1$ correspond to CSB dominant in the Higgs sector, RSB dominant in the Higgs sector and the mixed scenario respectively. In the mixed scenario both CSB and RSB contribute to the EW symmetry breaking and we are not able to separate one from the other. Inputting the results $\lambda_1 = 0.53$, $\lambda_3 = 1.926, \lambda_2 = -2.95, \langle S \rangle = 156\,\text{GeV}$ of the broken case, we obtain $r = 0.1$ which implies conventional EW symmetry breaking in the Higgs sector triggered by the CW mechanism in the hidden sector. Note that the Higgs quartic coupling $\lambda_1 = 0.53$ obtained in our case is around four times larger than the SM one which is $\lambda_{\text{SM}} = 0.13$ implying large radiative corrections in the Higgs sector.

4.5 Results and Conclusions

In summary, we have studied a conformally symmetric complex singlet extension of the SM with a Higgs portal interaction, whose global $U(1)$ symmetry is spontaneously broken or unbroken. In the unbroken case, radiative EW symmetry breaking in the SM Higgs sector is induced by the CW mechanism [12]. The complex singlet is protected from decay, making it an ideal $\sim 100\,\text{GeV}$ dark matter candidate comprising a significant proportion of the thermal relic abundance that is within the detection region of the upcoming XENON1T [155] and LUX 300 day [51] experiments. Including an extra vector-like fermion F, this case can also provide an ideal explanation for diphoton excesses without violating the experimental bounds only if extra terms are introduced to increase the singlet mass. In the broken case, generalizing and improving upon the optimization method inspired by [151], we found a sequential symmetry breaking scenario, in which RSB in the singlet sector triggers conventional EW symmetry breaking in the Higgs sector. We found there exists a second Higgs boson with an approximate $550\,\text{GeV}$ mass and a mixing angle $\sin\theta \approx 0.47$, which satisfies the current experiment bound $\sin\theta \leq 0.5$ at around $500\,\text{GeV}$ Higgs mass region provided by the LHC signal rates [53] that will be strengthened during LHC run 2. Moreover, including the extra vector-like fermion F we find a set of coupling solutions where the second Higgs boson mass increases to around $720\,\text{GeV}$ and the extra vector-like fermion mass is $830\,\text{GeV}$, addressing the $750\,\text{GeV}$ diphoton anomaly observed at the LHC [59, 60].

Scenarios	Dark Matter	Diphoton Excess	Second Higgs	$\sin\theta$
Unbroken; $y_S = 0$	Yes; Cold	No	No	0
Unbroken; $y_S \neq 0$	No	No; Singlet mass too small	No	0
Broken; $y_S = 0$	Yes; Axion	No	Yes; $550\,\text{GeV}$	0.47
Broken; $y_S \neq 0$	No	Yes	Yes; $720\,\text{GeV}$	0.67

Table 4.1: Two categories (unbroken and broken phase) and four scenarios (each phase with either $y_S = 0$ or $y_S \neq 0$ where y_S is the scalar-vector like fermion coupling) are summarized in the table where $\sin\theta$ corresponds to the mixing angle between the Higgs field and the singlet.

Chapter 5

Asymptotic Safety in the Conformal Hidden Sector?

The work presented in this chapter was done in collaboration with Tom Steele, Robert Mann and Fred Sage and has been submitted to Phys. Rev. D [17]. I have played a major role in motivation (initial ideas), calculations and writing the manuscript except for the dark matter section which is mostly finished by Fred Sage.

In the previous chapter, we have studied the complex singlet extension of the SM where there exists a global $U(1)$ symmetry in the hidden sector. In this chapter, we add further complication and gauge the global $U(1)$ symmetry leading to a famous $U(1)'$ model. Note that the detailed construction of a $U(1)'$ model depends on the charge assignments which are further constrained by the anomaly cancellations. In this work, in order to address the recent LHC diboson excess, we select the leptophobic $U(1)'$ model.

In addition, in the previous chapters, when we use the notion of conformal symmetry we always mean the model satisfies the classically conformal symmetry. In this work, we have strengthened this idea and clarified that the classically conformal symmetry actually means the model satisfying the conformal symmetry at a UV scale implying that the couplings in the model run into a fixed point at a UV scale. In this way, the conformal symmetry of the model becomes a certain UV boundary condition. We make a connection between the fixed point in the conformal theory and the fixed point in asymptotic safety theory (asymptotic safety was originally proposed by Steven Weinberg [163]). Thus, the conformal theory obtains the good property to be valid to an arbitrarily high energy scale. Due to the above insights, we employ a different technique (rather than leading logarithmic summation technique) to solve the system:

the RG running of the couplings. Technically, the technique we have employed is to solve the RG equation of the running couplings satisfying certain UV boundary conditions. By using this technique, we find the UV boundary conditions can substantially influence the EW/ TeV scale physics and we take the recent LHC diboson excess as a detailed realization of our framework. In the context of leptophobic $U(1)'$ model, we find one of the AS boundary conditions may address the diboson excess and it will be testable in the LHC run 2.

5.1 Introduction and Motivation

5.1.1 Abstract

We combine the notion of asymptotic safety (AS) with conformal invariance in a hidden sector beyond the Standard Model. We use the renormalization group (RG) equations as a bridge to connect UV boundary conditions and EW/TeV scale physics and furnish a detailed example in the context of a leptophobic $U(1)'$ model to address the diboson excess recently observed at the LHC. Investigating a broad selection of UV boundary conditions corresponding to differing AS scenarios, we find that AS scenarios have very strong predictive power, allowing unique determination of most of the parameters in the model. We obtain the interrelationships among the couplings, the transition scale of the fixed point M_{UV} and the generations of quarks coupled to the Z', and especially the correlation between M_{UV} and the top quark Yukawa coupling Y_t. We find one of the AS boundary conditions provides a diboson excess of around 4 fb, which is close to the current best fit value. In addition, this model also admits dark matter with a mass around $M_{Z'}/2$.

5.1.2 Introduction

Recently the ATLAS collaboration reported excesses in the search for a resonance that decays into a pair of standard model (SM) gauge bosons [164]. The narrow width excesses were observed around 2 TeV in the WZ, WW and ZZ channels, with local significance of 3.4σ, 2.6σ, and 2.9σ respectively [164]. Interestingly, at around 1.8 TeV the CMS collaboration also observed excesses in the dijet distributions with a significance of 2.2σ [165]. Other ideas have been proposed to address these excesses [167, 166, 168]. Although the excesses reported by the ATLAS collaboration are in the WZ, WW and ZZ channels, the ability to accurately distinguish between gauge bosons is still very limited, implying the possibility that a new 2 TeV

particle contributes to only one of the channels, with the peaks in the other channels being contaminations due to incomplete tagging selections (see e.g. [166] for a very clear description). Based on this idea, in this article we only focus on the excess in the ZZ channel, where Z' models become excellent candidates [169, 170, 171].

According to Bardeen's insight, conformal symmetry as a custodial symmetry protects Higgs mass from large UV contributions [9] addressing the naturalness problem [6]. Such a possibility can be realized if the conformal symmetry is only softly broken and is restored sufficiently quickly requiring the couplings run into a fixed point at a high energy scale using the renormalization group equation [31]. Moreover, the Coleman–Weinberg (CW) mechanism [12] can dynamically generate the natural scale hierarchies between the unification scale and the electroweak (EW) scale through the dimensional transmutation which is similar to QCD [99, 11]. In this work, we make a connection of the fixed point required in the conformal scenario to the notion of asymptotic safety which also requires a fixed point and is originally proposed to make the SM plus gravity valid up to arbitrary high energy scales without any singularities [175, 176]. Since there is no non-trivial fixed point within the SM, the requirement of a fixed point within the conformal scenario provides an excellent motivation for extending the SM. Although different versions of the extensions of the SM with classical conformal symmetry have been proposed [14, 15, 16, 18, 34, 35, 126, 128, 129, 130, 131, 132, 133, 150, 172, 173, 174], none have incorporated asymptotic safety (AS). In this paper, we implement the AS principle in conformal hidden sector models and apply this to a detailed example of a leptophobic $U(1)'$ model to address the diboson excess and possible dark matter candidate.

In this paper, we regard asymptotic safety as providing deep motivation for the existing non-AS flat scenarios proposed in [177], with an emphasis on the fixed points of the scalar couplings below the singularity to avoid Landau poles and provide a stable Higgs vacuum. We provide a categorization of different AS scenarios according to the gravity contribution to the RG functions above Planck scale. We use RG equation as a bridge to connect the UV boundary conditions to EW/TeV scale physics and explore implications for the SM observables. The predictive power of AS scenarios implies that most of the parameters in the model are uniquely determined, thereby providing interesting interrelationships among the couplings, the

scale of the fixed point (transition scale) M_{UV}, and the generations of quarks coupled to the Z'. Furthermore, it is not necessary to associate the transition scale M_{UV} with the Planck scale; indeed we find that M_{UV} is very sensitive to the top quark Yukawa coupling Y_t and for a fixed Y_t, there exists an interesting range of M_{UV}. In addition, we find diboson excesses are also sensitive to Y_t and correlations among M_{UV}, Y_t and diboson excesses are provided. We find one of the AS boundary conditions provides a diboson excess of around 4 fb, which is close to the current best fit value of 5 fb [167, 166]. This requires a top quark Yukawa coupling $Y_t = 0.954$ which is consistent with current bounds (see e.g. [178]), and a transition scale $M_{UV} = 1.85 \times 10^{11}\,\text{GeV}$, which is much lower than the Planck scale. Note that to avoid large threshold contributions to the Higgs mass, we assume there is no extra-heavy particles at the transition scale M_{UV}. The model also admits the possibility of a dark sector that interacts with the Z' through a purely vector coupling. We provide a brief discussion of the potential of this model to address the dark matter problem.

5.2 Theoretic Framework

We investigate the conformally symmetric complex singlet extension of the SM with an extra $U(1)'$ gauge coupling. The Lagrangian of the scalar sector is written as

$$L = D_\mu H^\dagger D^\mu H + D_\mu S^\dagger D^\mu S - \lambda_2 |S|^2 H^\dagger H - \lambda_3 |S|^4 - \lambda_1 \left(H^\dagger H\right)^2, \tag{5.1}$$

where H is the SM Higgs doublet, S is the complex singlet and D_μ is the extended covariant derivative. In the basis where the two $U(1)$ gauge kinetic terms are diagonal, the covariant derivative term is written as [177, 56]

$$D_\mu = \partial_\mu - i g_3 \frac{\lambda_a}{2} G^a_\mu - i g_2 \frac{\tau_i}{2} W^i_\mu - i Y \left(g_Y B_\mu + g_m B'_\mu\right) - i g' Q'_B B'_\mu, \tag{5.2}$$

where g_3, g_2, g_Y and g' are the gauge couplings of $SU(3)_c$, $SU(2)$, $U(1)_Y$ and $U(1)'$ respectively. The quantities Y and Q'_B denote the $U(1)_Y$ hypercharge and the $U(1)'$ charge. Note that since we focus on the leptophobic model, we choose a special case of the gauge group $U(1)'_{B-xL}$ where $x = 0$ and the gauge group in our case can be denoted $U(1)'_B$ with charge Q'_B [171]. To construct an anomaly free model, a right handed neutrino is needed, its mass arising from a Majorana

Yukawa coupling to the singlet [171, 177]: $L_M = -Y_M^{ij}\bar{\nu_{Ri}^c}\nu_{Rj}S + (\text{h.c.})$. For convenience, we list the charge assignments of the $U(1)'_B$ model in Table 5.1, where ψ_L^l and ψ_L^e are spectator particles required for anomaly cancellation. A more general set of charge assignments can be found in [171].

fermion	q_L	u_R	d_R	l_L	e_R	ν_R	ψ_L^l	ψ_L^e
$U(1)_B$	1/3	1/3	1/3	0	0	-1	-1	-1

Table 5.1: Fermion gauge charges.

At a particular high energy scale, gravity will affect the SM running coupling (see [175] for more details):

$$\beta_j = \beta_j^{\text{SM}} + \beta_j^{\text{grav}}\,. \tag{5.3}$$

For SM gauge couplings and the top quark Yukawa coupling, it has been shown that the gravity contribution to the RG functions is negative i.e. $\beta_j^{\text{grav}} < 0$ [175]. Thus, all SM gauge couplings and top Yukawa coupling are asymptotically safe and valid to arbitrarily high energy scales. However, for the SM Higgs quartic coupling, the gravity contribution is positive i.e. $\beta_{\lambda_1}^{\text{grav}} > 0$ [179]. Thus, to realize the asymptotic safety scenario, we require the Higgs quartic coupling λ_1 to reach a fixed point i.e. $\lambda_1(M_{UV}) = 0, \beta_{\lambda_1}(M_{UV}) = 0$, which provides a stable Higgs vacuum. In the complex singlet extension of the SM, the boundary conditions at the UV scale can be categorized according to the gravity contribution to the singlet quartic and Higgs portal running couplings λ_3 and λ_2 respectively. For $\beta_{\lambda_2}^{\text{grav}} > 0$, this implies the fixed point conditions $\lambda_2(M_{UV}) = 0,\ \beta_{\lambda_2}(M_{UV}) = 0$; however, $\beta_{\lambda_2}(M_{UV}) = 0$ is not consistent with (5.7) and (5.11). From Eq. (5.10), $\beta_{\lambda_2}(M_{UV}) = 0$ implies $g_m(M_{UV})\, g'(M_{UV}) = 0$. If $g'(M_{UV}) = 0$, g' will be negative below the scale M_{UV} since $\beta_{g'} > 0$, while if $g_m(M_{UV}) = 0$, the coupling λ_2 will run very slowly from M_{UV} to the EW scale, leading to a λ_2 at EW scale too small to satisify (5.7) and (5.11).

We therefore only consider $\beta_{\lambda_2}^{\text{grav}} < 0$. Although λ_2 consequently need not run into a fixed point at M_{UV}, it might still be of interest to consider $\lambda_2(M_{UV}) = 0$ as one of the conditions where the Higgs portal interaction is purely radiatively generated. We therefore focus on the

following three boundary conditions corresponding to different AS scenarios:

$$\beta_{\lambda_1}(\Lambda) = \beta_{\lambda_3}(\Lambda) = \lambda_1(\Lambda) = \lambda_2(\Lambda) = \lambda_3(\Lambda) = 0 \tag{5.4}$$

$$\beta_{\lambda_1}(\Lambda) = \lambda_1(\Lambda) = 0;\ \lambda_2(\Lambda),\ \lambda_3(\Lambda) \neq 0 \tag{5.5}$$

$$\beta_{\lambda_1}(\Lambda) = \lambda_1(\Lambda) = \lambda_2(\Lambda) = 0,\ \lambda_3(\Lambda) \neq 0 \tag{5.6}$$

where the UV scale $\Lambda \equiv M_{UV}$ is not necessarily the Planck scale M_{pl}. The cases (5.4), (5.5), (5.6) respectively correspond to $\beta_{\lambda_3}^{\text{grav}} > 0$, $\beta_{\lambda_3}^{\text{grav}} < 0$, $\beta_{\lambda_3}^{\text{grav}} < 0$. We begin with (5.4), which is particularly interesting because it has the strongest predictive power of the three scenarios, determining all parameters in the model.

In scenario (5.4), radiative symmetry breaking first occurs in the singlet sector at a very high energy scale v_1 through the CW mechanism [12] and then is communicated to the Higgs sector to trigger EW symmetry breaking associated with a small Higgs portal interaction (inversely proportional to v_1). We are thus able to study these two sectors separately. Letting $H = \frac{1}{\sqrt{2}}(\phi_1 + i\phi_2, \phi_3 + i\phi_4)$, $S = \frac{1}{\sqrt{2}}(\varphi_1 + i\varphi_2)$ and defining $\phi^2 = \sum_i \phi_i^2$ and $\varphi^2 = \sum_i \varphi_i^2$, we obtain the vacuum expectation value (VEV) condition of the Higgs sector $\frac{dV_{Higgs}}{d\phi}\big|_{\substack{\phi=v \\ \varphi=v_1}} = 0$, where $V_{Higgs} = \frac{1}{4}\lambda_1\phi^4 + \frac{1}{4}\lambda_2\phi^2\varphi^2$ is the Higgs effective potential and v, v_1 are identified with the electroweak scale $v = 246\,\text{GeV}$ and the singlet broken scale v_1 respectively. We only use the tree level Higgs effective potential because conventional symmetry breaking is completely determined by the tree level VEV condition. Combining the Higgs sector VEV condition with the 125 GeV Higgs mass observed [96, 97], we obtain

$$2v^2\lambda_1 = -v_1^2\lambda_2 = M_H^2\ , \tag{5.7}$$

where $M_H = 125\,\text{GeV}$ is the Higgs mass and λ_1, λ_2 are evaluated at the EW scale.

To realize radiative symmetry breaking in the singlet sector, we consider the one loop RG improvement of the singlet effective potential

$$V_S = \frac{1}{4}\lambda_3(t)\,G^4(t)\,\varphi^4 = \frac{1}{4}\lambda_3(t)\,G^4(t)\,v_1^4\exp(t)^4\ , \tag{5.8}$$

where $t \equiv \log(\varphi/v_1)$ with the renormalization scale at the VEV of the singlet, $G(t) \equiv \exp\left[-\int_0^t dt'\gamma(t')\right]$ and $\lambda_3(t)$ is the running singlet self-coupling. The VEV condition of the

singlet is defined by

$$\left.\frac{dV}{d\varphi}\right|_{\varphi=v_1} = \left(\frac{e^{-t}}{v_1}\right)\left.\frac{dV_{\rm S}}{dt}\right|_{t=0} = 0\ , \tag{5.9}$$

where t=0 corresponds to the singlet broken scale v_1. The RG functions are obtained using the formula in [177] with charge assignments in Table 5.1 and the assumption that Z' only couples to the first generation of quarks (discussed below) while the anomalous dimension is provided in [180]. At one loop level for the beyond-SM part and three loop level for the SM part, they are written as:

$$\begin{aligned}
16\pi^2\beta_{\lambda_1} &= \lambda_2^2 - 3\lambda_1 g_m^2 + \frac{3}{8}g_m^4 + \beta_{\lambda_1}^{SM} \\
16\pi^2\beta_{\lambda_2} &= 12 g_m^2 g'^2 + 6Y_t^2\lambda_2 - 24 g'^2\lambda_2 + 4Y_M^2\lambda_2 + 4\lambda_2^2 + 12\lambda_1\lambda_2 + 8\lambda_2\lambda_3 - \frac{3}{2}\lambda_2\left(g_m^2 + 3g_2^2 + g_1^2\right) \\
6\pi^2\beta_{\lambda_3} &= 96 g'^4 - 16Y_M^4 + 2\lambda_2^2 - \lambda_3\left(48 g'^2 + 8Y_M^2 + 20\lambda_3\right) \\
16\pi^2\beta_{Y_t} &= -\frac{17}{12}Y_t g_m^2 - \frac{2}{3}Y_t g'^2 - \frac{5}{3}Y_t g' g_m + \beta_{Y_t}^{SM} \\
16\pi^2\beta_{g'} &= \frac{1}{18}g'\left(76 g'^2 + 64 g' g_m + 123 g_m^2\right) \\
16\pi^2\beta_{g_m} &= g_m\left(\frac{41}{6}\left(g_m^2 + 2g_1^2\right) + \frac{38}{9}g'^2\right) + \frac{32}{3}g'\left(g_m^2 + g_1^2\right) \\
16\pi^2\beta_{Y_M} &= -6Y_M g'^2 + 6Y_M^3;\quad 32\pi^2\gamma_\varphi = Y_M^2 - 24 g'^2
\end{aligned} \tag{5.10}$$

where $\beta_{\lambda_1}^{SM}$ and $\beta_{Y_t}^{SM}$ are the three loop SM RG functions provided in [181]. Three-loop SM RG functions are necessary because higher-loop contributions from Y_t are too large to be ignored, while the effects of hidden-sector couplings are small enough to be well-approximated by the one-loop RG functions. We also include a 2 TeV Z' mass constraint [164, 165]

$$M_{Z'} = 2g'(0)\, v_1 = 2\,\text{TeV}\,. \tag{5.11}$$

We now solve the RG equations with the UV boundary conditions (5.4) using the RG functions (5.10), reducing the system of nine unknowns (λ_1, λ_2, λ_3, g', g_m, Y_M, Y_t, v_1, M_{UV}) to that of five (g_m, v_1, Y_M, Y_t, M_{UV}) by employing the constraints (5.7), (5.9), (5.11). Our solutions are shown in I of Table 5.2. Interestingly, we find $M_{UV} \sim M_{pl}$ and the predicted $Y_t = 0.93$ to be very close to the current experimental central value $Y_t^c = 0.936$ [181].

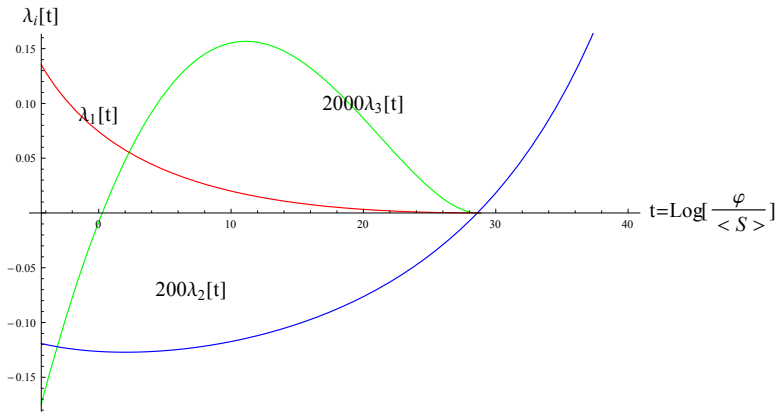

Figure 5.1: Running scalar couplings are shown as a function of the scale $t = \log(\varphi/\langle S \rangle)$. The red, blue, and green curves represent $\lambda_1(t)$, $200\lambda_2(t)$, $2000\lambda_3(t)$ respectively.

We plot the running scalar couplings from the EW scale to the Planck scale in Figure 5.1. To satisfy the boundary condition (5.4), Z' can only couple to at most two generations of quarks, a point also emphasized in [177] for the $U(1)_{B-L}$ model. This is because, the more generations of quarks Z' couples to, the larger $\beta_{g'}$ would be. Large $\beta_{g'}$ leads to fast running of λ_3, which is not consistent with the slow running of λ_3 required to satisfy the boundary conditions (5.4); see also Figure 5.1. Thus, we assume Z' only couples to the first generation of quarks. While it might be interesting to assume Z' only couples to the third generation of quarks, this would heavily suppress the Z' production rate at the LHC, forbidding observation of the dibson excess.

The singlet quartic coupling λ_3, from the Planck scale to the EW scale, runs from positive to negative. The transition point where λ_3 runs to zero defines the singlet broken scale v_1 by the CW mechanism [12], a point also emphasized in [150]. It might seem surprising that the singlet quartic coupling can run to negative values. However, the true effective coupling defined as $\lambda_{eff} = \frac{e^{-4t}}{v_1^4}\frac{d^4 V_s}{dt^4}|_{t=0}$ provides a positive effective coupling value of $\lambda_{eff}(0) = 1.2 \times 10^{-4}$. In addition, we are able to show the singlet mass predictions in both MS scheme and CW scheme are within 2% difference implying the consistency in both schemes.

Using the above results, we can study whether or not this conformal $U(1)'$ model in an AS scenario can account for the diboson excess. The production cross section of Z' at the LHC8

is estimated to be [169, 170, 166]

$$\sigma\left(pp \to Z'\right) \simeq 5.2 \left(\frac{2\Gamma\left(Z' \to u\bar{u}\right) + \Gamma\left(Z' \to d\bar{d}\right)}{\text{GeV}} \right), \tag{5.12}$$

where the Z' decay modes to quarks are given by [166]. For the diboson decay mode, we have

$$\Gamma\left(Z' \to WW\right) = \frac{g_m^2}{48\pi} Y_H^2 M_{Z'}, \tag{5.13}$$

where Y_H is the hypercharge of the Higgs field. The mixing angle of Z and Z' is strongly constrained by the electroweak precision measurements. In our leptophobic model, this constraint is $\sin\theta \leq 0.008$ [182] and our coupling solutions are comfortably within the constraint. Using (5.12)(5.13) with the coupling solutions shown in I of Table 5.2

, we obtain $\sigma\left(pp \to Z'\right) \times \text{BR}\left(\text{Z}' \to \text{WW}\right) = 0.034$ fb which is a hundred times smaller than the best fit of around 5 fb [167, 166] indicating a tension with the large diboson excess at 2 TeV.

A larger diboson excess requires large (g', g_m), especially a large g_m, in tension with the conditions $\lambda_2\left(M_{UV}\right) = 0$ and $\lambda_3\left(M_{UV}\right) = 0$ in (5.4). To satisfy the condition $\lambda_2\left(M_{UV}\right) = 0$, since running coupling λ_2 is governed by (g', g_m), a large (g', g_m) will lead to a large Higgs portal interaction λ_2 which results in a small singlet VEV using Eq. (5.7). A small singlet VEV will be too small to provide a 2 TeV Z' mass since $M_{Z'} = 2g'\left(t\right)v_1$. Moreover, a larger ($g'$, g_m) will force the singlet quartic coupling λ_3 to keep increasing rather than run into a fixed point at M_{UV}, violating $\lambda_3\left(M_{UV}\right) = 0$. Thus, to satisfy Eq. (5.4), small (g', g_m) are required.

To overcome this tension, consider the alternative boundary condition (5.5). In this case, we arbitrarily set $Y_M = 0$ since it only governs the running of λ_3 and does not affect other parameters in the model. We also input very small g'. Only by setting $Y_M \sim 0$ will the vacuum in the singlet sector be UV stable and IR unstable, consistent with radiative symmetry breaking in the singlet sector. The system has seven unknowns (λ_1, λ_2, λ_3, g', g_m, $\langle S\rangle$, M_{UV}), where we choose M_{UV} as output and Y_t as input to illustrate the sensitivity between the unification scale and the top quark Yukawa coupling. Using the constraints (5.7), (5.9), and (5.11), we are able to simplify the system to a problem of finding the three unknowns (g_m, $\langle S\rangle$, M_{UV}). The boundary condition (5.5) provides two constraints and one more constraint is necessary to fully determine the system. We find for a particular input Y_t, there exists a range for M_{UV}. For $g_m/g' \ll 1$, we obtain the maximum M_{UV} while for $g_m/g' \gg 1$ we obtain the minimum M_{UV}.

We choose the extra constraint that the system provides the minimum M_{UV} with a particular input Y_t, thereby uniquely determining all parameters. Note that when $g_m/g' \gg 1$, we also have the maximum diboson excess. Although we want g' as small as possible, we can not directly set $g' = 0$ since it breaks the condition (5.11). Instead we set $g' = 0.0001$, and find that from $g' = 0.001$ to $g' = 0.0001$, M_{UV} varies less than 0.1%. The correlation between the input value of Y_t and the corresponding M_{UV} is depicted in the blue curve in Figure 5.2, indicating M_{UV} is very sensitive to Y_t. In addition, using (5.12)(5.13), we also obtain the correlation between the input value of Y_t and the corresponding diboson excesses shown in the purple curve (the upper one is for Z' coupled to one generation of quarks while the lower one is for three generations) in Figure 5.2. With input $Y_t = 0.954$ which is 2% larger than the central value $Y_t^c = 0.936$ [181] and is viable (see e.g. [178]), we obtain the diboson excesses at 4 fb which is very close to the best fit value of 5 fb [167, 166] and the corresponding transition scale at $M_{UV} = 1.8 \times 10^{11}$ GeV where some new physics may occur. The coupling solutions with input $Y_t = 0.93$ and $Y_t = 0.954$ are shown in IIa and IIb of Table 5.2 respectively.

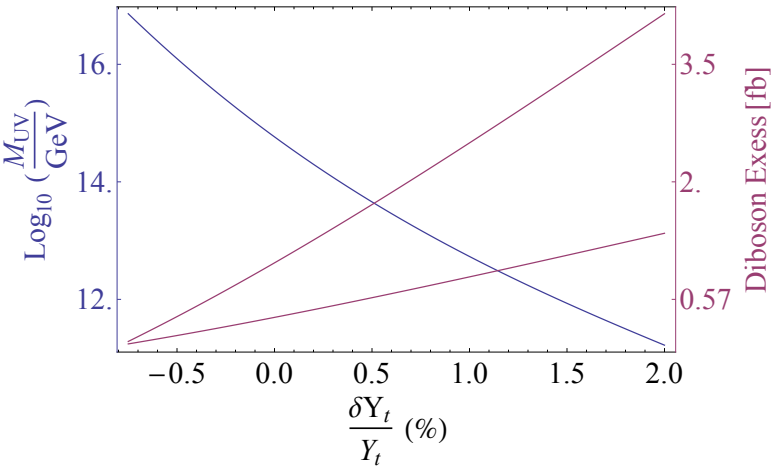

Figure 5.2: The correlation between the transition scale M_{UV} and the top Yukawa coupling Y_t is shown in blue while the correlation between the diboson excess and Y_t is shown in red. δY_t is defined as the deviation from the central experimental value $\delta Y_t = Y_t - Y_t^c$.

BC	$10^4\lambda_2$	$10^4\lambda_3$	g'	g_m	Y_M	Y_t	v_1	ex
I	-6	-0.8	0.18	0.034	0.28	0.93	5.1	0.03
III	-1.6	-3	0.1	0.045	0.1	0.93	9.8	0.01
BC	$10^9\lambda_2$	$10^{16}\lambda_3$	$10^3 g'$	g_m	Y_M	Y_t	$10^{-6}v_1$	ex
IIa	-0.17	-7.07	0.1	0.1	0	0.93	9.5	0.23
IIb	-0.17	-7.07	0.1	0.37	0	0.954	9.5	4

Table 5.2: This table summarizes all the coupling solutions and VEV of the singlet v_1 in TeV units according to the boundary conditions (BC) and scenarios (I–III) are respectively based on BC (5.4–5.6). The diboson excesses (ex) with one generation of quarks coupled to Z' in fb units are also included. a/b represent different solutions in the same AS scenario.

5.3 Dark Matter Possibility

The model admits a Dirac fermion charged under $U(1)'$ that can act as cold dark matter. We briefly discuss the properties of such a fermion χ in that context. The coupling between the fermion and the Z' will be governed by the coupling g' and the fermion charge, which we take to be purely vector (thereby avoiding introduction of new anomalies) and set $Q'_B = 1$ for simplicity. The Z' will interact with quarks through their vector and axial $U(1)'$ and $U(1)_Y$ charges. The basic form of the interaction is $\sum_i \bar{q}_i \gamma^\mu Z'_\mu \left(v_i - a_i \gamma^5\right) q_i$ [183, 184]. For each of the scenarios presented in Table 5.2, using the charges in Table 5.1, we compute the thermally averaged annihilation cross section of the dark fermion (using only the dominant contribution of $\chi\bar{\chi} \to Z' \to q\bar{q}$; the cross section has been reported in [184]) and compare these cross sections to the annihilation cross section required to reproduce the observed dark matter abundance as estimated in [139]. The cross sections for scenarios I and III are plotted in Figure 5.3 for a range of dark fermion masses using the couplings in Table 5.2. The small couplings g' in the scenarios IIa and IIb prevent them from reproducing the required abundance in this model. These results are largely insensitive to the properties of the right handed neutrinos included in this model. Our results indicate that the dark fermion can satisfy the required abundance constraints to be a thermal relic in a mass region around $M_{Z'}/2$. Using the expressions for the

nuclear recoil cross section in [184], we find this resonance is only slightly above the mass range ruled out by the XENON100 experiment [50]. If our model is correct, a signal should be seen by the next generation liquid noble gas detectors [185].

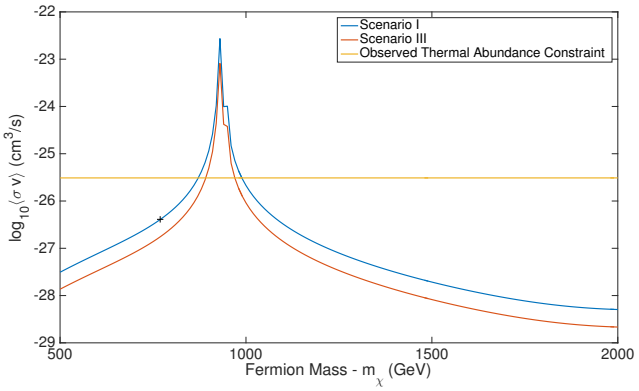

Figure 5.3: The thermally averaged annihilation cross sections for scenarios I and III in Table 5.2 are plotted against the fermion mass m_χ. Also included is the cross section required to reproduce the observed cold dark matter abundance, following the estimation procedure in [139]. The markers + indicate lower bounds on the fermion mass from XENON100 for scenario I.

5.4 Results and Conclusions

Table 5.2 categorizes the different AS scenarios we explored. Their strong predictive power allows determination of most of the parameters in the model and allows us to find their inter-relationships, especially the correlations among M_{UV}, Y_t and diboson excesses.

To conclude, we have shown that different UV boundary conditions can substantially affect electroweak/ TeV scale physics, via the very different coupling solutions shown in table 5.2. We find that one of the AS scenarios IIb can explain diboson excesses of 4 fb albeit with a slightly larger top Yukawa coupling $Y_t = 0.954$ and a much lower transition scale $M_{UV} = 1.8 \times 10^{11}$ GeV. In addition, this model also admits a dark matter particle with a mass around $\frac{1}{2}M_{Z'}$. The framework we have provided is broad and far-reaching, making it possible to investigate other new LHC phenomena with corresponding UV physics/boundary conditions. This will be the subject of future research.

Chapter 6

Multi-scale Renormalization Group Methods for Effective Potentials with Multiple Scalar Fields

The work presented in this chapter was done in collaboration with Tom Steele, and Gerry McKeon and has been published in Phys. Rev. D [18].

In chapter 3 and chapter 4, we have developed the generalized leading logarithmic summation technique for multiple scalar fields based on the Gildener Weinberg method which itself is a generalization of the Coleman Weinberg mechanism. However, the Gildener Weinberg method itself has limitations which have not been emphasized seriously in the previous chapters. Firstly, the Gildener Weinberg method normally assumes the couplings are small. However, from chapter 1, we notice that radiative symmetry breaking in the Higgs sector normally requires a large perturbative coupling. Although the summation technique implemented is based on the RG equation which is able to optimize the couplings, the Gildener Weinberg method is still realized approximatedly in our case. Secondly, the Gildener Weinberg method is normally used to provide a mass prediction of the scalon which in our case is attached to the Higgs leading to a Higgs mass prediction. However, we have also pushed this method further to provide a mass prediction of the singlet, where part of the information may be lost due to the simplification of the form of the logarithm. Thus, the singlet mass prediction based on the Gildener Weinberg method is an approximation. However, we are able to prove (not shown in this thesis) that the singlet mass prediction based on the Gildener Weinberg method (in the broken case) is very close to the mass prediction when the full information of the logarithmic terms are included. In this chapter, we will develop a multi-scale renormalization group method which addresses

the above two points (small coupling approximation and missing information of the logarithmic terms) at once. By introducing an extra renormalization scale, we are able to map the effective potential onto an RG-equivalent form with a certain symmetric structure along a particular trajectory in the multiple renormalization-scale space. The effective potential can be simplified into a form where the logarithmic terms possessing the exact form as the one we have implemented in Gildener Weinberg method. However, in this case, the form of the logarithmic terms are exact rather than approximation and there is no small coupling assumption required. The method we have developed can be useful to simplify the calculation of effective potential.

6.1 Introduction and Motivation

6.1.1 Abstract

Multi-scale renormalization group (RG) methods are reviewed and applied to the analysis of the effective potential for radiative symmetry breaking with multiple scalar fields, allowing an extension of the Gildener & Weinberg (GW) method beyond the weak coupling limit. A model containing two interacting real scalar fields is used to illustrate multi-scale RG methods and the multi-scale RG functions of this model are calculated to one-loop order for the β function and two-loop order for the anomalous mass dimension. The introduction of an extra renormalization scale allows the mapping of the effective potential in this model onto an RG-equivalent form with an $O(2)$ symmetric structure along a particular trajectory in the multiple renormalization-scale space, leading to a simplified form of the effective potential. It is demonstrated that the physical content of the effective potential in the original model, referenced to a single conventional renormalization scale, can be extracted from a particular RG-trajectory that connects to this multi-scale $O(2)$-symmetric form of the effective potential. Extensions of these multi-scale methods for effective potentials in models containing multiple scalars with $O(M) \times O(N)$ symmetry are also discussed.

6.1.2 Introduction

Following the discovery of the Higgs boson [96, 97], one of the most important outstanding challenges in particle physics is to reveal the underlying mechanism for spontaneous electroweak (EW) symmetry breaking. Amongst the numerous underlying mechanisms, radiative symmetry breaking where spontaneous symmetry breaking can occur through loop (radiative) corrections

to the effective potential with a conformal invariant tree-level Lagrangian [12] is conceptually appealing since it addresses aspects of the hierarchy and fine-tuning problems [5, 9]. The Higgs mass is protected by classical scale invariance in the radiative Higgs loop corrections [9, 6], and similar to dimensional transmutation in QCD, leads to natural scale hierarchies in a unification context [99, 11]. It has been demonstrated by Gildener & Weinberg (GW) that the above mechanism can be generalized to incorporate arbitrary numbers of elementary scalars beyond the single Higgs EW doublet of the conventional minimal Higgs sector [186]. The GW approach is very useful in models with Higgs portal interactions which lead to natural dark matter predictions [126, 127, 128, 129, 131, 187, 130, 132, 133, 35, 134, 135, 136, 137, 15]. However, the GW approach has the limitation that the scalars should be weakly coupled [186, 188, 35]. This limitation of GW methods precludes analyses of multi-scalar extensions of interesting radiative EW symmetry-breaking scenarios [33, 101], including those that can describe a 125 GeV Higgs boson [14]. For example, extensions of the Coleman-Weinberg (CW) effective potential [12] with an additional heavy Higgs doublet require a large coupling between the two doublets [11].

In this article, we use multi-scale renormalization group methods [188, 189] to extend the GW method beyond the weak coupling regime. With the introduction of an extra renormalization scale, we are able to choose a particular trajectory in the multiple renormalization-scale space which results in the GW form of logarithmic terms in the effective potential. The resulting simplification facilitates typical renormalization-group (RG) analyses of effective potentials [36] and allows higher-loop calculations of the effective potential using only the RG functions of the theory [33, 100, 11, 105, 14]. To make connection with the physical content of the theory referenced to a conventional single renormalization scale, we map the multi-scale couplings onto a physical trajectory in the renormalization-scale space to extract solutions for the physical predictions.

In Section 6.2 we apply the multiple-renormalization scale methods of Ref. [188, 189] to a theory of two interacting real scalars, obtaining the multi-scale RG functions and verifying some self-consistency requirements of the approach. In Section 6.3, we study the effective potential in the conformal limit of this model to illustrate how the GW method can be extended using multi-scale RG methods. Generalizations to other models are discussed in Section 6.4.

6.2 Multi-scale Renormaliztion Group Equation

Any conformal invariance present in a classical renormalizable field theory is broken by radiative corrections as the process of renormalization inevitably results in the introduction of a non-physical parameter with the dimension of mass. Any change in this parameter must be accompanied by a corresponding change in the quantities that characterize the theory (the couplings, masses, and fields). This results in Green's functions satisfying the RG equation. Satisfying this equation ensures that physical processes are not dependent on the choice of mass scale; one compensates for explicit dependence on the mass scale by having implicit dependence on the mass scale through the couplings, masses and fields that are present [190, 191, 192, 193, 194, 195, 196, 197, 198].

It is apparent that there are widely varying mass scales in nature; the electroweak, strong, grand unified and gravitational mass scales differ by orders of magnitude. This has resulted in a discussion in the literature on how the effective potential (and subsequent spontaneous symmetry breaking it includes) can have different mass scales [188, 189]. The most convenient approach to the problem is through using the so-called "minimal subtraction" (MS) approach to renormalization [192, 197, 198]; this is a mass-independent renormalization scheme that employs dimensional regularization (DR) [199].

In this MS scheme, a bare coupling g_B^i is dimensionful as it appears in an n-dimensional Lagrangian. If this is a renormalizable scalar coupling in four dimensions, then g_B^i is expanded in powers of the renormalized couplings g_R^j (which are dimensionless)

$$g_B^i = \mu^{-\epsilon}\left(g_R^i + \sum_{\nu=1}^{\infty}\frac{a_v^i\left(g_R^j\right)}{\epsilon^\nu}\right) \quad (\epsilon = n-4)\ . \tag{6.1}$$

The massive parameter μ is the renormalization scale mentioned above; its contribution to Green's functions cannot be physical and this observation that results in the RG equation.

In what follows, we consider the approach of [188, 189] to multi-scale problems and replace the single parameter μ in (6.1) with a series of parameters μ_i a separate one for each coupling. As none of these parameters are physical, each results in its own RG equation.

For purposes of illustration, we consider a model with two scalars ϕ_1 and ϕ_2 in four dimensions possessing the symmetries $\phi_1 \leftrightarrow \phi_2$ and $\phi_i \rightarrow -\phi_i$. The simplest renormalizable model with these properties has the action

$$S = \int d^4x \left[\frac{1}{2} \left(\partial_\mu \phi_1\right)^2 + \frac{1}{2} \left(\partial_\mu \phi_2\right)^2 - \frac{m_B^2}{2} \left(\phi_1^2 + \phi_2^2\right) - \frac{\lambda_B}{4!} \left(\phi_1^4 + \phi_2^4\right) - \frac{g_B}{2!2!} \phi_1^2 \phi_2^2 - \Lambda \right] \quad (6.2)$$

where Λ is a cosmological term [200]. If one employs DR with different mass scales for the couplings λ_B and g_B, then

$$\lambda_B = \mu_\lambda^{-\epsilon} \left(\lambda_R + \sum_{\nu=1}^{\infty} \frac{a_\nu}{\epsilon^\nu} \right) \quad (6.3)$$

$$g_B = \mu_g^{-\epsilon} \left(g_R + \sum_{\nu=1}^{\infty} \frac{b_\nu}{\epsilon^\nu} \right) \quad (6.4)$$

$$m_B^2 = m_R^2 \left(1 + \sum_{\nu=1}^{\infty} \frac{c_\nu}{\epsilon^\nu} \right) \quad (6.5)$$

If $\mu_\lambda = \mu_g$, then a_ν, b_ν and c_ν are dependent only on λ_R and g_R [192, 193, 197, 198]. However, in general, these functions also acquire a dependence on $l = \log \left[\frac{\mu_g^2}{\mu_\lambda^2} \right]$.

The bare quantities are independent of μ_λ and μ_g. This means that in order for Eqs. (6.3)–(6.5) to be satisfied, the renormalized quantities depend on μ_λ and μ_g; this dependency results in the expansions

$$\mu_\lambda \frac{\partial \lambda_R}{\partial \mu_\lambda} = \sum_{\nu=0}^{\infty} x_\nu^{\lambda/\lambda} \epsilon^\nu \quad (6.6)$$

$$\mu_\lambda \frac{\partial g_R}{\partial \mu_\lambda} = \sum_{\nu=0}^{\infty} x_\nu^{g/\lambda} \epsilon^\nu \quad (6.7)$$

$$\mu_\lambda \frac{\partial m_R^2}{\partial \mu_\lambda} = \sum_{\nu=0}^{\infty} x_\nu^{m/\lambda} \epsilon^\nu \quad (6.8)$$

with similar expansions for derivatives with respect to μ_g for these renormalized quantities.

Following ref.[197, 198], we find from Eq. (6.3) that

$$\begin{aligned} \mu_\lambda \frac{d\lambda_B}{d\mu_\lambda} = 0 = \mu_\lambda^{-\epsilon} \Bigg[& \left(1 + \sum_{\nu=1}^{\infty} \frac{a_{\nu,\lambda}}{\epsilon} \right) \left(\sum_{\nu=0}^{\infty} x_\nu^{\lambda/\lambda} \epsilon^\nu \right) + \left(\sum_{\nu=1}^{\infty} \frac{a_{\nu,g}}{\epsilon^\nu} \right) \left(\sum_{\nu=0}^{\infty} x_\nu^{g/\lambda} \epsilon^\nu \right) \\ & - 2 \left(\sum_{\nu=1}^{\infty} \frac{a_{\nu,l}}{\epsilon^\nu} \right) - \epsilon \left(\lambda_R + \sum_{\nu=1}^{\infty} \frac{a_\nu}{\epsilon^\nu} \right) \Bigg] \end{aligned} \quad (6.9)$$

If now $x_\nu^{i/j} = 0$ for $\nu > 1$, then at order ϵ, Eq. (6.9) shows that

$$x_1^{\lambda/\lambda} = \lambda_R \tag{6.10}$$

and consequently at order ϵ^0, it follows that

$$x_0^{\lambda/\lambda} = a_1 - \lambda_R a_{1,\lambda} - x_1^{g/\lambda} a_{1,g}\,. \tag{6.11}$$

In a similar fashion, we find that

$$\begin{aligned}
x_1^{g/g} &= g_R \\
x_0^{g/g} &= b_1 - g_R b_{1,g} - x_1^{\lambda/g} b_{1,\lambda} \\
x_1^{g/\lambda} &= x_1^{\lambda/g} = x_1^{m/\lambda} = x_1^{m/g} = 0 \\
x_0^{\lambda/g} &= -g_R a_{1,g} \\
x_0^{g/\lambda} &= -\lambda_R b_{1,\lambda} \\
x_0^{m/\lambda} &= -m_R^2 \lambda_R c_{1,\lambda} \\
x_0^{m/g} &= -m_R^2 g_R c_{1,g}
\end{aligned} \tag{6.12}$$

If terms of order $\epsilon^{-\nu}$ ($\nu \geq 1$) are considered in Eq. (6.9) and its analogues, we find consistency conditions that are to be satisfied for the functions a_ν, b_ν and c_ν. For example, at order ϵ^{-1}, the equation for $\mu_\lambda \frac{dm_B^2}{d\mu_\lambda} = 0$ results in having

$$\begin{aligned}
-\lambda_R c_{1,\lambda} c_1 + c_{1,\lambda}\left(a_1 - \lambda_R a_{1,\lambda}\right) + \lambda_R c_{2,\lambda} \\
-\lambda_R b_{1,\lambda} c_{1,g} - 2c_{1,l} = 0
\end{aligned} \tag{6.13}$$

From Eq. (6.10)-(6.12) it follows that in the $\epsilon = 0$ limit,

$$\begin{aligned}
\mu_\lambda \frac{\partial \lambda_R}{\partial \mu_\lambda} &= a_1 - \lambda_R a_{1,\lambda} \\
\mu_g \frac{\partial g_R}{\partial \mu_g} &= b_1 - g_R b_{1,g} \\
\mu_\lambda \frac{\partial g_R}{\partial \mu_\lambda} &= -\lambda_R b_{1,\lambda} \\
\mu_g \frac{\partial \lambda_R}{\partial \mu_g} &= g_R a_{1,g} \\
\mu_\lambda \frac{\partial m_R^2}{\partial \mu_\lambda} &= -m_R^2 \lambda_R c_{1,\lambda} \\
\mu_g \frac{\partial m_R^2}{\partial \mu_g} &= -m_R^2 g_R c_{1,g}
\end{aligned} \tag{6.14}$$

If we were to have $\mu_\lambda = \mu_g = \mu$ at the outset, then [192, 197, 198] we find that

$$\begin{aligned}
\mu\frac{d\lambda_R}{d\mu} &= a_1 - \lambda_R a_{1,\lambda} - g_R a_{1,g} \\
\mu\frac{dg_R}{d\mu} &= b_1 - g_R b_{1,g} - \lambda_R b_{1,\lambda} \\
\mu\frac{dm_R^2}{d\mu} &= -m_R^2\left(\lambda_R c_{1,\lambda} + g_R c_{1,g}\right) .
\end{aligned} \tag{6.15}$$

We now will follow ref.[197] and compute the coefficients a_1, b_1, c_1 to the second order in the couplings. The relevant Feynman diagrams are shown in Figs. 6.1–6.3. The results keeping terms of order $\frac{1}{\epsilon}, \frac{1}{\epsilon^2}$ are shown in Table 6.1 and in the equations below. We express our results in terms of renormalized quantities.

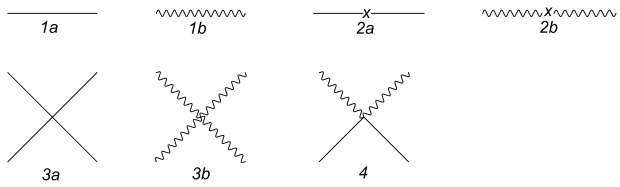

Figure 6.1: Tree level Feynman diagrams are shown for the action (6.2). The solid line represents ϕ_1 and wavy line represents ϕ_2.

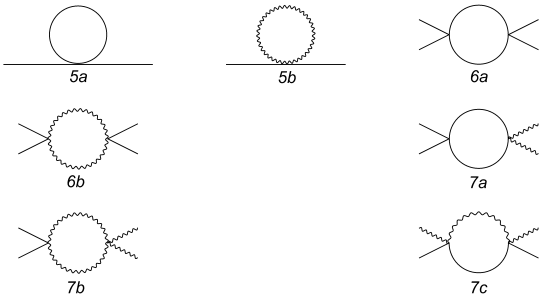

Figure 6.2: One loop level Feynman diagrams for the two point Green functions and four point Green functions.

$$\begin{aligned}
\text{diag.}\,(5a,b) =& \frac{im_R^2}{(4\pi)^2\epsilon^2}\left(3\lambda_R^2 + 2\lambda_R g_R + 7g_R^2\right) + \frac{im_R^2}{\epsilon}\Bigg[\frac{-\left(\lambda_R + g_R\right)}{(4\pi)^2} \\
&+ \frac{1}{(4\pi)^4}\Bigg(\frac{1}{2}\left(\gamma - 1\right)\left(3\lambda_R^2 + 2\lambda_R g_R + 7g_R^2\right) + \frac{1}{2}\Bigg(3\left(\lambda_R^2 + g_R^2\right)\log\frac{m_R^2}{4\pi\mu_\lambda^2} \\
&+ 2\left(\lambda_R g_R + 2g_R^2\right)\log\frac{m_R^2}{4\pi\mu_g^2}\Bigg)\Bigg)\Bigg]
\end{aligned} \tag{6.16}$$

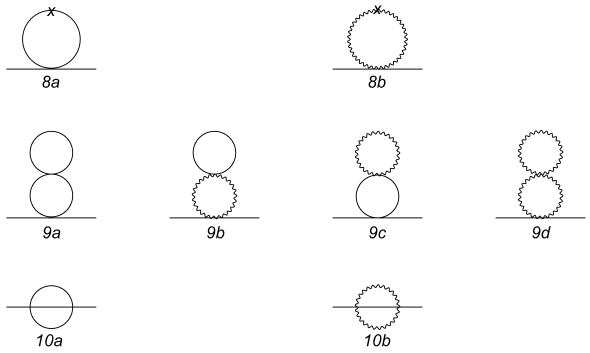

Figure 6.3: Feynman diagrams for two loop order mass anomalous dimension.

diag. $(1a, b)$	$\frac{i}{k^2 - m_R^2}$
diag. $(2a, b)$	$-i\left(m_B^2 - m_R^2\right)$
diag. $(3a, b)$	$-i\lambda_B$
diag. (4)	$-ig_B$
diag. $(6a, b)$	$\frac{-3i\left(\lambda_R^2 + g_R^2\right)}{(4\pi)^2 \epsilon}$
diag. $(7a, b, c)$	$\frac{-2i\left(\lambda_R^2 g_R + 2g_R^2\right)}{(4\pi)^2 \epsilon}$

Table 6.1: Feynman diagram results for tree level and one loop level.

$$\text{diag.}\,(8a, b) = \frac{i m_R^2}{(4\pi)^2}\left[\frac{\left(\lambda_R + g_R\right)^2}{\epsilon^2} + \frac{1}{\epsilon}\left(\frac{\gamma}{2}\left(\lambda_R + g_R\right)^2 + \left(\lambda_R + g_R\right)\left(\lambda_R \log\frac{m_R^2}{4\pi\mu_\lambda^2} + g_R \log\frac{m_R^2}{4\pi\mu_g^2}\right)\right)\right] \tag{6.17}$$

$$\begin{aligned}\text{diag.}\,(9a, b, c, d) = \frac{-i m_R^2}{(4\pi)^4}\Bigg[\frac{\left(\lambda_R + g_R\right)^2}{\epsilon^2} + \frac{1}{\epsilon}\Bigg(&\left(\lambda_R + g_R\right)^2\left(\gamma - \frac{1}{2}\right) \\ &+ \left(\lambda_R + g_R\right)\left(\lambda_R \log\frac{m_R^2}{4\pi\mu_\lambda^2} + g_R \log\frac{m_R^2}{4\pi\mu_g^2}\right)\Bigg)\Bigg]\end{aligned} \tag{6.18}$$

$$\begin{aligned}\text{diag.}\,(10a, b) = \frac{i}{(4\pi)^4}\Bigg[&-\frac{m_R^2}{\epsilon^2}\left(\lambda_R^2 + 3g_R^2\right) + \frac{1}{\epsilon}\Bigg(-\frac{1}{2}p^2\left(\frac{\lambda_R^2}{6} + \frac{g_R^2}{2}\right) \\ &+ m_R^2\left(-\gamma + \frac{3}{2}\right)\left(\lambda_R^2 + 3g_R^2\right) - m_R^2\left(\lambda_R^2 \log\frac{m_R^2}{4\pi\mu_\lambda^2} + 3g_R^2 \log\frac{m_R^2}{4\pi\mu_g^2}\right)\Bigg)\Bigg]\end{aligned} \tag{6.19}$$

The integrals and renormalization conventions we use are in refs. [197, 198]. We found from

the one-loop four point function and the one and two-loop two point functions that

$$\begin{aligned}
\lambda_B &= \mu_\lambda^{-\epsilon}\left[\lambda_R - \frac{3}{(4\pi)^2\,\epsilon}\left(\lambda_R^2+g_R^2\right)\right]\\
g_B &= \mu_g^{-\epsilon}\left[g_R - \frac{2}{(4\pi)^2\,\epsilon}\left(\lambda_R g_R+2g_R^2\right)\right]\\
m_B^2 &= m_R^2\left(1-\frac{\lambda_R+g_R}{(4\pi)^2\,\epsilon}+\frac{5\left(\lambda_R^2+3g_R^2\right)}{12\,(4\pi)^4\,\epsilon}+\frac{3g_R^2-\lambda_R g_R}{2\,(4\pi)^4\,\epsilon}\log\left(\frac{\mu_g^2}{\mu_\lambda^2}\right)+\frac{2}{(4\pi)^4\,\epsilon^2}\left(\lambda_R^2+\lambda_R g_R+2g_R^2\right)\right)
\end{aligned} \tag{6.20}$$

and

$$Z = 1+\frac{1}{12\,(4\pi)^2\,\epsilon}\left(\lambda_R^2+3g_R^2\right) \tag{6.21}$$

where Z is the wavefunction renormalization. From Eqs. (6.14) and (6.20) we obtain

$$\begin{aligned}
\beta_\lambda^\lambda &= \mu_\lambda\frac{\partial\lambda_R}{\partial\mu_\lambda} = \frac{3\left(\lambda_R^2-g_R^2\right)}{(4\pi)^2}\\
\beta_g^\lambda &= \mu_g\frac{\partial\lambda_R}{\partial\mu_g} = \frac{6g_R^2}{(4\pi)^2}\\
\beta_g^g &= \mu_g\frac{\partial g_R}{\partial\mu_g} = \frac{4g_R^2}{(4\pi)^2}\\
\beta_\lambda^g &= \mu_\lambda\frac{\partial g_R}{\partial\mu_\lambda} = \frac{2\lambda_R g_R}{(4\pi)^2}\\
\gamma_\lambda^m &= \mu_\lambda\frac{\partial m_R^2}{\partial\mu_\lambda} = \frac{m_R^2}{(4\pi)^2}\left[\lambda_R-\frac{5}{6\,(4\pi)^2}\lambda_R^2+\frac{\lambda_R g_R}{2\,(4\pi)^4}\log\left(\frac{\mu_g^2}{\mu_\lambda^2}\right)\right]\\
\gamma_g^m &= \mu_g\frac{\partial m_R^2}{\partial\mu_g} = \frac{m_R^2}{(4\pi)^2}\left[g_R-\frac{5}{2\,(4\pi)^2}g_R^2-\frac{6g_R^2-\lambda_R g_R}{2\,(4\pi)^4}\log\left(\frac{\mu_g^2}{\mu_\lambda^2}\right)\right]
\end{aligned} \tag{6.22}$$

The RG functions should be compared with the standard one-loop RG functions that follow from Eq. (6.15)

$$\begin{aligned}
\beta^\lambda &= \mu\frac{\partial\lambda_R}{\partial\mu} = \frac{3}{(4\pi)^2}\left(\lambda_R^2+g_R^2\right)\\
\beta^g &= \mu\frac{\partial g_R}{\partial\mu} = \frac{2}{(4\pi)^2}\left(\lambda_R g_R+2g_R^2\right)\\
\gamma^m &= \mu\frac{\partial m_R^2}{\partial\mu} = m_R^2\left(\frac{\lambda_R+g_R}{(4\pi)^2}-\frac{5}{6}\frac{\lambda_R^2+3g_R^2}{(4\pi)^2}\right)
\end{aligned} \tag{6.23}$$

It is apparent that at one-loop order, the RG functions are independent of $l = \log\left(\frac{\mu_g^2}{\mu_\lambda^2}\right)$; however, in general, the form of the RG functions with couplings $\xi_i = (\lambda_R, g_R)$ is

$$\beta_j^i = \mu_j \frac{\partial \xi_i}{\partial \mu_j} = \sum_{n=2}^{\infty} \sum_{a=0}^{n-2} \frac{1}{n!} c_{k_1 \ldots k_n}^{i/j(a)} l^a \tag{6.24}$$

$$\gamma_i^m = \mu_i \frac{\partial m_R^2}{\partial \mu_i} = m_R^2 \sum_{n=1}^{\infty} \sum_{a=0}^{n-1} \frac{1}{n!} d_{k_1 \ldots k_n}^{i(a)} \xi_{k_1} \ldots \xi_{k_n} l^a \tag{6.25}$$

Diagrams with n-loops contribute to $c_{k_1 \ldots k_n}^{i/j(a)}$ and $d_{k_1 \ldots k_n}^{i(a)}$. These coefficients are related on account of the consistency condition

$$\left[\mu_i \frac{\partial}{\partial \mu_i}, \mu_j \frac{\partial}{\partial \mu_j}\right] = 0 \tag{6.26}$$

For example, $d_{k_1,0}^{i(0)}$ $d_{k_1,k_2}^{i(1)}$ and $c_{k_1,k_2}^{i/j(0)}$ are related as can be seen by applying the above equation to m_R^2 and keeping only terms bilinear in ξ_i:

$$\begin{aligned}
&\left[\mu_\lambda \frac{\partial}{\partial \mu_\lambda}, \mu_g \frac{\partial}{\partial \mu_g}\right] m_R^2 \\
&= \mu_\lambda \frac{\partial}{\partial \mu_\lambda} \left[m_R^2 \left(\frac{g_R}{(4\pi)^2} - \frac{6g_R^2 - \lambda_R g_R}{(4\pi)^4} \log \frac{\mu_g}{\mu_\lambda}\right)\right] - \mu_g \frac{\partial}{\partial \mu_g} \left[m_R^2 \left(\frac{\lambda_R}{(4\pi)^2} + \frac{\lambda_R g_R}{(4\pi)^4} \log \frac{\mu_g}{\mu_\lambda}\right)\right] \\
&= \frac{m_R^2}{(4\pi)^4} \left[\left(\lambda_R g_R + 2\lambda_R g_R + \left(6g_R^2 - \lambda_R g_R\right)\right) - \left(g_R \lambda_R + 6g_R^2 + \lambda_R g_R\right)\right] \\
&= 0
\end{aligned} \tag{6.27}$$

In general $c_{k_1 \ldots k_n}^{i/j(a)}$ $(a > 0)$ is fixed by $c_{k_1 \ldots k_{n-1}}^{i/j(b)}$ as follows from applying Eq. (6.26) to ξ_i; Similarly $d_{k_1 \ldots k_n}^{i(a)}$ $(a > 0)$ is fixed by applying Eq. (6.26) to m_R^2. Furthermore, $c_{k_1 \ldots k_n}^{i/j(0)}$ and $d_{k_1 \ldots k_n}^{i(0)}$ can be determined from the usual RG functions. To see this, we first note that upon setting $\mu_R = \mu$ Eq. (6.14) and Eq. (6.15) show that

$$\begin{aligned}
\beta^i &= \sum \beta_j^i \\
\gamma^m &= \sum_j \gamma_j^m
\end{aligned} \tag{6.28}$$

as, in general if

$$\xi_{iR} = (\mu_i)^{-\epsilon} \left[\xi_i + \sum_{\nu=1}^{\infty} \frac{a_\nu^i}{\epsilon^\nu}\right] \tag{6.29}$$

then

$$\beta^i = \mu \frac{\partial \xi_i}{\partial \mu}\bigg|_{\mu=\mu_R} = a_1^i - \sum_j \xi_j a_{1,\xi_j}^i \tag{6.30}$$

$$\beta_j^i = \mu_j \frac{\partial \xi_i}{\partial \mu_j} = \delta_j^i a_1^i - \xi_j a_{1,\xi_j}^i \tag{6.31}$$

Next, we note that at n-loop order

$$a_1^{i(n)} = \sum_{k_1 \ldots k_{n+1}} \frac{1}{(n+1)!} a_{k_1 \ldots k_{n+1}}^i \xi_{k_1} \ldots \xi_{k_n+1} \tag{6.32}$$

and so by Eq. (6.30)

$$\beta^i = \sum_{n=1}^{\infty} \left(\frac{1}{(n+1)!} - \frac{1}{n!} \right) \sum_{k_1 \ldots k_{n+1}} a_{k_1 \ldots k_{n+1}}^i \xi_1 \ldots \xi_{k+1} \tag{6.33}$$

This is shows that $a_{k_1 \ldots k_{n+1}}^{i(n)}$ can be found when $\mu_i = \mu$ by examining β^i and thus by Eqs. (6.24) and (6.31), $c_{k_1 \ldots k_{n+1}}^{i/j(0)}$ can be found.

Actually integrating Eq. (6.14) to determine ξ_1 and m_R^2 is complicated beyond one loop order by dependence of the right side on l; at one-loop order integration of Eq. (6.22) is feasible.

6.3 Multi-scale Renormaliztion Group Methods for the Effective Potential

In this Section we use multi-scale renormalization group methods to simplify analysis of the effective potential. In models with multiple scalar fields the (one-loop) effective potential depends on the eigenvalues of the mass matrix, which can become complicated non-polynomial functions of the fields if there are no simplifying symmetries [101, 188]. The GW approach addresses this complexity, but is limited to weakly coupled theories [186, 188, 35] which may preclude studies of interesting symmetry-breaking scenarios and Standard-Model extensions [11, 33, 100, 33, 14, 15, 101]. It is thus desirable to generalize the GW method to avoid the weak-coupling limitation. The original CW analysis with the Standard Model Higgs scalar field

was based on this weak-coupling assumption, leading to a light Higgs mass of approximately 10 GeV [12]. However, the weak-coupling limit in CW analysis of the Standard Model can be addressed by a full leading-logarithm RG analysis, increasing the Higgs mass prediction [33]. Similarly, the weak-coupling limitation of the GW approach, which is the generalization of CW model to incorporate extra scalar fields, can be addressed by multi-scale RG methods.

For the model introduced in Section 6.2, the multi-scale RG method requires two renormalization scales μ_λ and μ_g (i.e., one for each coupling) [188]. In the limit when $\mu_\lambda = \mu_g$ the multi-scale method reverts to conventional single-scale RG techniques.

The presence of a second renormalization scale gives the freedom to choose a special relationship between μ_λ and μ_g to constrain the couplings to satisfy $\lambda = 3g$, leading to an $O(2)$-symmetric version of the Lagrangian (6.2) and resulting in a simplified logarithmic term in the one-loop level effective potential. By contrast to conventional (single-scale) RG methods where the $\lambda = 3g$ constraint may be satisfied at a certain fixed scale, with multiple scales the constraint will be satisfied along a particular trajectory in the μ_λ, μ_g plane. Because the effective potential will satisfy a modified RG equation along this $O(2)$-symmetric trajectory, we can exploit RG methods to analyze the effective potential along this trajectory. We can then use RG invariance to map the predictions from the symmetric trajectory to obtain the physical content of the model for a conventional (single) renormalization scale. Thus instead of a complicated and possibly intractable effective potential in the single-scale RG approach, we simplify the analysis of the effective potential on the symmetric RG trajectory and the challenges are shifted to obtaining the multi-scale RG functions on the symmetric RG trajectory and the process of mapping back to the physical single-scale trajectory. However, because this mapping is governed by both the single- and multi-scale RG functions, the procedure is well-established and has no inherent challenges. It should be noted that the multiple renormalization scales can also be attached to the kinetic terms [107]. However, the implementation of this approach in a generalized $O(M) \times O(N)$ model discussed later will be difficult since it does not provide enough renormalization scales, which leads to insufficient freedom to choose a special relationship between the scales to constrain the couplings. Thus, the approach in Ref. [188] will be employed, with each renormalization scale attached to one coupling.

We begin by studying the conformal (massless) version of the model given in Eq. (6.2) with multiple renormalization scales (note that the cosmological term is not needed in the massless theory [200]). Since our primary interest is in radiative symmetry-breaking, we assume that $g > 0$ so that there is no conventional symmetry-breaking at tree-level. The one loop effective potential has the form

$$V_1 = \frac{1}{2}\int d^n k \log\left[\det\left(k^2 I + M\right)\right] \tag{6.34}$$

where we are integrating over Euclidean moment k and the mass matrix M is

$$M = \begin{pmatrix} \frac{1}{2}\left(\lambda_B {\phi_1}^2 + g_B {\phi_2}^2\right) & g_B \phi_1 \phi_2 \\ g_B \phi_1 \phi_2 & \frac{1}{2}\left(\lambda_B {\phi_2}^2 + g_B {\phi_1}^2\right) \end{pmatrix}. \tag{6.35}$$

The results of the loop integration can be expressed in terms of the eigenvalues M_+ and M_- of the matrix M

$$V_1 = \frac{1}{32\pi^2\epsilon}\left(M_+^2 M_+^{\epsilon/2} + M_-^2 M_-^{\epsilon/2}\right) \tag{6.36}$$

where counter-terms that are polynomials in the fields have been omitted. As emphasized in Ref. [188], we note that the explicit form of the one-loop contributions contains non-polynomial terms contained in $M_\pm$ and thus presents many complications for analysis of the effective potential.

By contrast with a single renormalization scale, where a variety of ways for introducing the scale will lead to the the same result because there is only a single dimensionless combination possible for the logarithms resulting from (6.36), a more systematic approach is needed for multiple renormalization. Including the tree-level contribution V_0 into the effective potential

$$V_{\text{eff}} = V_0 + V_1 \tag{6.37}$$

$$V_0 = \frac{\lambda_B}{24}\left(\phi_1^4 + \phi_2^4\right) + \frac{g_B}{4}\phi_1^2\phi_2^2\,, \tag{6.38}$$

using the relation (6.20) between the bare and renormalized couplings (note that the anomalous field dimension is zero at one-loop order, so the bare and renormalized fields are identical), and

expanding to appropriate order in the couplings and in ϵ to obtain all finite terms, gives

$$V_{\text{eff}} = \frac{\lambda_R}{24}\left(\phi_1^4 + \phi_2^4\right) + \frac{g_R}{4}\phi_1^2\phi_2^2 + \frac{1}{64\pi^2}\left(M_+^2 \log M_+ + M_-^2 \log M_-\right) + A_\lambda \log \mu_\lambda + A_g \log \mu_g \tag{6.39}$$

$$A_\lambda = -\frac{1}{16\pi^2}\left[\frac{1}{8}\left(\lambda_R^2 - g_R^2\right)\left(\phi_1^4 + \phi_2^4\right) + \frac{1}{2}\lambda_R g_R \phi_1^2\phi_2^2\right] \tag{6.40}$$

$$A_g = -\frac{1}{16\pi^2}\left[\frac{1}{4}g_R^2\left(\phi_1^4 + \phi_2^4\right) + g_R^2\phi_1^2\phi_2^2\right] \tag{6.41}$$

where counter-terms have again been omitted. Note that

$$A_\lambda + A_g = \frac{1}{32\pi^2}\left(M_+^2 + M_-^2\right) \tag{6.42}$$

as required to recover the limit of a single renormalization scale. The quantities A_λ and A_g are also completely determined by the multi-scale RG functions (6.22)

$$-A_\lambda = \frac{1}{24}\beta_\lambda^\lambda\left(\phi_1^4 + \phi_2^4\right) + \frac{1}{4}\beta_\lambda^g\phi_1^2\phi_2^2 \tag{6.43}$$

$$-A_g = \frac{1}{24}\beta_g^\lambda\left(\phi_1^4 + \phi_2^4\right) + \frac{1}{4}\beta_g^g\phi_1^2\phi_2^2 \tag{6.44}$$

and hence the agreement between Eqs. (6.41), (6.44) and Eqs. (6.40), (6.43) demonstrate that our calculations are self-consistent.

The typical strategy for analyzing effective potentials is to choose a renormalization scale where the logarithmic terms are zero (see, e.g., Ref. [36]). However, even with multiple renormalization scales this is not possible because of the complicated field dependence of the eigenvalues $M_\pm$, and thus a more sophisticated implementation of the multi-scale RG methods is needed. We can simplify the eigenvalues $M_\pm$ by exploiting the additional degree of freedom provided by the multi-scale RG to choose a special relationship between μ_λ and μ_g to constrain the couplings λ and g to fulfill

$$g\left(\mu_\lambda, \mu_g\right) = \frac{1}{3}\lambda\left(\mu_\lambda, \mu_g\right) , \tag{6.45}$$

such that the tree-level Lagrangian has $O(2)$ symmetry. Then the simplified eigenvalues M'_+ and M'_- become

$$M'_+ = \frac{1}{2}\lambda\left(\phi_1^2 + \phi_2^2\right); M'_- = \frac{1}{6}\lambda\left(\phi_1^2 + \phi_2^2\right) . \tag{6.46}$$

Using these eigenvalues, rearranging the logarithms in (6.39) via $\log \mu_g = \log (\mu_g/\mu_\lambda) + \log \mu_\lambda$, and ignoring counter-terms (which could thus contain coefficients with explicit $\log (\mu_g/\mu_\lambda)$ dependence), the one-loop effective potential for the constrained RG trajectory (6.45) becomes

$$V_{\text{eff}} = \frac{\lambda_R}{24} \left(\phi_1^2 + \phi_2^2\right)^2 + \frac{5\lambda_R^2}{1152\pi^2} \left(\phi_1^2 + \phi_2^2\right)^2 \log \left(\frac{\lambda_R \left(\phi_1^2 + \phi_2^2\right)}{\mu_\lambda^2} \right). \tag{6.47}$$

Thus along the symmetric RG trajectory, the effective potential assumes the simplified GW form [186], but with no implicit small-coupling assumptions.

Finally, by using the scheme transformation [107]

$$\frac{\lambda_R (\mu_\lambda)}{\mu_\lambda^2} = \frac{1}{\mu^2}\,, \tag{6.48}$$

we obtain the CW form of the effective potential along the symmetric RG trajectory at leading-logatrithm order

$$V_{LL} = V_{tree} + \left(\phi_1^2 + \phi_2^2\right)^2 \left(BL + CL^2 + DL^3 + EL^4 + \ldots\right) \ , \ L \equiv \log \left[\frac{\phi_1^2 + \phi_2^2}{\mu^2} \right] \tag{6.49}$$

where the coefficients $B, C, D, E \ldots$ are functions of the renormalized coupling λ_R. These coefficients can be determined from the renormalization group equation [33, 100, 11, 105]. Although Eq. (6.49) superficially resembles an effective potential for an $O(2)$-symmetric ϕ^4 theory, the imprint of the underlying original theory is contained in the RG functions which must be modified to reflect the effect of both the symmetric RG trajectory (6.45) and the scheme transformation (6.48).

From Section 6.2, we already know how each coupling runs with the scales μ_λ, μ_g. However, we have chosen a particular trajectory in the $\mu_\lambda - \mu_g$ plane to simplify the form of the effective potential and we need to know how the couplings λ, g run on this symmetric trajectory. Thus we have:

$$\begin{aligned} \beta_\mu^\lambda = \frac{d\lambda}{d\log\mu} &= \left(\frac{\partial\lambda}{\partial \log \mu_\lambda} + \frac{\partial\lambda}{\partial \log \mu_g} \frac{d\log\mu_g}{d\log\mu_\lambda} \right) \frac{d\log\mu_\lambda}{d\log\mu} \\ &= \left(\beta_\lambda^\lambda + \beta_g^\lambda \frac{d\log\mu_g}{d\log\mu_\lambda} \right) \frac{d\log\mu_\lambda}{d\log\mu} \end{aligned} \tag{6.50}$$

$$\begin{aligned} \beta_\mu^g = \frac{dg}{d\log\mu} &= \left(\frac{\partial g}{\partial \log \mu_\lambda} + \frac{\partial g}{\partial \log \mu_g} \frac{d\log\mu_g}{d\log\mu_\lambda} \right) \frac{d\log\mu_\lambda}{d\log\mu} \\ &= \left(\beta_\lambda^g + \beta_g^g \frac{d\log\mu_g}{d\log\mu_\lambda} \right) \frac{d\log\mu_\lambda}{d\log\mu}\,. \end{aligned} \tag{6.51}$$

For the anomalous dimension we have

$$\begin{aligned}\gamma_\mu^{\phi_i} = \frac{d\log Z_{\phi_i}}{d\log\mu} &= \left(\frac{\partial \log Z_{\phi_i}}{\partial \log \mu_\lambda} + \frac{\partial \log Z_{\phi_i}}{\partial \log \mu_g}\frac{d\log\mu_g}{d\log\mu_\lambda}\right)\frac{d\log\mu_\lambda}{d\log\mu} \\ &= \left(\gamma_i^\lambda + \gamma_i^g \frac{d\log\mu_g}{d\log\mu_\lambda}\right)\frac{d\log\mu_\lambda}{d\log\mu}\end{aligned} \tag{6.52}$$

where $\frac{d\log\mu_g}{d\log\mu_\lambda}$ is determined from the symmetry constraint (6.45) and $\frac{d\log\mu_\lambda}{d\log\mu}$ is determined from Eq. (6.48). In particular, we find

$$\frac{d\log\mu_g}{d\log\mu_\lambda} = -\frac{\left(\beta_\lambda^\lambda - 3\beta_\lambda^g\right)}{\left(\beta_g^\lambda - 3\beta_g^g\right)}\,. \tag{6.53}$$

By using Eq. (6.22), the above expression can be simplified to

$$\frac{d\log\mu_g}{d\log\mu_\lambda} = -\frac{1}{2} - \frac{\lambda_R}{g_R} + \frac{1}{2}\frac{\lambda_R^2}{g_R^2}\,. \tag{6.54}$$

Inputting Eqs. (6.22) and (6.54) into Eqs. (6.50) and (6.51), we have

$$\begin{aligned}\beta_\mu^\lambda &= \frac{1}{(4\pi)^2}\left(6\lambda_R^2 - 6g_R^2 - 6\lambda_R g_R\right) \\ \beta_\mu^g &= \frac{1}{(4\pi)^2}\left(2\lambda_R^2 - 2g_R^2 - 2\lambda_R g_R\right)\,.\end{aligned} \tag{6.55}$$

We can now impose the constraint (6.45) that defines the symmetric trajectory to obtain

$$\frac{d\log\mu_g}{d\log\mu_\lambda} = -\frac{1}{2} - \frac{\lambda_R}{g_R} + \frac{1}{2}\frac{\lambda_R^2}{g_R^2} = 1 \tag{6.56}$$

$$\beta_\mu^\lambda = \frac{1}{(4\pi)^2}\frac{10}{3}\lambda_R^2 \tag{6.57}$$

$$\beta_\mu^g = \frac{1}{(4\pi)^2}\frac{10}{9}\lambda_R^2\,. \tag{6.58}$$

We speculate that the simple relationship (6.56) is a one-loop artifact, and would become non-trivial at higher-loop order.

As outlined in Refs. [33, 100, 105, 14], effective potentials of the $O(2)$ form (6.49) are best analyzed by choosing the scale $\mu^2 = v^2 = \langle\phi_1^2 + \phi_2^2\rangle$, which results in predictions of the coupling $\lambda_R(\mu = v) = \lambda_s$ and scalar mass M_s (i.e., the mass matrix is diagonal). It should be noted that vacuum expectation value v is a physical RG-invariant observable. However, these predictions from the symmetric RG trajectory must be mapped back to physical values in the original theory for a conventional single-renormalization scale. We describe this process

in general, keeping in mind that the one-loop case has a number of simplifications including (6.56) and trivial anomalous dimensions for the fields. Although the effective potential has an $O(2)$-symmetric form along the symmetric trajectory, it is important to recognize that the vacuum configuration of the original theory retains its imprint along the symmetric trajectory through the vacuum angle $\langle\phi_1\rangle/\langle\phi_2\rangle = \tan\theta$.

First, consider a geometric description of the constraint (6.45) defining the symmetric RG trajectory. The multi-scale couplings $g\left(\mu_\lambda, \mu_g\right)$ and $\lambda\left(\mu_\lambda, \mu_g\right)$ can be represented by surfaces parameterized by the renormalization scales μ_λ and μ_g. The constraint (6.45) represents an intersection of surfaces defining a three-dimensional curve, whose projection onto the $\mu_\lambda,\ \mu_g$ plane represents the symmetric RG trajectory. The single-scale limit $\mu_\lambda = \mu_g$ defines the physical RG trajectory, and the symmetric and physical trajectories intersect at the scale $\mu_\lambda = \mu_g = \mu^*$ (questions related to the existence of μ^* are discussed below).

Consider the physical content of the original theory parameterized by the RG-invariant vacuum configuration of the fields ($\phi_1 = v_1$, $\phi_2 = v_2$, $v^2 = v_1^2 + v_2^2$), scalar mass spectrum (M_{ϕ_1}, M_{ϕ_2}), and couplings referenced to these symmetry-breaking scales ($\lambda_p(v) = \lambda_v$, $g_p(v) = g_v$). Using the single- and multi-scale RG functions, the physical couplings λ_v and g_v are sufficient to determine the scale μ^* by noticing that at the intersection point of the symmetric and physical trajectories, the physical couplings satisfy the constraint $g_p\left(\mu^*\right) = \frac{1}{3}\lambda_p\left(\mu^*\right)$. The symmetric RG trajectories governed by Eqs. (6.50) and (6.51) are also uniquely determined after we obtain μ^*. We can thus evolve λ along the symmetric trajectory to $\mu = v$ until it reaches the value λ_s, and the correct value of the physical coupling λ_p therefore self-consistently leads to the numerical value λ_s. Thus, the physical couplings of the original theory are now determined.

A similar procedure is used to obtain the physical mass spectrum. The physical-trajectory values of the mass matrix $M_{ij}^p(v) = M_{ij}^p$ (from which the mass eigenvalues M_{ϕ_1}, M_{ϕ_2} are obtained) must be evolved using the RG equation to the scale μ^* where the mass matrix becomes diagonal with a single mass scale as required to connect with the $O(2)$-symmetric trajectory. RG evolution of the (diagonal) mass matrix then continues along the symmetric trajectory to $\mu = v$ until it reaches the value M_s. Just as for the couplings, the correct value of the physical-trajectory mass matrix M_{ij}^p self-consistently leads to M_s, and the physical content

of the original theory is now completely determined.

The existence of the scale μ^* that connects the physical and symmetric trajectories can be determined by using the single-scale RG functions to evolve the physical couplings from their values at the scale v until the constraint (6.45) is satisfied. One might become concerned in the extreme cases $\mu* \ll v$ or $\mu^* \gg v$ that would result from a hierarchy of the couplings $\lambda_v \gg g_v$. However, in this situation where one of the couplings is small enough to be ignored, the eigenvalues of the mass matrix are simplified, and alternative approaches are needed. Finally, we note that the scale μ^* will always exist in this model, because the single-scale β function for the ratio $r = 3g/\lambda$

$$\beta_r = \mu \frac{dr}{d\mu} = \lambda \left(-7r + \frac{4}{3} r^2 - r^3 \right) \ , \tag{6.59}$$

does not change sign, and hence r can be increased monotonically by evolution to a smaller scale or decreased monotonically by evolution to a larger scale.

6.4 Discussions and Conclusions

The method we described in the above section for the two-scalar model can be generalized to the case with $O(M) \times O(N)$ symmetry. For the generalized scalar sector:

$$L_s = \frac{1}{6}\lambda_1 \left(\Phi_1^\dagger \Phi_1 \right)^2 + \frac{1}{6}\lambda_2 \left(\Phi_2^\dagger \Phi_2 \right)^2 + \lambda_3 \left(\Phi_1^\dagger \Phi_1 \right) \left(\Phi_2^\dagger \Phi_2 \right) \tag{6.60}$$

where $\Phi_1^\dagger \Phi_1$ and $\Phi_2^\dagger \Phi_2$ fulfill $O(M)$ and $O(N)$ symmetries respectively. The explicit calculation of the effective potential at one loop level in the $\overline{MS}$ scheme is [186, 101]:

$$\begin{aligned} V_{eff} = & \frac{N-1}{256\pi^2} \left(\frac{2}{3}\lambda_1 H^2 + 2\lambda_3 \phi^2 \right)^2 \ln \left(\frac{\frac{2}{3}\lambda_1 H^2 + 2\lambda_3 \phi^2}{v^2} \right) \\ & + \frac{M-1}{256\pi^2} \left(\frac{2}{3}\lambda_2 \phi^2 + 2\lambda_3 H^2 \right)^2 \ln \left(\frac{\frac{2}{3}\lambda_2 \phi^2 + 2\lambda_3 H^2}{v^2} \right) \\ & + \frac{1}{64\pi^2} F_+^2 \ln \left(\frac{F_+}{v^2} \right) + \frac{1}{64\pi^2} F_-^2 \ln \left(\frac{F_-}{v^2} \right) \end{aligned} \tag{6.61}$$

where $H^2 = \Phi_1^\dagger \Phi_1$, $\phi^2 = \Phi_2^\dagger \Phi_2$ and

$$\begin{aligned} & F_\pm (H, \phi) := \frac{\lambda_1 + \lambda_3}{2} H^2 + \frac{\lambda_2 + \lambda_3}{2} \phi^2 \\ & \pm \sqrt{\left[\frac{\lambda_1 - \lambda_3}{2} H^2 - \frac{\lambda_2 - \lambda_3}{2} \phi^2 \right]^2 + 4\lambda_3^2 \phi^2 H^2} \, . \end{aligned} \tag{6.62}$$

It should be noted that the above expression of the effective potential is calculated by using $Tr\left[M^4 \ln\left(\frac{M^2}{v^2}\right)\right]$ where M^2 is the $(M+N)\times(M+N)$ mass matrix calculated from the Lagrangian and logarithmic terms emerge from the eigenvalues of the mass matrix. By associating each coupling $\lambda_1, \lambda_2, \lambda_3$ with the scale $\mu_{\lambda_1}, \mu_{\lambda_2}, \mu_{\lambda_3}$, we have the freedom to choose a particular trajectory in the renormalization scale space $\mu_{\lambda_1} - \mu_{\lambda_2} - \mu_{\lambda_3}$, as we did in the last section, such that a tree-level $O(N+M)$-symmetric Lagrangian would be obtained:

$$\begin{aligned} \lambda_1\left(\mu_{\lambda_1}, \mu_{\lambda_2}, \mu_{\lambda_3}\right) &= \lambda_2\left(\mu_{\lambda_1}, \mu_{\lambda_2}, \mu_{\lambda_3}\right) \\ \lambda_1\left(\mu_{\lambda_1}, \mu_{\lambda_2}, \mu_{\lambda_3}\right) &= 3\lambda_3\left(\mu_{\lambda_1}, \mu_{\lambda_2}, \mu_{\lambda_3}\right) . \end{aligned} \tag{6.63}$$

By using the above relationships, we are able to simplify the four logarithm terms in the above leading order effective potential expression to obtain a GW form [186] of the logarithmic terms along the symmetric RG trajectory. The methodology developed in the previous Section can then be extended to more complicated models with multiple scalars.

In summary, we have applied the multi-scale RG methods originally developed in Refs. [188, 189] to the study of effective potentials with multiple scalar fields, using a model with two interacting real scalar fields as a specific example. The additional degree of freedom represented by the second renormalization scale allows the identification of a RG trajectory where the effective potential exhibits an $O(2)$ symmetry, aligning with the GW form of the effective potential [186]. However, in contrast to the GW method [186, 188, 35], there is no explicit requirement for small scalar couplings in this approach. Although the functional form of the effective potential on the symmetric trajectory has an $O(2)$ symmetry, the imprint of the original theory remains in the vacuum configuration and in the multi-scale RG functions explicitly calculated for our example model in Section 6.2. Thus we have exchanged a complicated (and possibly intractable) non-polynomial structure of the effective potential with a single renormalization scale for a simpler $O(2)$-symmetric structure with multiple renormalization scales; at one- or two-loop order, this simplification is offset by only a marginal increase in the complexity of the RG functions resulting from multiple renormalization scales. RG evolution of the effective potential along a specific trajectory connecting the multi-scale symmetric and single-scale regimes then allows the physical content of the effective potential to be extracted, further emphasizing the imprint of the original model that determines the RG functions governing evolution along

this trajectory.

Chapter 7

Summary and Future Work

7.1 Summary

In this thesis, we have studied the conformally symmetric SM and the hidden sector extensions to address the hierarchy/ naturalness problem, the origin of EW symmetry breaking, possible dark matter candidates and recent LHC diphoton/ diboson anomalies.

In chapter 1, we introduced the notion of custodial symmetry and conformal symmetry as a custodial symmetry can address the naturalness problem. We have demonstrated that this conformal scenario may imply new physics around EW/ TeV scale, which makes this scenario particularly important in the LHC era. In addition, we have also provided a brief review of Coleman Weinberg mechanism where the scale hierarchies are dynamically generated through dimensional transmutation. Moreover, the SM itself is not sufficient to address the dark matter problem which requires an extension of the SM. In this thesis, we focus on the hidden sector extension of the SM. The notion that conformal symmetry as a custodial symmetry, Coleman Weinberg mechanism and the hidden sector extensions of the SM lay the foundation of this thesis.

In chapter 1, we have also introduced two key techniques in this thesis: the effective potential and the renormalization group method. Combining these two techniques results in the leading logarithmic summation technique where the RG improvement of the effective potential is obtained. However, this technique normally applies to the case with single scalar field while the hidden sector extensions of the SM normally contain multiple scalar fields. The generalization of the leading logarithmic summation technique requires generalizing the Coleman Weinberg mechanism to incorporate multiple scalar fields leading to the well-known Gildener

Weinberg method. We are able to develop a generalized summation technique built upon the Gildener Weinberg method. Thus, the effective potential, renormalization group and Gildener Weinberg method lay the technical foundation of this thesis.

From chapter 2 to chapter 5, we start with the conformally symmetric SM and gradually add further complexity to the models. In chapter 2, we focus on the conformally symmetric SM. We have developed the Padé approximations and averaging method to extend the Higgs mass predictions from five- to nine-loop order, resulting in an upper bound on the Higgs mass of 141 GeV. By noticing that the Higgs mass predictions are well-described by a geometric series, we find the series converged to an asymptotic Higgs mass of 124 GeV consistent with the ATLAS/ CMS observations. Similarly, we find the Higgs quartic coupling converges to $\lambda = 0.23$, which is significantly larger than its conventional symmetry breaking counterpart. This large coupling solution will lead to a significant enhancement of the process $HH \to HH$ and will be testable in the future ILC (International Linear Collider). This simple model also captures some essential features of the conformal models such as how radiative symmetry breaking is realized through the Coleman Weinberg mechanism.

In chapter 3, we have studied the minimal extension of the SM: the conformally symmetric real singlet extension, which is also the simplest hidden sector model. We have only considered the case where the Z_2 symmetry in the singlet sector is unbroken and the singlet decay is protected by the Z_2 symmetry. Thus, the real singlet in this model can be a dark matter candidate. In order to incorporate the extra real scalar field, we have developed a generalized leading logarithmic summation technique built upon the Gildener Weinberg method. In addition, we have proposed two scenarios to generate the singlet mass: the sequential scenario and the dynamical scenario. In the sequential scenario, we are able to address less than 35 % of the dark matter abundance for dark matter mass $M_s > 80\,\mathrm{GeV}$. However, in the dynamical scenario, we obtain much higher dark matter abundance. At one loop level, we find abundance of $10\% - 100\%$ with dark matter mass $106\,\mathrm{GeV} < \mathrm{M_s} < 120\,\mathrm{GeV}$. The predictions are within the detection region of the next generation XENON experiment.

In chapter 4, we have studied the next minimal extension of the SM: the conformally symmetric complex singlet extension of the SM where there is a global $U(1)$ symmetry in

the hidden sector. The global $U(1)$ symmetry can be either broken or unbroken and we have studied each scenario. In the unbroken case, the decay of complex singlet is protected by the global $U(1)$ symmetry leading to an ideal $\sim 100\,\text{GeV}$ cold dark matter candidate comprising a significant proportion of the thermal relic abundance within the detection region of the upcoming XENON1T [155] and LUX 300 day [51] experiments. Including an extra vector-like fermion F, this case can also provide an explanation for diphoton excesses without violating the experimental bounds if extra terms are introduced to increase the singlet mass. In the broken case, we have developed a renormalization-scale optimization technique to significantly narrow the parameter space and provide unique predictions for the model's couplings and masses. We find there exists a second Higgs boson with an approximate 550 GeV mass and a mixing angle $\sin\theta \approx 0.47$ consistent with current experimental limits. We have also explored the possibility of the LHC diphoton excess in the broken case upon including interactions of the complex scalar with an additional vector-like fermion. We find a set of coupling solutions that yield a second Higgs boson of mass around 720 GeV and an 830 GeV extra vector-like fermion F, which is able to address the 750 GeV LHC diphoton excess. Criteria to determine the symmetry breaking pattern in both the Higgs and hidden sectors is provided.

In chapters 2, 3 and 4, we have studied models with classical conformal symmetry. In chapter 5, we clarify that classical conformal symmetry actually means the model possesses the conformal symmetry at a UV scale implying the couplings of the model run into a fixed at a UV scale. We make a connection between the conformal scenario and the asymptotic safety theory by noticing there exists fixed point in both theories. We combine the notion of asymptotic safety (AS) with conformal invariance in a hidden sector beyond the SM. We use the renormalization group equations as a bridge to connect UV boundary conditions and EW/ TeV scale physics and furnish a detailed example in the context of a leptophobic $U(1)'$ model to address the recent LHC diboson excess. Upon investigating a broad selection of UV boundary conditions corresponding to different AS scenarios, we find that AS scenarios have very strong predictive power, allowing unique determination of most of the parameters in the model. We obtain the interrelationships among the couplings, the transition scale of the fixed point M_{UV} and the generations of quarks coupled to the Z'. We find one of the AS scenarios may address

the diboson excess with a rate of 4 fb. In addition, we have also explored the possibility of dark matter and find this model admits dark mater with a mass around $M_{Z'}/2$.

In chapter 3 and chapter 4, we have developed the generalized leading logarithmic summation technique built upon the Gildener Weinberg method. However, the Gildener Weinberg method is implemented with two approximations: the weak coupling approximation and the simplification of the form of the logarithm (may lead to missing information for the singlet mass prediction). In chapter 6, we develop the multi-scale renormalization group method to address the above two limitations. We use a model containing two interacting real scalar fields to illustrate the method. By introducing of an extra renormalization scale, we are allowed to map the effective potential of the model onto an RG-equivalent form with an $O(2)$ symmetric structure along a particular trajectory in the multiple renormalization-scale space, leading to a simplified form (Gildener Weinberg form) of the effective potential. It is demonstrated that the physical content of the effective potential in the original model, referenced to a single conventional renormalization scale, can be extracted from a particular RG-trajectory that connects to this multi-scale $O(2)$-symmetric form of the effective potential.

7.2 Future Work

7.2.1 Future Work of Conformally Symmetric Extension of SM (Hierarchy Problem, Origin of Higgs Mass and Dark Matter)

With stronger dark matter bounds provided by direct detection experiments (e.g., XENON/LUX) or collider experiments (e.g., LHC), richer structures may be necessary in the dark sector. Also, compared with the complicated structure of the existing SM, the dark sector may not be as simple as a basic Higgs portal or $U(1)'$ extension. So, in my future work, I want to consider richer hidden sectors (e.g., partially interacting dark matter [44], asymmetric dark matter [45]) both in and outside the conformal scenario and try to connect theoretical predictions to direct detection experiments (e.g., XENON/LUX), collider constraints (e.g., LHC/LEP) and cosmic ray signals (e.g., Fermi Telescope/AMS). Also, most of my work so far is in the conformal scenario. In my future work, I also want to explore other scenarios motivated by the hierar-

chy problem (e.g., supersymmetry, little Higgs, composite Higgs, extra dimension, twin Higgs) which at the same time could provide interesting dark matter candidates. Among them, the twin Higgs scenario [201, 202] is of particular interest to me since it not only provides solutions to the little hierarchy problem but also generally leads to hidden sector phenomenology which is closely related to my research experience. In addition, I am also very interested in the composite Higgs scenario [203]. In this scenario, electroweak scale is dynamically generated through the strong new dynamics above the electroweak scale, which is related to my research experience in conformal scenario where electroweak scale is dynamically generated through the dimension transmutation [204]. Both the twin Higgs scenario and the composite Higgs scenario may provide very interesting dark matter candidates.

7.2.2 Future Work of Vacuum Stability and Asymptotic Safety Scenario

The renormalization group equations provide a bridge to connect physics at the UV scale to physics at the EW scale. The UV physics can be encoded in the UV scale boundary conditions [176] and the asymptotic safety scenario is one of them. In my future work, in addition to the asymptotic safety scenario, I want to study alternative UV boundary conditions and try to find new phenomenological implications at EW/TeV scale (e.g. dynamically generated dark matter mass, top Yukawa coupling). Conversely, I also want to study versions of the SM with hidden sector/portal parameter inputs at the EW/TeV scale which may or may not be strongly constrained by experiment and explore their UV behavior. To realize the asymptotic safety scenario, we need to consider the running of the couplings to the unification scale by using the renormalization group. Thus, higher loop contributions to the RG functions could be very important. One thing I could do in the future is to calculate the higher loop order RG functions for a particular model (e.g., Z' model).

7.2.3 Future Work of Effective Potential Calculation Techniques and Applications

With the effective potential calculation techniques we have developed, in my future work, I want to generalize these techniques to incorporate temperature and study electroweak phase transitions and baryogenesis. Also, it is well known that electroweak baryogenesis does not work in the pure SM since it requires a strong first-order electroweak phase transition (see E.g. [205]). This provides another motivation for new beyond-SM physics. In my future work, I could study versions of SM extensions (hidden sector) to address the electroweak baryogenesis and at the same time possibly explain dark matter. In addition, I also want to implement the effective potential calculation techniques to study the quantum effects on the inflationary scenarios with a connection to the vacuum stability of the effective potential at high energies (e.g. Higgs portal inflationary scenarios [156]). Furthermore, I am very interested in cosmological signatures of the dark matter (see e.g. "A light particle solution to the cosmic lithium problem " [206]).

References

[1] S.L. Glashow, Nucl. Phys. 22 (1961) 579.

[2] S. Weinberg, Phys. Rev. Lett. 19 (1967) 1264.

[3] A. Salam, Elementary Particle Theory, ed. N. Swartholm, Almquist and Wissell, Stockholm (1968).

[4] A. Salam, J. Strathdee, Nuovo Cimento 11A (1972) 397.

[5] L. Susskind, Phys. Rev. D **20** (1979) 2619.

[6] G. 't Hooft, NATO Adv. Study Inst. Ser. B Phys. **59** (1980) 135.

[7] M. Dine, Ann. Rev. Nucl. Part. Sci. **65** (2015) 43 [arXiv:1501.01035 [hep-ph]].

[8] N. Craig, "Naturalness in the LHC Era", Lectures at the 21st International Summer Institute on Phenomenology of Elementary Particles and Cosmology (SI2015).

[9] W. A. Bardeen, FERMILAB-CONF-95-391-T, 1995.

[10] C. T. Hill, hep-th/0510177.

[11] C. T. Hill, Phys. Rev. D **89** (2014) 073003.

[12] S. R. Coleman and E. J. Weinberg, Phys. Rev. D **7** (1973) 1888.

[13] E. Gildener, S. Weinberg, Phys. Rev. D **13** (1976) 3333.

[14] T.G. Steele, Zhi-Wei Wang, Phys. Rev. Lett **110** (2013) 151601.

[15] T. G. Steele, Z. W. Wang, D. Contreras and R. B. Mann, Phys. Rev. Lett. **112** (2014) 17, 171602.

[16] Z. W. Wang, T. G. Steele, T. Hanif and R. B. Mann, JHEP **08** (2016) 065.

[17] Z. W. Wang, F. S. Sage, T. G. Steele and R. B. Mann, arXiv:1511.02531 [hep-ph].

[18] T. G. Steele, Z. W. Wang and D. G. C. McKeon, Phys. Rev. D **90** (2014) 10, 105012

[19] S. Weinberg, Phys. Rev. D **19** (1979) 1277.

[20] Y. Nambu, Proc. of Tenth Intern. Conf. on High Energy Physics, Rochester, Studer, Geneva (1960).

[21] Y. Nambu, G. Jona-Lasinio, Phys. Rev. 122 (1961) 345.

[22] J. Goldstone, Nuovo Cimento 19 (1961) 154.

[23] J. Goldstone, A. Salam, S. Weinberg, Phys. Rev. 127 (1962) 965.

[24] A. Djouadi, Phys. Rept. **457** (2008) 1 [hep-ph/0503172].

[25] E.S. Abers, B.W. Lee, Phys. Rep. 9C (1973) 1.

[26] S. R. Coleman and J. Mandula, Phys. Rev. **159** (1967) 1251.

[27] C. P. Burgess, Phys. Rept. **330** (2000) 193 [hep-th/9808176].

[28] S. Weinberg, Phys. Rev. Lett. **29** (1972) 1698.

[29] N. Arkani-Hamed, A. G. Cohen and H. Georgi, Phys. Lett. B **513** (2001) 232 [hep-ph/0105239].

[30] Z. Chacko, H. S. Goh and R. Harnik, Phys. Rev. Lett. **96** (2006) 231802 [hep-ph/0506256].

[31] G. Marques Tavares, M. Schmaltz and W. Skiba, Phys. Rev. D **89** (2014) no.1, 015009 doi:10.1103/PhysRevD.89.015009 [arXiv:1308.0025 [hep-ph]].

[32] V.A. Miransky, Dynamical Symmetry Breaking in Quantum Field Theory, World Scientific, (1993).

[33] V. Elias, R. B. Mann, D. G. C. McKeon and T. G. Steele, Phys. Rev. Lett. **91** (2003) 251601.

[34] S. Iso and Y. Orikasa, "TeV Scale B-L model with a flat Higgs potential at the Planck scale - in view of the hierarchy problem -," PTEP **2013** (2013) 023B08. [arXiv:1210.2848 [hep-ph]].

[35] L. Alexander-Nunneley and A. Pilaftsis, JHEP **1009** (2010) 021.

[36] M. Sher, Phys. Rept. **179** (1989) 273.

[37] F. Zwicky, "Spectral displacement of extra galaxtic nebulae", Helv. Phys. Acta **6** (1933) 110.

[38] V. C. Rubin and W. K. Ford, Jr. , "Rotation of the Andormeda Nebula from a Spectroscopic Survey of Emission Regions", Astrophys. J. **159** (1970) 379.

[39] M. Markevitch, A. H. Gonzalez, D. Clowe *et al.*, Astrophys. J. **606** (2004) 819.

[40] Particle Data Group Collaboration, B. D. Fields and S. Sarkar, "Big Bang nuclesynthesis", Phys. Lett. B **667** (2008) 228.

[41] E. Komatsu et al., "Seven-Year Wilkinson Microwave Anisotropy Probe (WMAP) Observations: Cosmological Interpretation", arXiv: 1001. 4538.

[42] G. Bertone *et al.*, "Particle Dark Matter: Observations, Models and Searches," Cambridge, UK: Univ. Pr. (2010) 738 p.

[43] Y. Mambrini, "Histories of Dark Matter in the Universe".

[44] J. Fan, A. Katz, L. Randall and M. Reece, "Double-Disk Dark Matter," Phys. Dark Univ. **2** (2013) 139 [arXiv:1303.1521 [astro-ph.CO]].

[45] T. Cohen, D. J. Phalen, A. Pierce and K. M. Zurek, Phys. Rev. D **82** (2010) 056001 [arXiv:1005.1655 [hep-ph]].

[46] K. M. Zurek, "Multi-Component Dark Matter," Phys. Rev. D **79** (2009) 115002.

[47] M. A. Buen-Abad, G. Marques-Tavares and M. Schmaltz, Phys. Rev. D **92** (2015) no.2, 023531 [arXiv:1505.03542 [hep-ph]].

[48] S. Alekhin *et al.*, arXiv:1504.04855 [hep-ph].

[49] J. M. Cline, K. Kainulainen, P. Scott and C. Weniger, Phys. Rev. D **88** (2013) 055025.

[50] E. Aprile *et al.* [XENON100 Collaboration], Phys. Rev. Lett. **109** (2012) 181301.

[51] D. S. Akerib *et al.* [LUX Collaboration], Phys. Rev. Lett. **112** (2014) 091303.

[52] N. Craig, H. K. Lou, M. McCullough and A. Thalapillil, JHEP **1602** (2016) 127 [arXiv:1412.0258 [hep-ph]].

[53] T. Robens, T. Stefaniak, Eur. Phys. J. C **75** (2015) 104.

[54] D. Lpez-Val and T. Robens, Phys. Rev. D **90** (2014) 114018 [arXiv:1406.1043 [hep-ph]].

[55] B. Holdom, Phys. Lett. B **166** (1986) 196.

[56] P. H. Chankowski, S. Pokorski and J. Wagner, Eur. Phys. J. C **47** (2006) 187.

[57] T. G. Rizzo, hep-ph/0610104.

[58] D. Hooper, Phys. Rev. D **91** (2015) 035025 [arXiv:1411.4079 [hep-ph]].

[59] M. Kado, "Results with the Full 2015 Data Sample from the ATLAS Experiment", LHC seminar of ATLAS and CMS physics results from Run 2, CERN, 15 December 2015.

[60] J. Olsen, "CMS 13 TeV results", LHC seminar of ATLAS and CMS physics results from Run 2, CERN, 15 December 2015

[61] R. Franceschini *et al.*, JHEP **1603** (2016) 144 [arXiv:1512.04933 [hep-ph]].

[62] M. Redi, A. Strumia, A. Tesi and E. Vigiani, arXiv:1602.07297 [hep-ph].

[63] E. Molinaro, F. Sannino and N. Vignaroli, arXiv:1512.05334 [hep-ph].

[64] S. Knapen, T. Melia, M. Papucci and K. Zurek, arXiv:1512.04928 [hep-ph].

[65] J. Zhang and S. Zhou, arXiv:1512.07889 [hep-ph].

[66] N. Craig, P. Draper, C. Kilic and S. Thomas, arXiv:1512.07733 [hep-ph].

[67] M. Carena, I. Low and C. E. M. Wagner, JHEP **1208** (2012) 060 [arXiv:1206.1082 [hep-ph]].

[68] D. Buttazzo, A. Greljo and D. Marzocca, Eur. Phys. J. C **76** (2016) no.3, 116 [arXiv:1512.04929 [hep-ph]].

[69] [CMS Collaboration], "*Search for an Higgs Like resonance in the diphoton mass spectra above 150 GeV with 8 TeV data*", Tech. Rep. CMS-PAS-HIG-14-006.

[70] G. Aad *et al.* [ATLAS Collaboration], Phys. Rev. D **92** (2015) 032004 [arXiv:1504.05511 [hep-ex]].

[71] [ATLAS Collaboration], Phys. Rev. D **90** (2014) 052005.

[72] G. Aad *et al.* [ATLAS Collaboration], JHEP **1411** (2014) 056 [arXiv:1409.6064 [hep-ex]].

[73] G. Aad *et al.* [ATLAS Collaboration], Phys. Lett. B **738** (2014) 428 [arXiv:1407.8150 [hep-ex]].

[74] G. Aad *et al.* [ATLAS Collaboration], Eur. Phys. J. C **76** (2016) 45 [arXiv:1507.05930 [hep-ex]].

[75] G. Aad *et al.* [ATLAS Collaboration], Phys. Lett. B **744** (2015) 163 [arXiv:1502.04478 [hep-ex]].

[76] [ATLAS Collaboration], "*A search for resonant Higgs-pair production in the bb bb final state in pp collisions at* $\sqrt{s} = 8\,\text{TeV}$", Tech. Rep. ATLAS-CONF-2014-005.

[77] V. Khachatryan *et al.* [CMS Collaboration], JHEP **1510** (2015) 144 [arXiv:1504.00936 [hep-ex]].

[78] G. Aad *et al.* [ATLAS Collaboration], JHEP **1601** (2016) 032 [arXiv:1509.00389 [hep-ex]].

[79] S. Chatrchyan *et al.* [CMS Collaboration], Phys. Rev. Lett. **111** (2013) 211804 Erratum: [Phys. Rev. Lett. **112** (2014) no.11, 119903]

[80] V. Khachatryan *et al.* [CMS Collaboration], Eur. Phys. J. C **75** (2015) 235 [arXiv:1408.3583 [hep-ex]].

[81] V. Khachatryan *et al.* [CMS Collaboration], JHEP **1511** (2015) 071 [arXiv:1506.08329 [hep-ex]].

[82] R. Barbieri and R. Torre, Phys. Lett. B **695** (2011) 259 [arXiv:1008.5302 [hep-ph]].

[83] G. Aad *et al.* [ATLAS Collaboration], Phys. Rev. D **91** (2015) 052007 [arXiv:1407.1376 [hep-ex]].

[84] G. Jona-Lasinio, Nuovo Cim. 34A, 1790 (1964).

[85] R.H. Brandenberger, Rev. Mod. Phys. 57 (1985) 8.

[86] M.E. Peskin, D.V. Schoreder, An Introduction to Quantum Field Theory, Perseus Books Publishing, (1995).

[87] R. Jackiw, Phys. Rev. D9 (1974) 1686.

[88] K.G. Wilson and J. Kogut, Phys. Reports. 12C, (1974) 75.

[89] C.G. Callan, Phys. Rev. D2 (1970) 1541.

[90] K. Symanzik, Comm. Math. Phys. 18 (1970) 227.

[91] S. Coleman, Aspects of Symmetry, Cambridge University Press, (1985).

[92] T. J. Hollowood, arXiv:0909.0859 [hep-th].

[93] S. Weinberg, Phys. Rev. 118 (1960) 838.

[94] K. Nishijima and Y. Tomozawa, Prog. Theor. Phys. 57 (1977) 654.

[95] T. P. Cheng and L. F. Li, Oxford, Uk: Clarendon (1984) 536 P. (Oxford Science Publications)

[96] G. Aad *et al.* [ATLAS Collaboration], Phys. Lett. B **716** (2012) 1.

[97] S. Chatrchyan *et al.* [CMS Collaboration], Phys. Lett. B **716** (2012) 30.

[98] T. Aaltonen *et al.* [CDF and D0 Collaborations], Phys. Rev. Lett. **109** (2012) 071804.

[99] S. Weinberg, Phys. Lett. B **82** (1979) 387.

[100] V. Elias, R. B. Mann, D. G. C. McKeon and T. G. Steele, Nucl. Phys. B **678** (2004) 147 [Erratum-ibid. B **703** (2004) 413].

[101] K. A. Meissner and H. Nicolai, Phys. Lett. B **648** (2007) 312.

[102] V. Elias, R. B. Mann, D. G. C. McKeon and T. G. Steele, Phys. Rev. D **72** (2005) 037902.

[103] F. A. Chishtie, T. Hanif, J. Jia, R. B. Mann, D. G. C. McKeon, T. N. Sherry and T. G. Steele, Phys. Rev. D **83** (2011) 105009.

[104] R. Jackiw, Phys. Rev. D **9** (1974) 1686.

[105] F. A. Chishtie, D. G. C. McKeon and T. G. Steele, Phys. Rev. D **77** (2008) 065007.

[106] H. Kleinert, J. Neu, V. Schulte-Frohlinde, K. G. Chetyrkin and S. A. Larin, Phys. Lett. B **272** (1991) 39 [Erratum-ibid. B **319** (1993) 545].

[107] C. Ford and D. R. T. Jones, Phys. Lett. B **274** (1992) 409 [Erratum-ibid. B **285** (1992) 399].

[108] F. A. Chishtie, D. G. C. McKeon and T. G. Steele, Can. J. Phys. **86** (2008) 623.

[109] J. R. Ellis, M. Karliner and M. A. Samuel, Phys. Lett. B **400** (1997) 176.

[110] V. Elias, T. G. Steele, F. Chishtie, R. Migneron and K. B. Sprague, Phys. Rev. D **58** (1998) 116007.

[111] F. Chishtie, V. Elias and T. G. Steele, Phys. Lett. B **446** (1999) 267.

[112] F. A. Chishtie, V. Elias and T. G. Steele, Int. J. Mod. Phys. A **20** (2005) 6241.

[113] M. A. Samuel, J. R. Ellis and M. Karliner, Phys. Rev. Lett. **74** (1995) 4380.

[114] J. R. Ellis, I. Jack, D. R. T. Jones, M. Karliner and M. A. Samuel, Phys. Rev. D **57** (1998) 2665.

[115] W. H. Press, et al, "Numerical Recipes", Cambridge University Press (1986).

[116] A. Papaefstathiou, L. L. Yang and J. Zurita, Phys. Rev. D **87** (2013) 011301 [arXiv:1209.1489 [hep-ph]].

[117] M. J. Dolan, C. Englert and M. Spannowsky, JHEP **1210** (2012) 112 [arXiv:1206.5001 [hep-ph]].

[118] B. W. Lee, C. Quigg and H. B. Thacker, Phys. Rev. D **16** (1977) 1519.

[119] V. Silveira, A. Zee, Phys. Lett. B 161 (1985) 136.

[120] J. McDonald, Phys. Rev. D 50 (1994) 3637.

[121] C.P. Burgess, M. Pospelov, T. ter Veldhuis, Nucl. Phys. B 619 (2001) 709.

[122] H. Davoudiasl, R. Kitano, T. Li, H. Murayama, Phys. Lett. B 609 (2005) 117.

[123] B. Patt, F. Wilczek, hep-ph/0605188.

[124] R. Dick, R. B. Mann, K. E. Wunderle, Nucl. Phys. B 805 (2008) 207.

[125] J. M. Cline and K. Kainulainen, JCAP **1301** (2013) 012.

[126] R. Hempfling, Phys. Lett. B **379** (1996) 153.

[127] R. Foot, A. Kobakhidze and R. R. Volkas, Phys. Lett. B **655** (2007) 156.

[128] R. Foot, A. Kobakhidze, K. L. McDonald, R. R. Volkas, Phys. Rev. D **77** (2008) 035006.

[129] R. Foot, A. Kobakhidze and R. R. Volkas, Phys. Rev. D **82** (2010) 035005.

[130] C. Englert, J. Jaeckel, V. V. Khoze and M. Spannowsky, JHEP **1304** (2013) 060.

[131] V. V. Khoze and G. Ro, JHEP **1310** (2013) 075.

[132] W. -F. Chang, J. N. Ng and J. M. S. Wu, Phys. Rev. D **75** (2007) 115016.

[133] C. D. Carone, R. Ramos, Phys. Rev. D **88** (2013) 055020.

[134] A. Farzinnia, H. -J. He and J. Ren, Phys. Lett. B **727** (2013) 141.

[135] E. Gabrielli, M. Heikinheimo, K. Kannike, A. Racioppi, M. Raidal and C. Spethmann, Phys. Rev. D **89** (2014) 015017.

[136] T. Hambye, M.H.G. Tytgat, Phys. Lett. B **659** (2008) 651.

[137] M. Heikinheimo, A. Racioppi, M. Raidal and C. Spethmann, Phys. Lett. B **726** (2013) 781.

[138] D. Chway, T. H. Jung, H. D. Kim and R. Dermisek, Phys. Rev. Lett. **113** (2014) 051801 [arXiv:1308.0891 [hep-ph]].

[139] G. Steigman, B. Dasgupta and J. F. Beacom, Phys. Rev. D **86** (2012) 023506

[140] S. Dittmaier *et al.*, arXiv:1101.0593.

[141] J. R. Espinosa, C. Grojean, M. Muhlleitner and M. Trott, JHEP **1212** (2012) 045

[142] K. Inoue, A. Kakuto and Y. Nakano, Prog. Theor. Phys. 63 (1980) 234.

[143] S. W. Randall, M. Markevitch, D. Clowe, A. H. Gonzalez and M. Bradac, Astrophys. J. **679** (2008) 1173.

[144] A. Djouadi, A. Falkowski, Y. Mambrini and J. Quevillon, Eur. Phys. J. C **73** (2013) 6, 2455.

[145] V. Barger, P. Langacker, M. McCaskey, M. Ramsey-Musolf and G. Shaughnessy, Phys. Rev. D **79** (2009) 015018

[146] M. Gonderinger, H. Lim and M. J. Ramsey-Musolf, Phys. Rev. D **86** (2012) 043511.

[147] R. Costa, A. P. Morais, M. O. P. Sampaio and R. Santos, Phys. Rev. D **92** (2015) 2, 025024.

[148] L. Basso, S. Moretti and G. M. Pruna, Phys. Rev. D **83** (2011) 055014.

[149] V. V. Khoze, C. McCabe, G. Ro, JHEP **1408** (2014) 026.

[150] W. Altmannshofer, W. A. Bardeen, M. Bauer, M. Carena and J. D. Lykken, JHEP **1501** (2015) 032.

[151] J. A. Casas, J. R. Espinosa, M. Quiros and A. Riotto, Nucl. Phys. B **436** (1995) 3.

[152] J. Elias-Miro, J. R. Espinosa, G. F. Giudice, H. M. Lee and A. Strumia, JHEP **1206** (2012) 031.

[153] F. S. Sage and R. Dick, Astropart. Phys. **71** (2015) 31

[154] A. Djouadi, O. Lebedev, Y. Mambrini and J. Quevillon, Phys. Lett. B **709** (2012) 65.

[155] E. Aprile [XENON1T Collaboration], arXiv:1206.6288; E. Aprile [XENON Collaboration], arXiv:1512.07501.

[156] G. Ballesteros and C. Tamarit, JHEP **1509** (2015) 210.

[157] J. A. Aguilar-Saavedra, R. Benbrik, S. Heinemeyer and M. Prez-Victoria, Phys. Rev. D **88** (2013) 094010.

[158] R. D. Peccei and H. R. Quinn, Phys. Rev. Lett. **38** (1977) 1440.

[159] S. Weinberg, Phys. Rev. Lett. **40** (1978) 223.

[160] K. A. Meissner, H. Nicolai, Eur. Phys. J. C **57** (2008) 493.

[161] A. Latosinski, K. A. Meissner and H. Nicolai, arXiv:1010.5417 [hep-ph].

[162] M. Shaposhnikov, arXiv:0708.3550 [hep-th].

[163] Weinberg, Steven (1979). "Ultraviolet divergences in quantum theories of gravitation".

[164] G. Aad *et al.* (ATLAS), arXiv:1506.00962.

[165] V. Khachatryan *et al.* (CMS), Phys. Rev. D **91** (2015) 5, 052009.

[166] J. Hisano, N. Nagata and Y. Omura, Phys. Rev. D **92** (2015) 5, 055001.

[167] J. Brehmer, J. Hewett, J. Kopp, T. Rizzo and J. Tattersall, arXiv:1507.00013.

[168] K. Cheung, W. Y. Keung, P. Y. Tseng and T. C. Yuan, arXiv:1506.06064;
D. Gonalves, F. Krauss and M. Spannowsky, Phys. Rev. D **92** (2015) 053010;
A. Thamm, R. Torre and A. Wulzer, arXiv:1506.08688;
A. Carmona, A. Delgado, M. Quiros and J. Santiago, arXiv:1507.01914;
Q. H. Cao, B. Yan and D. M. Zhang, arXiv:1507.00268;
P. S. Bhupal Dev and R. N. Mohapatra, Phys. Rev. Lett. **115** (2015) 181803.

[169] A. Leike, Phys. Rept. **317** (1999) 143.

[170] P. Langacker, Rev. Mod. Phys. **81** (2009) 1199.

[171] M. Carena, A. Daleo, B. A. Dobrescu and T. M. P. Tait, Phys. Rev. D **70** (2004) 093009.

[172] S. Iso, N. Okada and Y. Orikasa, Phys. Lett. B **676**, 81 (2009).

[173] S. Oda, N. Okada and D. s. Takahashi, Phys. Rev. D **92** (2015) 015026.

[174] A. Karam and K. Tamvakis, Phys. Rev. D **92** (2015) 075010.

[175] M. Shaposhnikov and C. Wetterich, Phys. Lett. B **683** (2010) 196.

[176] M. Holthausen, K. S. Lim and M. Lindner, JHEP **1202** (2012) 037.

[177] M. Hashimoto, S. Iso and Y. Orikasa, Phys. Rev. D **89** (2014) 016019
M. Hashimoto, S. Iso and Y. Orikasa, Phys. Rev. D **89** (2014) 056010.

[178] F. Bezrukov and M. Shaposhnikov, J. Exp. Theor. Phys. **120** (2015) 335 [Zh. Eksp. Teor. Fiz. **147** (2015) 389].

[179] R. Percacci and D. Perini, Phys. Rev. D **68** (2003) 044018.

[180] S. Iso, N. Okada and Y. Orikasa, Phys. Rev. D **80** (2009) 115007.

[181] D. Buttazzo, G. Degrassi, P. P. Giardino, G. F. Giudice, F. Sala, A. Salvio and A. Strumia, JHEP **1312** (2013) 089.

[182] J. Erler, P. Langacker, S. Munir and E. Rojas, JHEP **0908** (2009) 017.

[183] A. Alves, A. Berlin, S. Profumo and F. S. Queiroz, JHEP **1510** (2015) 076.

[184] J. M. Cline, G. Dupuis, Z. Liu and W. Xue, JHEP **1408** (2014) 131.

[185] P.-A. Amaudruz *et al.*, arXiv:1410.7673.

[186] E. Gildener, S. Weinberg, Phys. Rev. D **13** (1976) 3333.

[187] F. S. Queiroz and K. Sinha, Phys. Lett. B **735** (2014) 69.

[188] M. B. Einhorn and D. R. T. Jones, Nucl. Phys. B **230** (1984) 261.

[189] C. Ford and C. Wiesendanger, Phys. Rev. D **55** (1997) 2202.

[190] E.C.G. Stueckelberg and A. Petermann, Helv. Phys. Acta 26 (1953) 499.

[191] M. Gell-Mann and F. Low, Phys. Rev. 95 (1954) 1300.

[192] G. 't Hooft, Nucl. Phys. B **61** (1973) 455.

[193] S. Weinberg, Phys. Rev. D **8** (1973) 3497.

[194] C. G. Callan, Jr., Phys. Rev. D **2** (1970) 1541.

[195] K. Symanzik, Commun. Math. Phys. **18** (1970) 227.

[196] P. M. Stevenson, Annals Phys. **132** (1981) 383.

[197] J. C. Collins, Phys. Rev. D **10** (1974) 1213.

[198] J. C. Collins and A. J. Macfarlane, Phys. Rev. D **10** (1974) 1201.

[199] G. 't Hooft and M. J. G. Veltman, Nucl. Phys. B **44** (1972) 189.

[200] B. M. Kastening, Phys. Rev. D **54** (1996) 3965.

[201] Z. Chacko, H. S. Goh and R. Harnik, Phys. Rev. Lett. **96** (2006) 231802 [hep-ph/0506256].

[202] N. Craig, A. Katz, M. Strassler and R. Sundrum, JHEP **1507** (2015) 105 [arXiv:1501.05310 [hep-ph]].

[203] F. Sannino, "Conformal Dynamics for TeV Physics and Cosmology," Acta Phys. Polon. B **40** (2009) 3533 [arXiv:0911.0931 [hep-ph]].

[204] T. Hambye and A. Strumia, Phys. Rev. D **88** (2013) 055022 [arXiv:1306.2329 [hep-ph]].

[205] D. E. Morrissey and M. J. Ramsey-Musolf, New J. Phys. **14** (2012) 125003 [arXiv:1206.2942 [hep-ph]].

[206] A. Goudelis, M. Pospelov and J. Pradler, arXiv:1510.08858 [hep-ph].